THERMOELASTIC PROPERTIES OF PARTICLE REINFORCED COMPOSITES AT THE MICRO AND MACRO SCALES

A Thesis

by

PRADEEP GUDLUR

Submitted to the Office of Graduate Studies of
Texas A&M University
in partial fulfillment of the requirements for the degree of

MASTER OF SCIENCE

December 2008

Major Subject: Mechanical Engineering

THERMOELASTIC PROPERTIES OF PARTICLE REINFORCED COMPOSITES AT THE MICRO AND MACRO SCALES

A Thesis

by

PRADEEP GUDLUR

Submitted to the Office of Graduate Studies of
Texas A&M University
in partial fulfillment of the requirements for the degree of

MASTER OF SCIENCE

Approved by:

Chair of Committee,	Anastasia Muliana
Committee Members,	Harry Hogan
	Ramesh Talreja
Head of Department,	Dennis L. O'Neal

December 2008

Major Subject: Mechanical Engineering

ABSTRACT

Thermoelastic Properties of Particle Reinforced Composites at the Micro and Macro Scales. (December 2008)

Pradeep Gudlur, B.Tech., Vidya Jyothi Institute of Technology, India;

M.S., Texas A&M University, USA

Chair of Advisory Committee: Dr. Anastasia Muliana

Particle reinforced composites are widely used in tires, heat exchangers, thermal barrier coatings and many other applications, as they have good strength to weight ratio, excellent thermal insulation, ease of manufacturing and flexibility in design. During their service life, these composites are often subjected to harsh environments, which can degrade the thermo-mechanical properties of the constituents in the composites, affecting performance and lifetime of the composites. This study investigates performance of particle reinforced composites subjected to coupled heat conduction and thermo-elastic deformation at the macro and micro levels. A micromechanical model is used to determine the effective thermal and mechanical properties of the homogenized composite by incorporating microscopic characteristics of the composites. The constituent's thermal conductivities of the composite are assumed to be functions of temperature and the elastic moduli to be functions of temperature and stress fields. The effective properties obtained from the micromechanical model represent average (macroscopic) properties. The effective heat conduction and thermo-elastic responses in

the homogenized composites are compared with the responses of the composite with particles randomly distributed in the matrix (heterogeneous materials) which represent microscopic responses. For this purpose, two sets of finite element (FE) models are generated for composites with particle volume contents 12.5, 25, and 50%. The first FE model represents a homogenized composite panel and the effective responses from the micromechanical model are used as input for the material properties. The second FE model mimics composite microstructure with discontinuous particles randomly dispersed in a homogeneous matrix. Parametric studies on effects of conductivity ratio between particle and matrix, degree of nonlinearity, and volume fraction on the temperature distribution and steady state times have been studied. For lower volume fractions the temperature profiles of homogenized and heterogeneous composite models are in good agreement with each other. But for higher volume fractions, the detailed model showed a wavy profile whereas the effective model showed no signs of it. When the nonlinearity in thermal conductivity of the particle and matrix constituents is increased, the steady state time significantly deviates from the ones with constant constituent properties. When the volume fraction of particles in the composite increases, the steady state is reached in less time, since the thermal conductivity of particles are taken larger than that of the matrix. Effects of coefficient of thermal expansion (CTE) ratio of particle and matrix, temperature change, and volume fraction on the discontinuity of stress and strain fields at the interphase of matrix and particle have been studied. The stresses developed were more for higher CTE ratios and the magnitude of discontinuity also follows the same trend. As the volume fraction increases, the stresses

developed and the magnitude of discontinuity also increase. Finally, sequentially coupled heat conduction and deformation analyses are performed on thermal barrier coating (TBC) systems to demonstrate the applicability of the micromechanical model in predicting overall thermo-elastic responses of the TBC.

ACKNOWLEDGEMENTS

I would like to thank my research advisor for master's program, Dr. Anastasia Muliana for her patience, guidance and support over the course of this research, along with her invaluable suggestions which were a constant inspiration towards the completion of this work. I would like to thank Dr. Harry Hogan and Dr. Ramesh Talreja for their helpful comments on the work. I would like to acknowledge and extend my gratitude to the Mechanical Engineering Department at Texas A&M University for giving me various opportunities that have helped to make this journey an educational as well as an enjoyable one.

I would like to dedicate my thesis work to my parents. Because of their love and affection along with constant encouragement to pursue my goals, I have learned to be the best that I can be. Thank you for being a part of my life.

TABLE OF CONTENTS

Page

CHAPTER Page

LIST OF FIGURES

FIGURE Page

FIGURE Page

FIGURE Page

LIST OF TABLES

TABLE Page

CHAPTER I

INTRODUCTION

Particle reinforced composites are a type of composites in which particles having specific properties are embedded into another material (matrix) having different properties in such a way that the overall systems will have a combination of properties of both constituents. By manufacturing particle reinforced composites with different microstructural geometries and constituent properties, one can achieve desired responses of the composite. Particle reinforced composites are used in tires, heat exchangers, thermal barrier coatings etc., which are often exposed to extremely harsh conditions. In order to have the component infallible even in these conditions, it is essential to understand the behavior of these composites under different loading conditions in terms of stresses and deformations. It is also important to monitor the deformations in composites during a transient heat transfer (heat conduction) process.

The overall response of the composite depends on the microscopic geometries and properties of the individual constituents of the composite. Hence it is necessary to study the influence of these microscopic characteristics on the overall macroscopic behavior of the composite. However, it is very complicated to incorporate the detailed microscopic characteristics of the composites in predicting effective (macroscopic) performance. Several approximate solutions based on volume averaging of individual constituents have been developed. This averaging technique, generally termed as

---

This thesis follows the style of Composites Science and Technology.

homogenization methods, allows us to calculate the effective properties of the composite from its microscopic constituents. Homogenization methods also help in reducing the computational time and effort. However, the main drawback of such a homogenization scheme is that the discontinuity of effective stress and strain fields at the particle and matrix interface, which plays a vital role in the debonding of the composite, cannot be properly quantified.

This chapter presents a literature review on analytical and numerical works proposed for predicting effective thermo-elastic properties of heterogeneous materials followed by research objectives.

1.1 Studies conducted on predicting effective thermo-elastic properties of a composite

As it is highly difficult to determine the detailed displacement (or) stress fields, attempts were made to simplify the geometry and behavior of constituents in order to obtain effective elastic properties. Hashin et al. [1] used variational principles based on linear theory of elasticity to derive upper and lower bounds for effective elastic moduli (bulk modulus & shear modulus). They have shown that as the stiffness of one phase is increased with respect to other, the distance between bounds increases. When one of the phases was rigid, their method gives upper bound as infinity and for an empty phase (porous or cavity) the lower bound goes to zero.

Kari et al. [2] used FE method to evaluate the effective properties of randomly distributed spherical particle reinforced composites with periodic boundary conditions. For linear elastic case and for volume fraction 30%, models were generated with

identical spherical particles and the effective properties (E, G and μ) for different sizes of cubic representative volume element (RVE) were evaluated. They concluded that the size of RVE should be at least L = (10/3)*D, where L is size of RVE and D is the diameter of the particles. By keeping size of RVE constant and volume fraction of particles constant at 30%, effective material properties were determined for different sizes of particles. There were no significant variations (only slight variations which can be attributed to particle-particle interactions when the size of particles is less and there are greater number of particles in RVE). Numerical simulations were conducted and it was observed that there was no significant difference in effective properties between random size of spherical particles and same size of spherical particles. From the numerical results, they concluded that effective material properties of spherical particle reinforced composite depend only on volume fraction. Size of particles and size of RVE has no significant effect on effective properties for linear case.

Chen et al. [3] developed a model to predict effective elastic modulus and Poisson's ratio of 2D & 3D two phase composite materials. Their model comprised of a specimen discretized into n x n domains, which are of equal size and assigned to a particular constituent of the two phase (glass & epoxy) composite and each domain is further divided into m x m finite elements. For constant volume fraction (50%) and for different distributions of constituents between domains they conducted studies on the sensitivity of the predictions to the domain size. They found that the effective elastic modulus does not vary significantly with increasing element density; however, the computational time increases tremendously. They compared the effective elastic

modulus obtained from all their studies with the Hashin-Shtrikman bounds and found that the values were lying between these bounds. They also found that for glass inclusion in the epoxy matrix, the effective elastic modulus was closer to the lower Hashin-Shtrikman bound, while the one of epoxy inclusion in glass matrix was closer to the upper Hashin-Shtrikman bounds.

Cho et al. [4] have used numerical and experimental methods to determine the effect of inclusion on the mechanical properties of composites. From the results, they conclude that as the particle size decreases, the tensile strength increases where as the debonding growth decreases. They also found that there would not be any effect of particle size on elastic modulus for the composite at micro scale or larger. But for nano scale, the elastic modulus increases with decrease in particle size.

According to Kanit et al. [5], RVE size must be treated as a function of different parameters such as: physical property e.g. thermal conductivity, bulk modulus, shear modulus, mismatch of phase properties, volume fraction of particles and desired precision in determining the effective properties. For example, to determine the effective thermal property and effective mechanical property for the same microstructure of the composite, one has to consider different sizes of RVE.

In order to transmit load between matrix and particles efficiently, it is highly important to choose the material for the interphase and its concentration carefully. Kari et al. [6] have evaluated the effect of interphase material properties and its volume fraction on the overall material behavior of the composite. By keeping the volume content of particles, volume content of interphase and material properties of matrix and

particle constant, they observed that overall properties significantly change by varying the elastic modulus for interphase material. By increasing the elastic modulus of interface the transverse modulus of the overall composite increased. They also found that when the volume fraction of interphase was increased by keeping all other parameters constant, the effective elastic and shear modulus decreased.

Hollister et al. [7] used asymptotic expansion homogenization method to estimate the effective properties of composites. The effective responses reach the exact solution as the ratio of RVE size to global structure size goes to zero. They compared the elastic behavior of the asymptotic homogenization model with the homogenization model based on volume averages for periodic composites with finite size RVEs. The two approaches are comparable as the ratio of RVE size to global size goes to zero. Since the accuracy of predicted effective stiffness increases as the ratio goes to zero, they concluded that for periodic composites, the effective stiffness of the asymptotic expansion homogenization theory are more accurate than that of the volume averaging schemes.

Kaminski [8] compared the FE based homogenization method with boundary element (BE) homogenization method for a linear elastic glass-epoxy periodic composite. Components of an effective stiffness tensor were calculated using both approaches and compared by plotting them against different volume fractions of fiber. With the increase of fiber radius, the effective stiffness tensors increase for both methods but the values obtained using BE method were always greater than that obtained from the FE method, which could be attributed to the general differences in the assumptions of both the methods.

Tszeng [9] and Segurado et al. [10] conducted virtual tests on particle reinforced composites to determine the effect of particle clustering on the mechanical properties of the composite. They concluded that cluster of particles weakly affects the overall behavior of the composite. It has no significant influence on the elastic modulus of the composite, on the stress and strain responses of the composite, and on the stress concentration of the particles in the composite. But with increase in degree of clustering, the ductility of the composites decreases as the fraction of broken particles increases. Clustered region starts yielding at a lower stress value than the unclustered region and when the particles in the cluster are very close, the chance of crack initiation at the particle matrix interface increases.

On two-phase particle reinforced linear elastic composites, Drugan et al. [11] used variational principles to derive the effective stiffness tensor which relates the volumetric averages of stress and strain. For spatially varying load, the minimum size of RVE was quantitatively determined by comparing the obtained constant effective stiffness tensor with the magnitude of nonlocal term in the constitutive equation. For a wide range of reinforcement types and their volume fractions and for a maximum error of 5% in determining the constant effective stiffness tensor, the minimum RVE size does not exceed 2.1 times reinforced spheres diameter. For a wide range of reinforcement types and concentrations, as the volume fraction of reinforcement increases, the minimum size of RVE required also increases. The minimum RVE size required in normal straining mode must be larger than that in shear straining mode, for the same accuracy in determining the stiffness tensor in both cases. Minimum RVE size required

for voids and rigid particles are greater than that of any other reinforcement type. The minimum RVE sizes required for voids are greater than that of rigid particles as discussed in Drugan [12].

If any one of the constituents of heterogeneous materials is nonlinear, the effective properties obtained through homogenization are not directly applicable. The nonlinear behavior has to be converted to linear elastic behavior before the homogenization principles can be applied on them. Levesque et al. [13] emphasizes this point by demonstrating a method to convert nonlinear visco-elastic material to linear elastic. They first use a linearization method to convert nonlinear visco-elastic behavior to linear visco-elastic behavior and then uses Laplace Carson transform to convert it to linear elastic material. Once the material is linear elastic, they use Mori-Tanaka scheme to homogenize the entire composite.

Hine et al. [14] predicted thermo-elastic properties of short glass fiber reinforced composites using numerical simulations. With the increase in volume fraction, the longitudinal and transverse modulus increased linearly and the shear modulus increased nonlinearly. The longitudinal Poisson's ratio and the longitudinal thermal expansion coefficient decreased slightly with increase in volume fraction. Whereas the transverse poisons ratio and transverse thermal expansion coefficient initially have increased slightly, reached a peak and then have reduced from there on.

Aboudi [15, 16] presented an analytical solution for a two-way thermo-mechanical coupled micromechanical analysis for multiphase composites where both temperature and deformation fields can influence each other. In the present work, a one

way thermo-mechanically coupled problem i.e., only temperature field is going to influence deformation field, is considered.

Li et al. [17] investigated the effect of particle shape and particle stiffness on the initial yielding and overall stress-strain relationship of the composite, under various loadings. Depending on the loading condition, different particle shapes have different effect on the overall response of the composite. For an axisymmetric loading, the strengthening effects are good for oblate and prolate shapes, as they give the largest increase in yield stress and load bearing capacity. For transverse and axisymmetric shearing loads, largest increment in yield stress and load bearing capacity are shown by the oblate shape. For longitudinal loading, spherical shapes are the best. Particle's stiffness can significantly contribute to initial yielding but not so much to the overall stress-strain response of the composite.

Muliana et al. [18, 19] developed a concurrent micromechanical model for determining the effective properties of a particle reinforced polymeric composite with matrix being nonlinear visco-elastic and the solid spherical particles exhibiting linear elastic characteristics. A unit cell model consisting of four particles and polymer sub-cells is generated and the micromechanical relations are developed in the sub-cells. A stress-strain correction scheme is developed in such a way that non-linear constitutive relations and the linearized micromechanical model are satisfied. Effective thermal conductivity and coefficient of expansion were determined, which allows simulating sequentially coupled heat conduction and deformation in composites.

1.2 Studies conducted on determining effective thermal properties of a composite

Analytical and numerical models have been developed to analyze effective transport properties of composites. Kolodziej et al. [20] proposed a method for determining effective thermal conductivity for a laminated composite slab, for which the thermal conductivity of constituents are linear functions of temperature. Their method consists of using an adaptive FEM in such a way that temperature is determined on the nodes generated at the beginning and on the nodes additionally generated in the adaptive mesh. An effective medium as a single layer with relevant effective temperature and effective thermal conductivity was introduced. The constants which characterize their effective thermal conductivity in effective medium were calculated based on the facts that the heat flux in effective and real medium are equal and that the temperature difference between effective and real medium is minimal in the least square sense.

Fan [21] used a microstructural approach for predicting the effective transport properties of two phase composites such as electrical conductivity, dielectric constant, magnetic permeability, thermal conductivity, and diffusion coefficient. The effective transport property of the overall composite depends not only on the transport properties of constituent phases but also on the volume fraction of constituent phases, geometrical distribution of phases and size of the phases. The proposed effective transport property was verified with bounds derived by Hashin et al. [1] and found it to be comfortably lying in between the upper and lower bounds. For a composite with high transport property of second phase, the upper bound of Hashin & Shtrikman becomes infinity and

for a composite with porous particle, the lower bound of Hashin & Shtikman vanishes. But the approach presented by Fan [21] works well even in these two extreme cases. Hence in terms of range of applicability and accuracy of prediction, this approach is superior to that of Hashin et al. [1].

In order to understand the overall effective thermal conductivity of the composite and the parameters that affect it, Yin and Tu [22] have studied two dimensional PTFE (Poly Tetra Floro Ethylene) composites with randomly distributed circular graphite particles. Their numerical work has yielded the fact that the effective conductivity for random distribution of particles is lower than that of uniform distribution of particles. This means that while fabricating the composite, the inclusion particles should be dispersed as uniform as possible to have a better effective conductivity of the composite. They also observed that as the number of particles increases, the effective thermal conductivity value for random distribution increases gradually and approaches the value of uniform distribution, i.e. for higher volume fraction the random distribution can be treated as a uniform distribution. As the conductivity ratio increases i.e., as the conductivity of particles increase, they observed that the effective conductivity of composite is at first increasing and reaches an asymptotic value. Improvement in effective conductivity can be made by increasing the conductivity ratio up to a certain degree.

Apparent properties are defined as those under essential (displacement or temperature), natural (traction or heat flux), mixed or periodic boundary conditions applied to finite size material domains (windows). Apparent property of a periodic

composite under periodic boundary condition is the effective property of that composite. Jiang et al. [23, 24, 25] describe the effects of boundary conditions, mismatch between constituent properties (modulus ratio or conductivity ratio) and window size (or scale) on apparent properties of 2D periodic composites with circular inclusions, for elastic, elasto-plastic and thermal properties. They concluded that apparent properties under mixed and periodic boundary conditions are equal. For elastic, elasto-plastic and thermal cases, they have shown that the effective properties obtained under periodic boundary condition are bounded above by that obtained under essential boundary condition and below by that obtained under natural boundary condition. The distance between bounds can be increased by increasing the mismatch between phases or by decreasing the window size. For soft inclusion case, the effective properties were closer to that of the upper bound (essential boundary condition) whereas for stiff inclusion case, the value was closer to that of the lower bound (natural boundary condition).

Kim et al. [26] have developed a boundary element method for determining the effective conductivity of a composite material. The method can be used for both periodic and random distribution of particles for arbitrary shapes. They demonstrate the method by determining the effective conductivities of Simple cubic, Face-centered cubic & Body-centered cubic arrays of spheroids and cubes for different volume fractions. In this method, even without knowing the temperature field beforehand, one can determine effective conductivity.

Hasselman [27] determined the effect of cracks on the thermal conductivity of the composite. Cracks formed in the composite lead to reduced strength and stiffness of

the composite. Cracked particles can be treated as voids, as their load transfer capacity will be negligible. The effect of cracks on thermal conductivity of the composite depends on the orientation of the cracks to the direction of heat flow. Thermal conductivity of the composite decreases drastically, if all the cracks developed are perpendicular to the direction of heat flow. However there will be no effect on thermal conductivity if all the cracks are parallel to the direction of heat flow. For any other arrangement of these cracks, thermal conductivity value lies between these two cases.

1.3 Research objectives

Determination of effective thermo-elastic properties and predicting the overall behavior of composites has been a long standing subject of study. Studies on effective mechanical properties of composites have been extensively done, while prediction of effective thermal properties has received less attention. Furthermore, coupled transient analyses of heat conduction and deformation at the composite microstructures are rarely done. Different thermal and mechanical properties in the constituents of composites often lead to significant mismatches in the stress/strain at the interphases between the inclusion and matrix constituents. These mismatches potentially cause debonding at the interlayers, reducing lifetime of the composites. The goals of this study are to determine the effective thermo-elastic properties of particle reinforced composites and to analyze the effect of different microscopic parameters on the overall behavior of these composites under different thermal and mechanical stimuli. This study considers a composite system made of linear elastic spherical particles and nonlinear elastic matrix. The thermal conductivities of both particle and matrix are assumed to degrade with

temperature field. The elastic moduli of the constituents are stress and temperature dependent.

CHAPTER II presents the micromechanical model for determining effective thermal conductivity of homogenized composites. The effective thermal properties determined with the help of micromechanical model are validated against analytical methods available in literature. To verify the accuracy of the micromechanical model, performance of the homogenized composites is compared with the ones of heterogeneous (detailed microstructure) composites. For this purpose, two FE meshes are generated. The first FE mesh uses the micromechanical model to predict effective properties and the second FE mimics the detailed microstructure of the composite. The responses of both FE models with particle volume contents 12.5, 25 and 50% are compared for different thermal stimuli. A parametric study is conducted on volume fraction of particles, conductivity ratio and degree of nonlinearity to determine the influence of these parameters on steady state time and temperature fields during transient heat conduction.

CHAPTER III presents the micromechanical relations to determine the effective thermo-mechanical properties. The FE meshes generated in CHAPTER II, one for determining effective properties using the micromechanical model and the other for representing the detailed microstructure of the composite, are used to analyze responses of composites subjected to coupled heat conduction and thermo-elastic deformation. The temperature profiles determined in CHAPTER II are used as prescribed conditions along with the mechanical boundary conditions. The effective thermo-elastic properties are

also validated against analytical methods available in literature. Parametric studies are to be conducted to determine the effects of CTE ratio of particle and matrix, volume fraction and temperature changes on the magnitude of discontinuity in stress and strain at the particle matrix interphase, which is vital for quantifying the debonding of the composite. For this purpose, FE model with detailed composite microstructures are used.

CHAPTER IV presents the application of micromechanical model to determine effective thermo-mechanical responses of composite structures, such as thermal barrier coatings (TBC). Developing a detailed microstructural model to determine the responses at the micro and macro scales is highly complicated and requires extensive computational time. The simplified micromechanical model is used to determine effective properties of homogenized composites. The example considered here consists of a rectangular laminate structure having metal substrate bonded to functionally graded plates, with varying particle concentration through the thickness of the layers. Both mechanical and thermal stimuli are applied on this composite structure and the behavior of the structure at macro scale is obtained.

CHAPTER V presents the conclusion and future scope of the project.

CHAPTER II

HEAT CONDUCTION IN PARTICLE REINFORCED COMPOSITES

"Heat is a form of energy that flows from a body at high temperature to a body at low temperature". Temperature gradient is the driving potential for the heat to flow. According to Rajput [28], the molecules of a substance are made up of one or more atoms which will be constantly translating, rotating and vibrating with respect to each other, resulting in kinetic energy. Kinetic energy of a substance increases with increasing temperature, which increases the agitation of the molecule to pass this energy to a neighboring molecule with lesser kinetic energy. There are three modes of heat transfer mechanisms and practical problems often involve a combination of these three modes.

Conduction is a transfer of heat between two regions of the same substance or between two different substances that are in physical contact. It occurs only between matters of same phases, i.e. between solids or liquids or gases. Conduction is greater in solids as the molecules or atoms are closely packed. As the spacing between molecules increases, there are lesser chances of collision between molecules such as in liquids and gases. Thus, liquids and gases have lower conductance compared to solids. Convection is a mode of heat transfer in which heat is transferred by virtue of motion of fluids. It occurs when a fluid flows over a surface of solid or another liquid and energy (heat) transfer takes place either from fluid to the surface or from surface to the fluid. The heat flow does not depend on material properties of the surface but it depends on the fluid properties and the surface shape over which fluid is flowing. Heat transmitted as

electromagnetic waves is called radiation. It requires no medium for propagation and can even travel through vacuum. During radiation, heat travels at the same speed as the light waves and exhibit reflection, diffraction and interference.

This chapter discusses a micromechanical model developed by Khan et al. [29] for determining effective thermal conductivities of particle reinforced composites. The responses from the micromechanical model represent homogenized composite media. These responses are compared with the ones obtained from particles dispersed in homogeneous matrix that represent heterogeneous composite microstructures. For this purpose, two sets of FE meshes are generated for composites at different particle volume contents i.e., 12.5%, 25%, and 50%. The first FE represents a homogeneous composite panel, which is used along with the micromechanical model to determine the effective thermal conductivity of the composite. Whereas the second FE mesh, mimics a more realistic composite microstructure with particles randomly distributed in matrix. For both cases an ABAQUS user material subroutine UMATHT is used to input the variation of thermal conductivity with temperature. A parametric study is conducted to determine the influence of different conductivity ratios of particle and matrix, volume fraction of particles in matrix and degree of nonlinearity in thermal conductivity on the temperature distribution and steady state times.

2.1 Analytical and numerical solutions of heat conduction in homogeneous media

According to Fourier's law, "the rate of heat flow through a homogeneous solid is directly proportional to the area of the section at right angles to the direction of heat flow, and to the gradient of temperature with respect to length of path of flow." It is

applicable to all solids, liquids and gases. Rate of heat transfer is given by, $Q = -KA\frac{dT}{dx}$; where K is the thermal conductivity of the solid, A is the cross-sectional area of the solid and dT is the temperature difference between two ends which are at a distance dx. The thermal conductivities of materials depend on the material molecular structure, temperature, moisture content, density of material, etc. For most metals, except Aluminum and Uranium, thermal conductivity decreases linearly with increase in temperature. For liquids, thermal conductivity decreases with increase in temperature whereas for gases it increases with increase in temperature. Thermal conductivity for porous materials depends on type of liquid or gas present in voids.

The rate of change of heat stored in a system is equal to the sum of net heat conducted into the system and the internal heat generated by the system. This results in the following Fourier's equation:

$$\frac{\partial}{\partial x}(KA\frac{\partial T}{\partial x}) + \frac{\partial}{\partial y}(KA\frac{\partial T}{\partial y}) + \frac{\partial}{\partial z}(KA\frac{\partial T}{\partial z}) + Ag = \rho Ac\frac{\partial T}{\partial t} \tag{2.1}$$

when the thermal conductivity of material is assumed constant, Eq. (2.1) becomes:

$$K\left[\frac{\partial^2 T}{\partial x^2} + \frac{\partial^2 T}{\partial y^2} + \frac{\partial^2 T}{\partial z^2}\right] + g = \rho c\frac{\partial T}{\partial t}$$

$$\frac{\partial^2 T}{\partial x^2} + \frac{\partial^2 T}{\partial y^2} + \frac{\partial^2 T}{\partial z^2} + \frac{g}{K} = \frac{\rho c}{K}\frac{\partial T}{\partial t} \tag{2.2}$$

$$\frac{\partial^2 T}{\partial x^2} + \frac{\partial^2 T}{\partial y^2} + \frac{\partial^2 T}{\partial z^2} + \frac{g}{K} = \frac{1}{\alpha}\frac{\partial T}{\partial t} \qquad (\text{where, } \alpha = \frac{K}{\rho c})$$

where ρc is the thermal capacity; and α is the thermal diffusivity of the material. If internal source of heat generation is absent then $g = 0$ and Eq. (2.2) reduces to:

$$\Rightarrow \frac{\partial^2 T}{\partial x^2} + \frac{\partial^2 T}{\partial y^2} + \frac{\partial^2 T}{\partial z^2} = \frac{1}{\alpha}\frac{\partial T}{\partial t} \tag{2.3}$$

Analytical solution for a heat conduction problem that involves simple geometry or when the material properties are constant can be easily obtained. For more complex structures and nonlinear material properties, numerical methods such as Finite difference and Finite element (FE) methods are often used to obtain the solution. In this study, the FE method is used.

Consider a solid at temperature T which is surrounded by a fluid medium at temperature T_∞ and having a heat transfer coefficient h (W/m^2K). The solid is generating internal energy at the rate of g (W/m^3). Consider one dimensional heat transfer. The energy equation is given as:

$$\underbrace{KA\frac{\partial^2 T}{\partial x^2}}_{\text{Conduction}} - \underbrace{Ph(T - T_\infty)}_{\text{Convection}} + \underbrace{Ag}_{\text{Heat generated}} = \underbrace{\rho Ac\frac{\partial T}{\partial t}}_{\text{Rate of energy stored}} \tag{2.4}$$

$$KA\frac{\partial^2 T}{\partial x^2} - PhT + PhT_\infty + Ag = \rho Ac\frac{\partial T}{\partial t} \tag{2.5}$$

$$\rho Ac\frac{\partial T}{\partial t} - \frac{\partial}{\partial x}[KA\frac{\partial T}{\partial x}] + PhT = Ag + PhT_\infty \tag{2.6}$$

We assume a solution of the form $T(x,t) = \sum_{j=1}^{n} T_j(t)\psi_j(x)$, where the temperatures $T(x,t)$ represent the spatial approximation of T for any time 't' and 'n' indicates the number of nodes in a finite element. Here we have divided the problem into element in space and element in time. This is called decoupled formulation. A weak form for the space part can now be obtained. It is noted that weak form can be written only for

element in space but not for element in time. Consider an element $\Omega = x_a, x_b$ as shown in Fig. 2.1.

Fig. 2.1. Axial element

Weak form is obtained using weighted residual method which states that the weighted integral over the element $\Omega = x_a, x_b$ is zero. If w is the weight function then

$$0 = \int_{x_a}^{x_b} w\left[\rho Ac\frac{\partial T}{\partial t} - \frac{\partial}{\partial x}\left(KA\frac{\partial T}{\partial x}\right) + PhT - Ag - PhT_\infty\right]dx$$

$$= \int_{x_a}^{x_b}\left[\rho Acw\frac{\partial T}{\partial t} + \left(KA\frac{\partial w}{\partial x}\frac{\partial T}{\partial x}\right) + PhwT - wAg - wPhT_\infty\right]dx$$

$$-w(x_a)Q_1 - w\ x_b\ Q_2 \tag{2.7}$$

$$\text{where, } Q_1(t) = -\left[KA\frac{dT}{dx}\right]_{x=x_a};\ Q_2(t) = \left[KA\frac{dT}{dx}\right]_{x=x_b} \tag{2.8}$$

Though Q_1 and Q_2 are evaluated at $x = x_a$ and $x = x_b$ from Eq. (2.8), they are not constants yet as they still are dependent on time.

Substituting $T(x,t) = \sum_{j=1}^{n} T_j(t)\psi_j(x)$ and $w = \psi_i(x)$ into Eq. (2.7), gives

$$\sum_{j=1}^{n} K_{ij}^{\ e} T_j^e + \sum_{j=1}^{n} M_{ij}^{\ e}\frac{\partial T_j^e}{\partial t} = F_i^e + Q_i^e$$

$$\left[K^e\right]\left[T^e\right] + \left[M^e\right]\left[\dot{T}^e\right] = \left[F^e\right] + \left[Q^e\right] \tag{2.9}$$

$$\text{where, } K^e_{ij} = \int_{x_a}^{x_b} \left(KA \frac{d\psi_i}{dx} \frac{d\psi_j}{dx} + Ph\,\psi_i \psi_j \right) dx$$

$$M^e_{ij} = \int_{x_a}^{x_b} \rho Ac\,\psi_i \psi_j dx$$

$$F^e_i = \int_{x_a}^{x_b} (Ag\,\psi_i + Ph\,\psi_i T_\infty) dx$$

$$Q_1(t) = -\left[KA \frac{dT}{dx} \right]_{x=x_a} ; Q_2(t) = \left[KA \frac{dT}{dx} \right]_{x=x_b}$$

Eq. (2.9) is called Semi-discrete FE model. To solve differential equation in time domain, Forward Difference method or Newmark's method can be used. Detailed formulation can be found in Reddy [30]. The solution obtained by FE method is an approximate one. It depends on the chosen mesh size, time increment, and chosen tolerance. Thus it is necessary to validate its responses. In this study, the temperature profiles during transient heat conduction in a homogeneous medium obtained using FE analyses will be compared to the analytical solution.

Consider a square plate as shown in Fig. 2.2 of length 'L=4', and it is initially at a temperature of T_i =303. The plate is subjected to the following prescribed boundary conditions:

$$\begin{aligned} T(x, y, 0) &= T_i = 303 \\ T(4, y, t) &= T_L = 803 \\ \frac{\partial T(0, y, t)}{\partial x} &= 0 \end{aligned} \qquad (2.10)$$

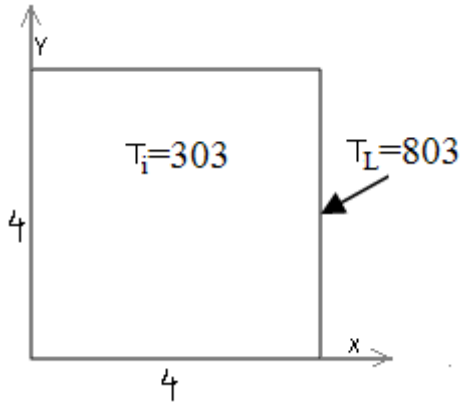

Fig. 2.2 Square plate

The transient behavior of the plate until it reaches steady state temperature can be observed by calculating the temperature distribution as a function of location(x,y) and time (t). The thermal conductivity and thermal diffusivity of the plate are taken as 1.3 W/mk and 0.622 m^2/s. Both analytical and numerical models are developed to solve heat conduction in the above plate. The temperature distribution is plotted at selective times until the plate reaches steady state. Fig. 2.3 shows the comparison of the temperature distribution from the analytical and numerical model.

Analytical Solution

This is a 1D problem i.e., heat is conducted along x-direction and from Fourier's law of heat conduction the governing equation of this problem is given by:

$$\frac{\partial T(x,t)}{\partial t} = \alpha \frac{\partial^2 T(x,t)}{\partial t^2} \tag{2.11}$$

The procedure described by White [31], has been used to obtain the temperature distribution in the rectangular plate. Let us assume a solution of the following form

$$T(x,t) = R(x,t) + S(x) \tag{2.12}$$

Substituting (2.12) in (2.11) gives:

$$\frac{\partial R(x,t)}{\partial t} + \cancelto{0}{\frac{\partial S(x)}{\partial t}} = \alpha \frac{\partial^2 R(x,t)}{\partial x^2} + \alpha \frac{\partial^2 S(x)}{\partial x^2}$$

$$\Rightarrow \frac{\partial R(x,t)}{\partial t} = \alpha \frac{\partial^2 R(x,t)}{\partial x^2} + \alpha \frac{\partial^2 S(x)}{\partial x^2} \tag{2.13}$$

Eq. (2.13) can be split into transient problem: $\frac{\partial R(x,t)}{\partial t} = \alpha \frac{\partial^2 R(x,t)}{\partial x^2}$ & steady state problem: $0 = \frac{\partial^2 S(x)}{\partial x^2}$

Using the boundary condition in Eq. (2.10), the steady state solution is $S(x) = 803$

The transient Solution is assumed as: $R(x,t) = F(x).G(t)$ (2.14)

Substituting Eq. (2.14) in the governing equation, we get:

$$G(t) = c.e^{-\alpha\lambda^2 t} \text{ and } F(x) = c_1 \sin\lambda x + c_2 \cos\lambda x;\ \text{where } \lambda \text{ is a constant} \tag{2.15}$$

Applying boundary conditions to Eq. (2.15), the following solutions are obtained:

$$c_1 = 0;\ \lambda_n = \left[(2n-1)\frac{\pi}{2L}\right]$$

$$\Rightarrow F_n(x) = c_2 \cos\lambda_n x = c_2 \cos\left[(2n-1)\frac{\pi}{2L}\right] \qquad (n = 1,2,3,....)$$

$$\Rightarrow T(x,t) = \sum_{n=1}^{\infty} c_n \cos(\lambda_n x) e^{-\alpha\lambda_n^2 t} + 803 \tag{2.16}$$

$$\text{where } \lambda_n = \left[(2n-1)\frac{\pi}{2L}\right];\ c_n = 2000.\frac{[-1^n]}{(2n-1).\pi};\ L = 4;\ \alpha = 0.622 \tag{2.17}$$

The analytical results were compared with the numerical results at different times and at different locations as shown in the following diagram.

Numerical Solution

A FE mesh of a square plate of dimensions 4x4 is generated with Continuum Plane stress elements (CPS4). The material properties used are k=1.37w/mk; density=2.58e-06 kg/m^3 and specific heat=810000 J/Kg^{o}K. Boundary and initial conditions as given in Eq. (2.10) are used. Transient heat transfer analysis is conducted until the plate reaches a steady state temperature.

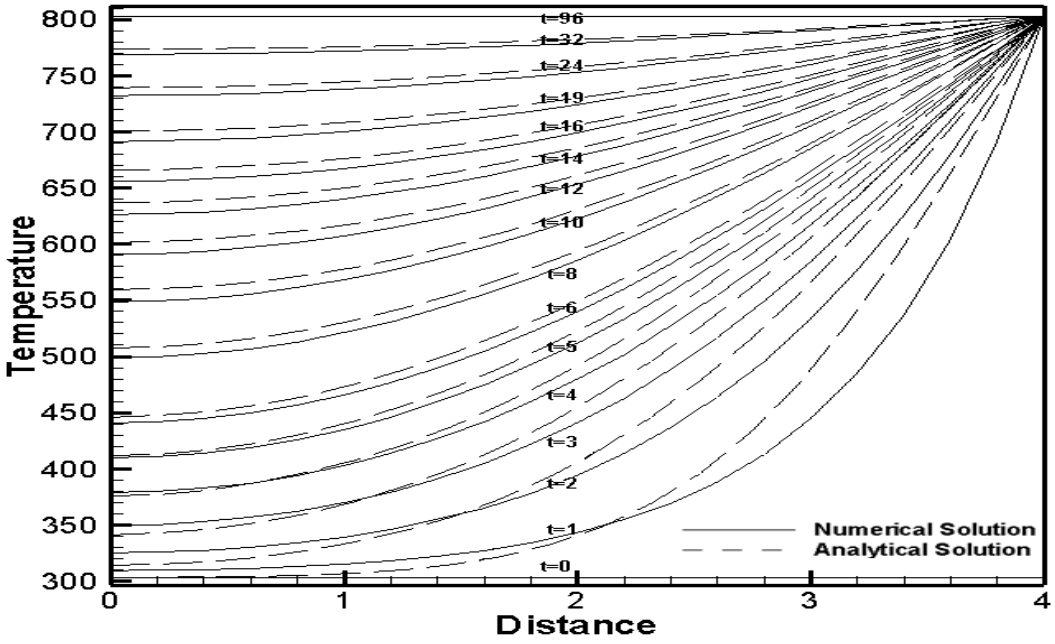

Fig. 2.3. Temperature distribution for 20 elements per edge of the square plate

Convergence Studies

(a) Effect of Refining the Mesh

Fig. 2.3 shows the temperature distribution for 20 elements per edge (seeds) of the square plate. As the accuracy of the FE method depends on how fine the mesh is, a study has been conducted by increasing the number of elements per edge or in other words decreasing the element size in the mesh. Figs. 2.4 and 2.5 shows 30 and 80 elements per edge of the square plate.

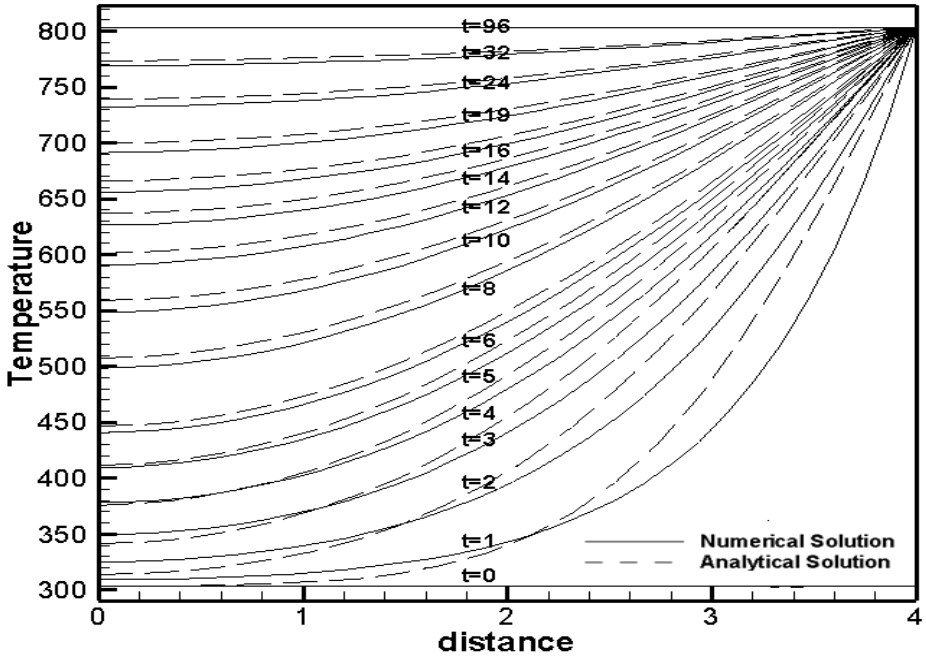

Fig. 2.4. Temperature distribution for 30 elements per edge of the square plate

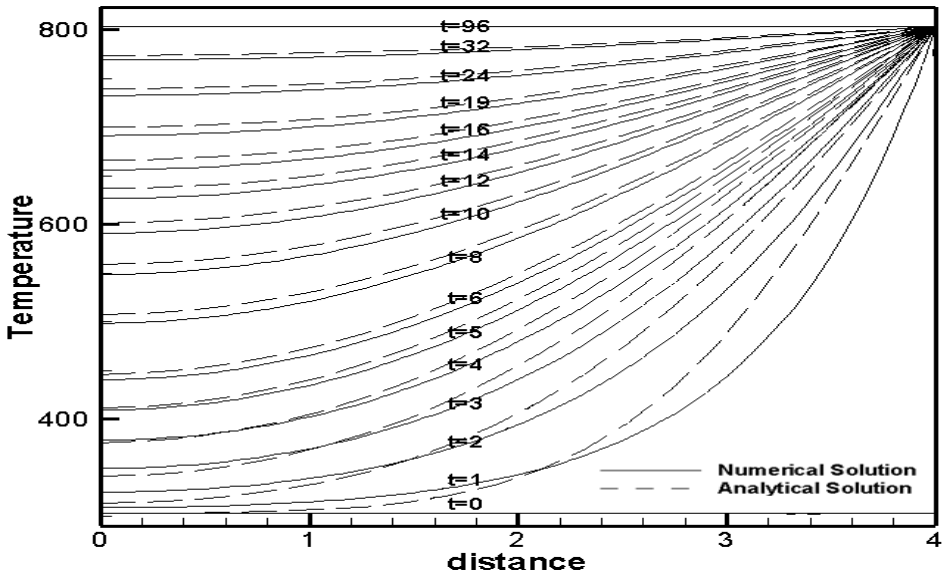

Fig. 2.5. Temperature distribution for 80 elements per edge of the square plate

The difference between numerical solution and the analytical solution was less in Fig. 2.4 than that in Fig. 2.3; and the difference is not so significant between Fig. 2.3 and 2.4. Hence for our case, 30 elements per edge (seeds) gives good enough result and any further increase in refining the mesh would require more computational time and effort but would not yield significant difference in the results.

(b) Effect of Initial Time Increment

The effect of initial increment time on steady state time has been studied for a mesh of 30 seeds (element size of 0.1333x0.1333) and a tolerance of 1e-2 to reach steady state. Table 2.1 shows the influence of initial time increment on the time taken to reach steady state. For an initial time increment of 15 sec, the steady state has been reached in 150 seconds whereas for an initial time increment of 5 second the steady state

has been reached in 115 seconds. A difference of approximately 23% has been observed in steady state times. Whereas for initial increments of 0.05 and 0.01, steady state time was attained in 90.9 seconds. This means that convergence has been achieved in terms of steady state times, at 0.05 seconds. Hence the minimum initial increment of 0.05 has to be used and anything less than this would result in unnecessary computational effort and time when speaking in terms of steady state times.

Table 2.1. Influence of initial time increment on steady state time

Initial Time	Steady state time taken
15	150
5	115
1	96
0.1	91.4
0.05	90.9
0.01	90.9

(c) Effect of Tolerance

The effect of tolerance on steady state time and temperature has been studied for a mesh of 30 seeds (element size of 0.1333x0.1333) and an initial increment of 1 second. From Table 2.2 it can be seen that for a tolerance of 1e-3, the temperature at the far end is within 1% of the temperature of the source (803), however the computational time involved in this was high. Whereas a tolerance of 1e-2 reduces this problem by allowing

the temperature at the far end to be within 10% of source's temperature. Hence it can be concluded that tolerance of 1e-2 is a good choice for this problem.

Table 2.2. Influence of tolerance on steady state time & temperature at farthest end

Tolerance	Steady state time	Temperature at the farthest distance
5	28	754.011
1	45	792.674
1e-1	71	802.045
1e-2	96	802.903
1e-3	121	802.99

2.2 Heat conduction in composites

No single material has all the desired and required properties for a particular application. Hence two or more materials are often engineered or intelligently combined to achieve specific properties for a particular application. Composites are usually made up of two constituents viz., matrix (continuous medium) and reinforcement (discontinuous medium). Reinforcements are made up of particles or fibers or sheets belonging to the same material or different material, which are dispersed in matrix constituents. Matrix acts as medium by which externally applied loads are transmitted to

the reinforcements. The matrix not only keeps the reinforcement in a set place, but also prevents catastrophic failure due to reinforcement breakage. Typically, materials for reinforcing constituent and matrix constituent are chosen in such a way that matrix material imparts ductility and toughness to the composite whereas the reinforcing material imparts stiffness and hardness to the composite. By varying the arrangement of reinforcement in the matrix, its volume fraction in the composite and material for reinforcement and matrix, the desired strength and the thermo-mechanical properties of the composite can be achieved.

This study focuses on composites having solid spherical particles. As the particle and matrix constituents have different material properties, analyzing heat conduction in this type of composites becomes more complicated. It is almost impossible to obtain closed form solution of temperature profile in the composite microstructures during heat conduction, especially when particles are randomly distributed in the matrix. One can only obtain solution for simple or a simplified composite system like one-dimensional heat transfer in a multi-layered composite. In addition to measuring temperature profiles in the composite system, it is desired to quantify effective thermal conductivity of composite systems.

Rule of mixtures has been widely used to determine the bounds for the effective thermal conductivity of the composites. According to the rule of mixtures, the upper and lower bounds are determined by two types of composite arrangements. The first one assumes that heat is transferred through the thickness (perpendicular direction) as shown in Fig. 2.6 and the second one assumes that heat is transferred in parallel direction as

shown in Fig. 2.7. The effective thermal conductivity obtained in both approaches is discussed as follows:

Case (1)

Consider the composite system made of materials A and B (shown in Fig. 2.6) If there is no temperature drop at the interface (i.e., if there is perfect contact between the two materials), then the amount of heat flowing in the two layers is equal which is given in the following equation:

$$Q = \frac{K_A A(T_1 - T_2)}{L_A} \Rightarrow (T_1 - T_2) = \frac{QL_A}{K_A A} \tag{2.18}$$

$$Q = \frac{K_B A(T_2 - T_3)}{L_B} \Rightarrow (T_2 - T_3) = \frac{QL_B}{K_B A} \tag{2.19}$$

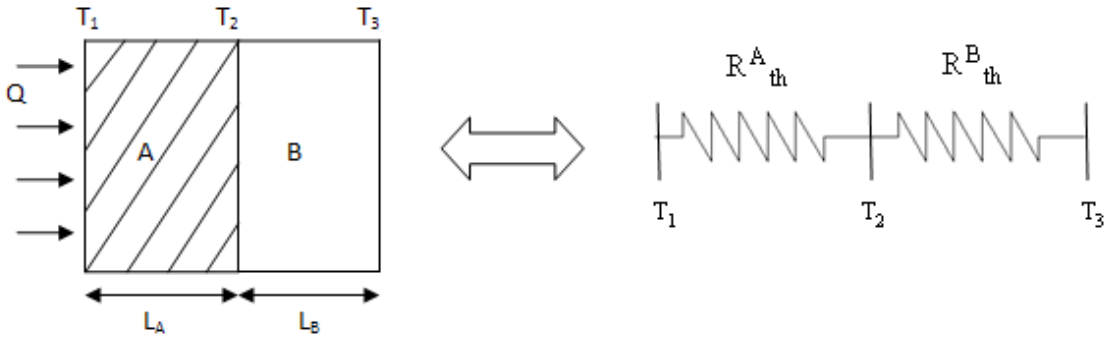

Fig. 2.6. Heat conduction in composite slab perpendicular to the direction of flow

$$T_1 \geq T_2 \geq T_3 \; ; \qquad R^A{}_{th} = \frac{L_A}{AK_A}; \qquad R^B{}_{th} = \frac{L_B}{AK_B}; \quad R^{eq}{}_{th} = R^A{}_{th} + R^B{}_{th}$$

where R_{th} is the thermal conduction resistance. Combining both (2.18) and (2.19), gives:

$$T_1 - T_3 = Q\left[\frac{L_A}{AK_A} + \frac{L_B}{AK_B}\right]$$

$$\Rightarrow Q = \frac{(T_1 - T_{3)}}{\left[\frac{L_A}{AK_A} + \frac{L_B}{AK_B}\right]} \tag{2.20}$$

but, $$Q = \frac{(T_1 - T_{3)}}{\left[\frac{L}{AK_{eq}}\right]} \tag{2.21}$$

where, $L = L_A + L_B$ and K_{eq} is the effective thermal conductivity for the composite.

By comparing (2.20) and (2.21), we get the equivalent thermal conductivity for the composite as $$K_{eq} = \frac{K_A K_B L}{K_A L_B + K_B L_A} \tag{2.22}$$

And the heat flux is obtained as $$Q = \frac{T_1 - T_3}{\left[\frac{L_A}{AK_A} + \frac{L_B}{AK_B}\right]} = \frac{T_1 - T_3}{\left[\frac{L}{AK_{eq}}\right]}$$

Case (2)

Consider the composite system made of materials A and B as shown in Fig. 2.7. For this case the temperature gradient for both the layers should be equal; however the heat flow is different for both the cases.

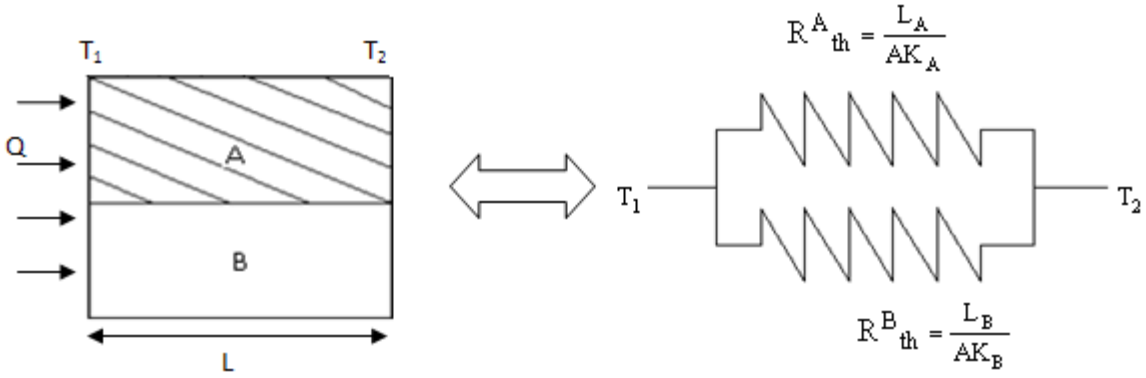

Fig. 2.7. Heat conduction in composite slab parallel to the direction of flow

The total heat flowing in the composite is equal to the sum of heats flowing in individual layers, which is:

$$Q = Q_A + Q_B$$

$$\frac{T_1 - T_2}{R^{eq}_{th}} = \frac{T_1 - T_2}{R^{A}_{th}} + \frac{T_1 - T_2}{R^{B}_{th}}$$

$$\frac{1}{R^{eq}_{th}} = \frac{1}{R^{A}_{th}} + \frac{1}{R^{B}_{th}} \qquad \left(\text{where } R^{eq}_{th} = \frac{L}{AK_{eq}} \right)$$

$$K_{eq} = \frac{(K_A L_B + K_B L_A)L}{L_B L_A} \qquad \text{where } L = L_A = L_B$$

$$\Rightarrow \text{Effective Thermal Conductivity, } \quad K_{eq} = K_A + K_B \tag{2.23}$$

And the heat flux is obtained as $Q = \dfrac{T_1 - T_2}{\left[\dfrac{L}{AK_{eq}}\right]}$

From Eqs. (2.22)-(2.23), we can clearly see that thermal conductivity depends on the arrangement of layers and the direction of heat flow and the properties of each constituent.

Cases (1) and (2) present heat conduction in simple composite media consisting of two layered constituents. In most composite systems, the effective thermal conductivity is not as simple as the above cases. It is necessary to understand different heterogeneities in composites and their influence on the thermal behaviors:

1. **Effect of inclusions:** In general, as the size of the particles increases, the thermal conductivity increases as noted by Geiger et al. [32]. However, for larger particles, there is more chance of particle cracking and load carrying capacity of these cracked particles decreases to zero and can be effectively treated as voids as discussed by Chawla et al. [33]. Different particle shapes have different effects on the overall response of the composite.
2. **Effect of voids:** The transport properties of void are very negligible compared to that of solid or liquid. Thermal conductivity for porous materials depends on type of liquid or gas present in voids. Conductivity of the composite decreases with increase in porosity**.**
3. **Effect of moisture and temperature:** Conductivity increases with increase in moisture content (amount of water absorbed) in the composite. Thermal conductivity of most materials decrease with increasing temperature. Specific heat also increases with increase in moisture content (as water has good specific heat) for most materials, as shown experimentally by Santos [34].
4. **Effect of cracks:** Cracks formed in the composite lead to reduced strength and stiffness of the composite. Cracked particles can be treated as voids, as their load transfer capacity will be negligible. Hasselman [27] studied the effect of cracks on

thermal conductivity of the composite and found that it depends on the orientation of the cracks to the direction of heat flow. Thermal conductivity of the composite decreases drastically, if all the cracks developed are perpendicular to the direction of heat flow. However there will be no effect on thermal conductivity if all the cracks are parallel to the direction of heat flow. For any other arrangement of these cracks, thermal conductivity value lies between these two cases.

It is very complicated to study the effects of all these heterogeneities mentioned above on the overall response of the composite. The present study considers perfectly solid spherical particles bonded to matrix system and randomly distributed. It is assumed that the composite is free of pores, moisture and cracks. The overall thermal behaviors depend on the temperatures. Micromechanical model is used to obtain effective thermal conductivity of composites. The results are compared with the responses of detailed microstructures of composite using FE analyses.

2.3 Effective thermal conductivity of particle reinforced composites

The micromechanical model formulated by Muliana et al. [18, 19] was used for the determination of effective thermal conductivity. Their model consisted of an RVE which is reduced to unit cell by virtue of symmetry, with four particle and matrix sub-cells. Each sub-cell is assumed to be homogeneous and sub-cell 1 is occupied entirely by Particle whereas sub cells 2, 3, 4 are occupied by Matrix, as shown in Fig. 2.8. The total volume of the unit cell is assumed to be unity. If length of the subcell1 is assumed to be b then the volume of all the sub cells are given as

$$V^{(1)} = b^3,\ V^{(2)} = b^2(1-b),\ V^{(3)} = b(1-b),\ V^{(4)} = (1-b) \qquad (2.24)$$

$$V = \sum_{\alpha=1}^{N} V^{(\alpha)} = 1$$, where number of sub cells, N=4

It is assumed that temperature gradient varies spatially in each sub-cell and volume averaging of properties was adopted to determine the effective thermal conductivity.

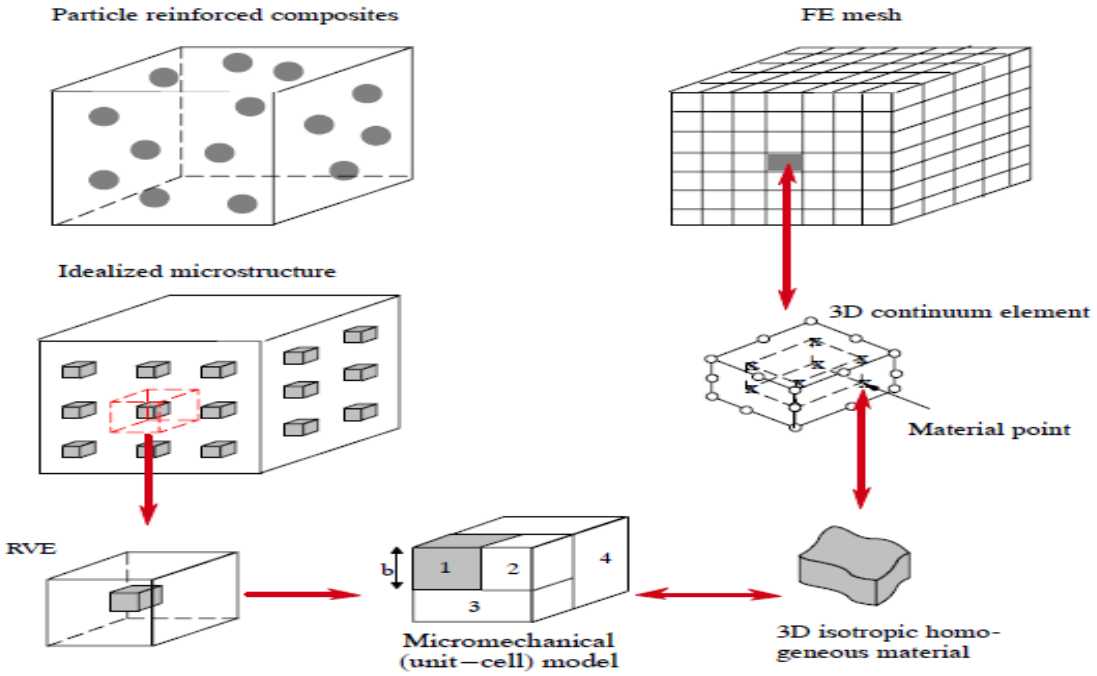

Fig. 2.8. Representative volume element and division of unit cell into sub cells

Volumetric average of a quantity is defined as the ratio of integral of that quantity over a region to the volume of that region. Average temperature gradient and heat flux are given as:

$$\bar{\varphi}_i = \frac{1}{V}\sum_{\alpha=1}^{N}\int_{V^{(\alpha)}} \varphi_i^{(\alpha)}(x_k^{(\alpha)})dV^{(\alpha)} \approx \frac{1}{V}\sum_{\alpha=1}^{N} V^{(\alpha)}\varphi_i^{(\alpha)} \tag{2.25}$$

$$\bar{q}_i = \frac{1}{V}\sum_{\alpha=1}^{N}\int_{V^{(\alpha)}} q_i^{(\alpha)}(x_k^{(\alpha)})dV^{(\alpha)} \approx \frac{1}{V}\sum_{\alpha=1}^{N} V^{(\alpha)}q_i^{(\alpha)} \tag{2.26}$$

The average heat flux and the average temperature gradient are related by Fourier's law of heat conduction, $\bar{q}_i^t = -\bar{K}_{ij}^t \bar{\varphi}_j^t$ (2.27)

It is noted that the thermal conductivities of particles and matrix are allowed to change with temperatures, resulting in nonlinear problems. To solve the heat conduction in the composite, numerical method and iterative solution are used.

The heat flux at current time is obtained by, $\bar{q}_i^t = \bar{q}_i^{t-\Delta t} + d\bar{q}_i^t$

Temperature gradient at current time is obtained by $\bar{T}_i^t = \bar{T}_i^{t-\Delta t} + d\bar{T}_i^t$

where the incremental heat flux and temperature gradient are related as, $d\bar{q}_i^t = -\bar{K}_{ij}^t d\bar{\varphi}_j^t$

The micromechanical relations Khan et al. [29], Muliana [19] are derived by assuming continuity of temperatures and heat flux at the interphase, resulting in the following equations:

$$d\bar{\varphi}_i^t = \frac{1}{V^{(1)}+V^{(2)}}\left[v^{(1)}d\varphi_i^{(1),t} + v^{(2)}d\varphi_i^{(2),t}\right] = d\varphi_i^{(3),t} = d\varphi_i^{(4),t} \tag{2.28}$$

$$d\bar{q}_i^t = \frac{1}{V}\left[v^{(A)}dq_i^{(A),t} + v^{(3)}dq_i^{(3),t} + v^{(4)}dq_i^{(4),t}\right]; dq_i^{(A),t} = dq_i^{(1),t} = dq_i^{(2),t} \tag{2.29}$$

where $V^{(A)} = V^{(1)} + V^{(2)}$

Using micromechanical relations and constitutive relation in each sub-cell, effewtive thermal conductivity and responses of equivalent homogeneous fictitious material can be obtained. The advantages of homogenization method are: it allows predicting effective responses of composite by incorporating microstructural constituent information, it is possible to incorporate nonlinear (temperature) dependent properties of the constituents due to the external stimuli, and it is computationally efficient and accurate. The homogenization method is useful for material and structural design. The main drawback of such a homogenization scheme is that the discontinuity of stress and strain fields at the particle and matrix interface, which plays a vital role in the debonding of the composite, cannot be properly quantified.

2.4 Verification of the effective thermal conductivity

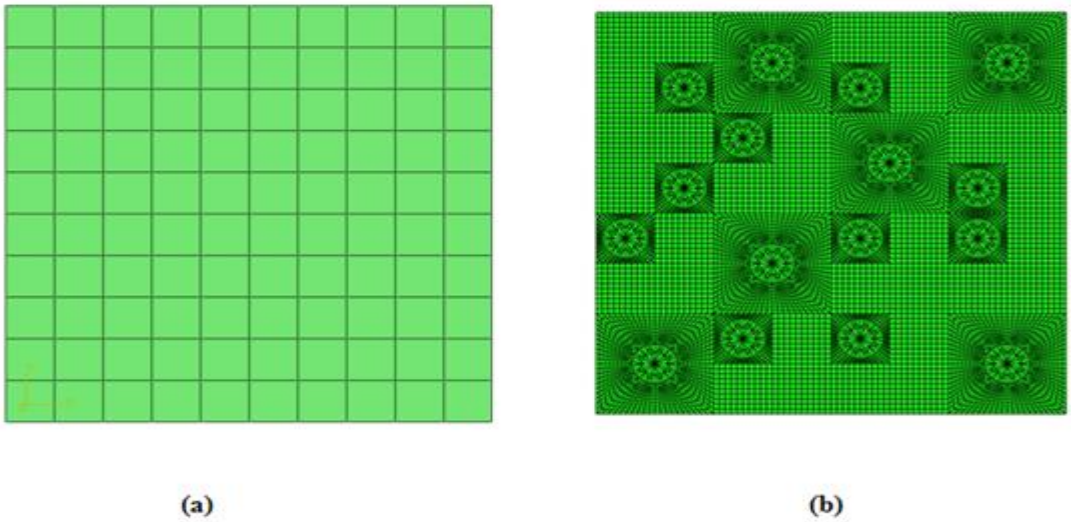

Fig. 2.9. FE meshes of effective and detailed model

A homogenized composite panel of 4µmx4µmx1µm as shown in Fig. 2.9(a) is developed. The length of each element in the mesh is 0.4µm. DC3D8 elements in ABAQUS are used to model the mesh. Different volume fractions are incorporated for the same geometry and mesh using a user subroutine. The inputs to the user subroutine are volume fraction and thermal conductivities for the particle and matrix which are temperature dependent. The effective conductivity assumes homogeneous media, thus it is necessary to compare the response with the ones of detailed composite microstructure. For that reason, a detailed FE model is developed with 4µmx4µm as shown in Fig. 2.9(b) and is made of fixed particle size, randomly distributed particles (glass) and matrix (epoxy). Fig. 2.9(b) shows the distribution of 12.5% volume fraction of particles distributed in the matrix randomly and similar models are developed for 25% and 50% volume fractions of particles. DC2D4 and DC2D3 (Continuum Plane Stress elements with 4 and 3 nodes) are the element types used to generate the mesh.

Transient thermal analysis is conducted on the detailed and effective model meshes, with temperature boundary condition at one of their ends and the temperature distribution throughout their lengths are noted. A parametric study is conducted by varying the volume fractions of particle in the matrix $V_f = 12.5\%, 25\%, 50\%$ and by varying the thermal conductivity ratio $(K_P / K_M = 6.84, 50, 200, 1000, 0.02)$ between particle and matrix for both the models. Thermal conductivities of the particles and matrix vary linearly with changes in temperatures, given as:

$$K_P = K_P{}^o + r^P (T - T_{ref}) \qquad (2.30)$$
$$K_M = K_M{}^o + r^M (T - T_{ref})$$

A parametric study is conducted by varying the r^P & r^M values for different conductivity ratios and volume fractions. Their steady state times and temperature distributions were compared.

Tables 2.3 to 2.7 compare the steady state times of effective and detailed models, for different conductivity ratios (K^o_P / K^o_M). The conductivity of the matrix is maintained at $K^o_M = 1.9 W/mK$ and the conductivity of particle is varied to obtain different ratios. Table 2.3 and 2.4 shows the steady state times for $K^o_P / K^o_M = 6.84 \& 50$. As the volume fraction is increased, the time taken to reach steady state has decreased. As the particle (higher conductivity constituent) concentration increases, the effective thermal conductivity of the composite increases and as a result it takes less time to reach steady state. It is also observed that as the degree of nonlinearity increases, time taken to reach steady state increases.

Table 2.5 and 2.6 shows the comparison of steady state times for effective and detailed model for conductivity ratios 200 and 1000. It can be observed there is no significant difference in the steady state times for Table 2.5 and Table 2.6 which is similar to the steady state time in Table 2.4. This behavior could be attributed to the fact that, the effective conductivity might have already reached a maximum value at the conductivity ratio of 200 (as proven later in the chapter) and by increasing the conductivity of the particle any further would not result in any significant difference in effective conductivity and thereby there would be no significant difference in steady state times. A more detailed discussion is given in the last part of CHAPTER II.

Table 2.3. Comparison of steady state times of effective & detailed model for K^o_P / K^o_M =6.84

	V_f	$K_P(T) = K^o_P + r^P(T-T_{ref})$ $K_M(T) = K^o_M + r^M(T-T_{ref})$	Steady state time	
			Effective Model	**Detailed FE model**
K^o_P / K^o_M =6.84 **K^o_P =13 w/mk,** **K^o_M= 1.9w/mk**	12.5	r^p= 0;r^M=0	34	34
		r^p= -0.05;r^M=-0.02	43	43
		r^p= -0.1;r^M=-0.04	64	64
		r^p= -0.15;r^M=-0.06	148	149
	25	r^p= 0;r^M=0	30	30
		r^p= -0.05;r^M=-0.02	38	38
		r^p= -0.1;r^M=-0.04	56	55
		r^p= -0.15;r^M=-0.06	131	130
	50	r^p= 0;r^M=0	23	24
		r^p= -0.05;r^M=-0.02	28	29
		r^p= -0.1;r^M=-0.04	39	40
		r^p= -0.15;r^M=-0.06	94	95

Table 2.4. Comparison of steady state times of effective & detailed model for K^{o}_{P}/K^{o}_{M} =50

	V_f	$K_P(T) = K^{o}_{P} + r^{P}(T-T_{ref})$ $K_M(T) = K^{o}_{M} + r^{M}(T-T_{ref})$	Steady state time	
			Effective Model	**Detailed FE model**
K^{o}_{P}/K^{o}_{M} =50 **K^{o}_{P} =95 w/mk,** **K^{o}_{M}= 1.9w/mk**	**12.5**	$r^{p}= 0; r^{M}=0$	33	33
		$r^{p}= -0.05; r^{M}=-0.02$	42	42
		$r^{p}= -0.1; r^{M}=-0.04$	63	63
		$r^{p}= -0.15; r^{M}=-0.06$	147	148
	25	$r^{p}= 0; r^{M}=0$	28	27
		$r^{p}= -0.05; r^{M}=-0.02$	35	35
		$r^{p}= -0.1; r^{M}=-0.04$	53	52
		$r^{p}= -0.15; r^{M}=-0.06$	129	128
	50	$r^{p}= 0; r^{M}=0$	18	19
		$r^{p}= -0.05; r^{M}=-0.02$	23	23
		$r^{p}= -0.1; r^{M}=-0.04$	34	34
		$r^{p}= -0.15; r^{M}=-0.06$	89	89

Table 2.5. Comparison of steady state times of effective & detailed model for K^{o}_{P}/K^{o}_{M} =200

	V_f	$K_P(T) = K^{o}_{P} + r^{P}(T-T_{ref})$ $K_M(T) = K^{o}_{M} + r^{M}(T-T_{ref})$	Steady state time	
			Effective Model	**Detailed FE model**
K^{o}_{P}/K^{o}_{M} =200 **K^{o}_{P}=380 w/mk** **K^{o}_{M}= 1.9w/mk**	**12.5**	$r^{p}= 0; r^{M}=0$	32	33
		$r^{p}= -0.05; r^{M}=-0.02$	42	42
		$r^{p}= -0.1; r^{M}=-0.04$	63	63
		$r^{p}= -0.15; r^{M}=-0.06$	147	147
	25	$r^{p}= 0; r^{M}=0$	27	27
		$r^{p}= -0.05; r^{M}=-0.02$	35	35
		$r^{p}= -0.1; r^{M}=-0.04$	53	52
		$r^{p}= -0.15; r^{M}=-0.06$	129	128
	50	$r^{p}= 0; r^{M}=0$	18	18
		$r^{p}= -0.05; r^{M}=-0.02$	23	22
		$r^{p}= -0.1; r^{M}=-0.04$	33	33
		$r^{p}= -0.15; r^{M}=-0.06$	89	88

Table 2.6. Comparison of steady state times of effective & detailed model for K^{o}_{P} /K^{o}_{M} =1000

	V_f	$K_P(T) = K^{o}_{P} + r^{P}(T-T_{ref})$ $K_M(T) = K^{o}_{M} + r^{M}(T-T_{ref})$	Steady state time	
			Effective	**Detailed**
K^{o}_{P} /K^{o}_{M}=1000 **K^{o}_{p}=1900w/mk** **K^{o}_{M}= 1.9w/mk**	**12.5**	r^{p}= 0;r^{M}=0	32	32
		r^{p}= -0.05;r^{M}=-0.02	42	42
		r^{p}= -0.1;r^{M}=-0.04	63	63
		r^{p}= -0.15;r^{M}=-0.06	147	147
	25	r^{p}= 0;r^{M}=0	27	27
		r^{p}= -0.05;r^{M}=-0.02	35	35
		r^{p}= -0.1;r^{M}=-0.04	52	52
		r^{p}= -0.15;r^{M}=-0.06	129	128
	50	r^{p}= 0;r^{M}=0	18	18
		r^{p}= -0.05;r^{M}=-0.02	22	22
		r^{p}= -0.1;r^{M}=-0.04	33	33
		r^{p}= -0.15;r^{M}=-0.06	89	88

Table 2.7 shows the steady state times for conductivity ratio 0.02 i.e., the conductivity of the matrix is taken to be more than that of the particle. As the

conductivity of the major constituent in the composite is more, the effective conductivity of the composite is going to be very high when compared to all other previous cases and hence the composite takes very less time to reach steady state.

Table 2.7. Comparison of steady state times of effective & detailed model for K^o_P / K^o_M =0.02

	V_f	$K_P(T) = K^o_P + r^P(T-T_{ref})$ $K_M(T) = K^o_M + r^M(T-T_{ref})$	Steady state time	
			Effective	**Detailed**
K^o_P / K^o_M=0.02 **K^o_P =1.9w/mk** **K^o_M = 95w/mk**	**12.5**	$r^p= 0; r^M=0$	5	5
		$r^p= -0.05; r^M=-0.02$	5	6
		$r^p= -0.1; r^M=-0.04$	5	5
		$r^p= -0.15; r^M=-0.06$	5	5
	25	$r^p= 0; r^M=0$	6	6
		$r^p= -0.05; r^M=-0.02$	6	6
		$r^p= -0.1; r^M=-0.04$	6	6
		$r^p= -0.15; r^M=-0.06$	6	6
	50	$r^p= 0; r^M=0$	7	8
		$r^p= -0.05; r^M=-0.02$	7	8
		$r^p= -0.1; r^M=-0.04$	7	8
		$r^p= -0.15; r^M=-0.06$	7	9

From the above studies, it is observed that:

1) At constant volume fraction, as the nonlinearity in thermal conductivity of the particle and matrix constituents increases, the steady state time significantly deviates from the ones with constant constituent properties.
2) As the volume fraction of particles in the composite increases, the steady state is reached in less time, since the thermal conductivity of particles are taken larger than that of the matrix.
3) As the conductivity ratio increases and for volume content of particle constant, the effective thermal conductivity reaches an asymptotic value.

The temperature distribution during transient heat transfer analysis is also monitored. Fig. 2.10 shows the contour plots of temperature distribution for effective and detailed model for 12.5% volume fraction of particles in the composite having conductivity ratio 6.84. A good agreement is observed between the models for different magnitudes of nonlinearity.

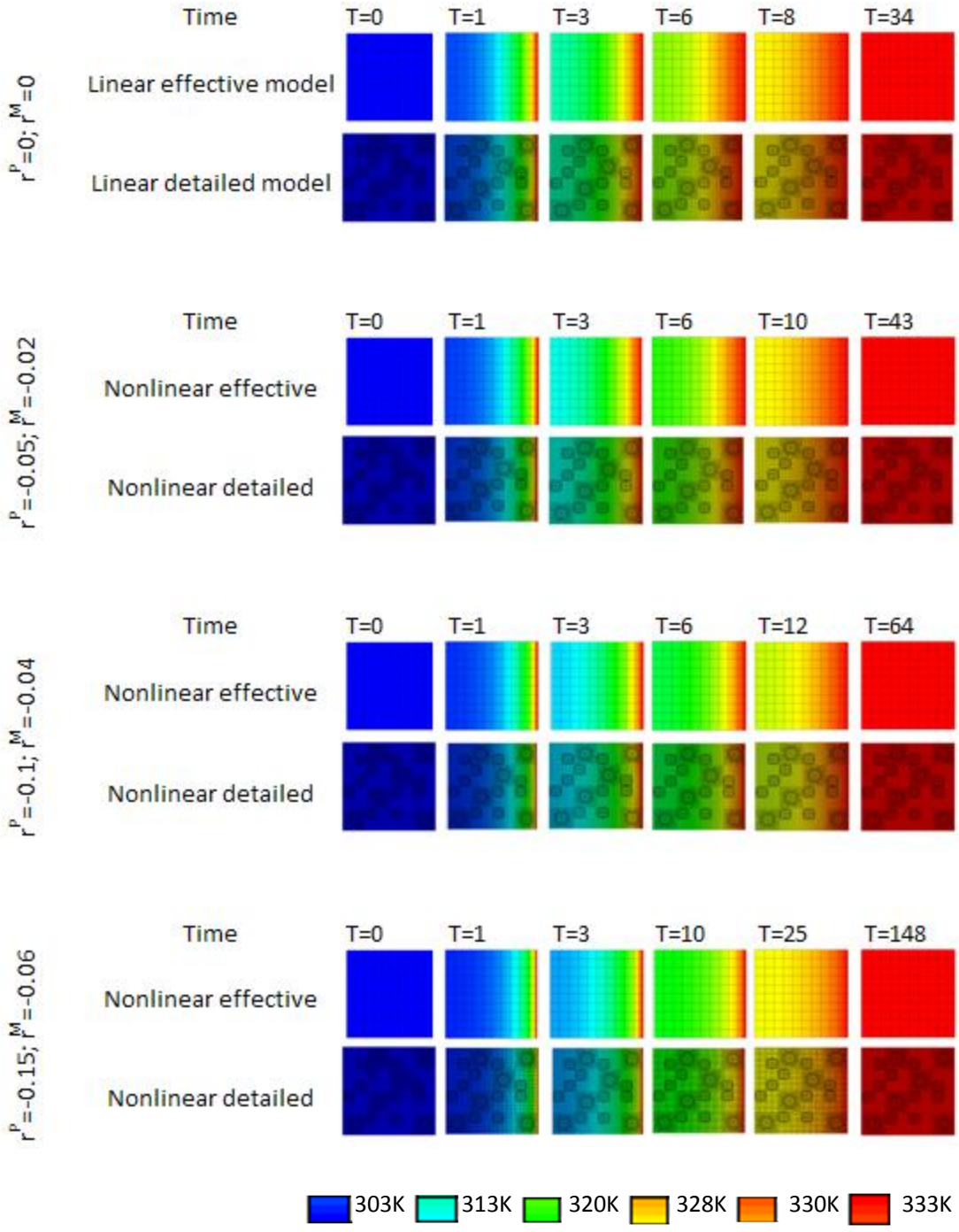

Fig. 2.10. Contour plots of temperature distribution for effective and detailed model for $K^{o}_{P}/K^{o}_{M}=6.84$; $V_f=12.5$ %

Figs. 2.11 to 2.22 show the temperature profiles for the homogenized composite and detailed microstructural composite at different times until the composite reaches steady state. For lower volume fractions (12.5 and 25%), the temperature profiles of both the models are in good agreement with each other. But for higher volume fractions (50%), deviation has been observed between the models. The detailed model showed a wavy profile for temperature but the effective model showed no signs of it. The cause for this could be attributed to two reasons:

- At higher volume fractions, there is a chance that particle-particle interactions could contribute to the effective conductivity and thereby to the temperature distribution. This could be the reason for the wavy behavior in detailed model. As these interactions are not possible in effective model, it has not shown any change in its temperature profile.
- The mesh used to represent the detailed model might not be fine enough to produce temperature profile identical to that of the effective model.

Case (1) K^o_P / K^o_M=6.84(K^o_P=13, K^o_M=1.9)

(a) V_f =12.5%

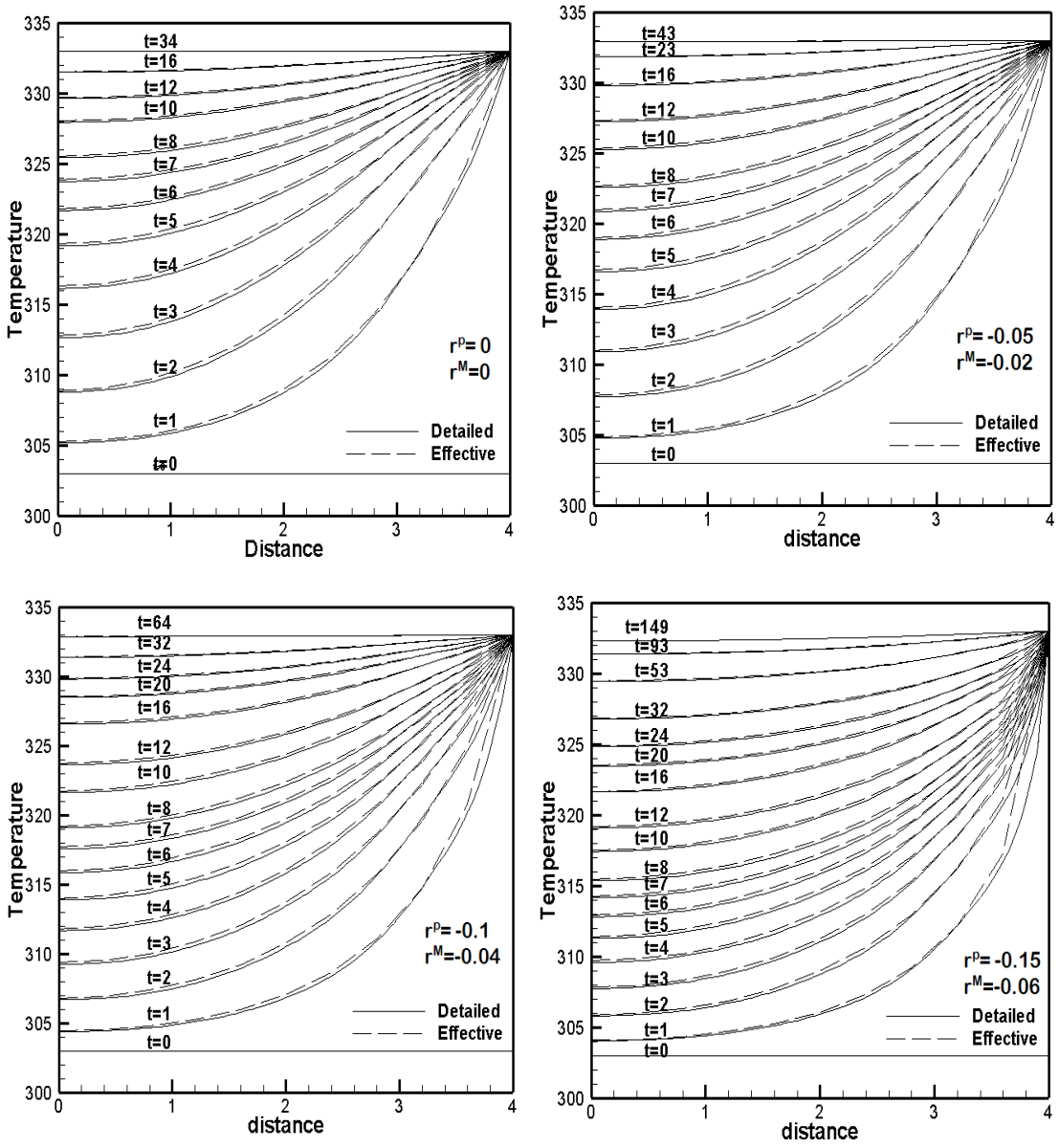

Fig.2.11. Temperature distribution along the slab for V_f =12.5% and K^o_P /K^o_M=6.84(K^o_P=13, K^o_M=1.9)

(b) V_f =25%

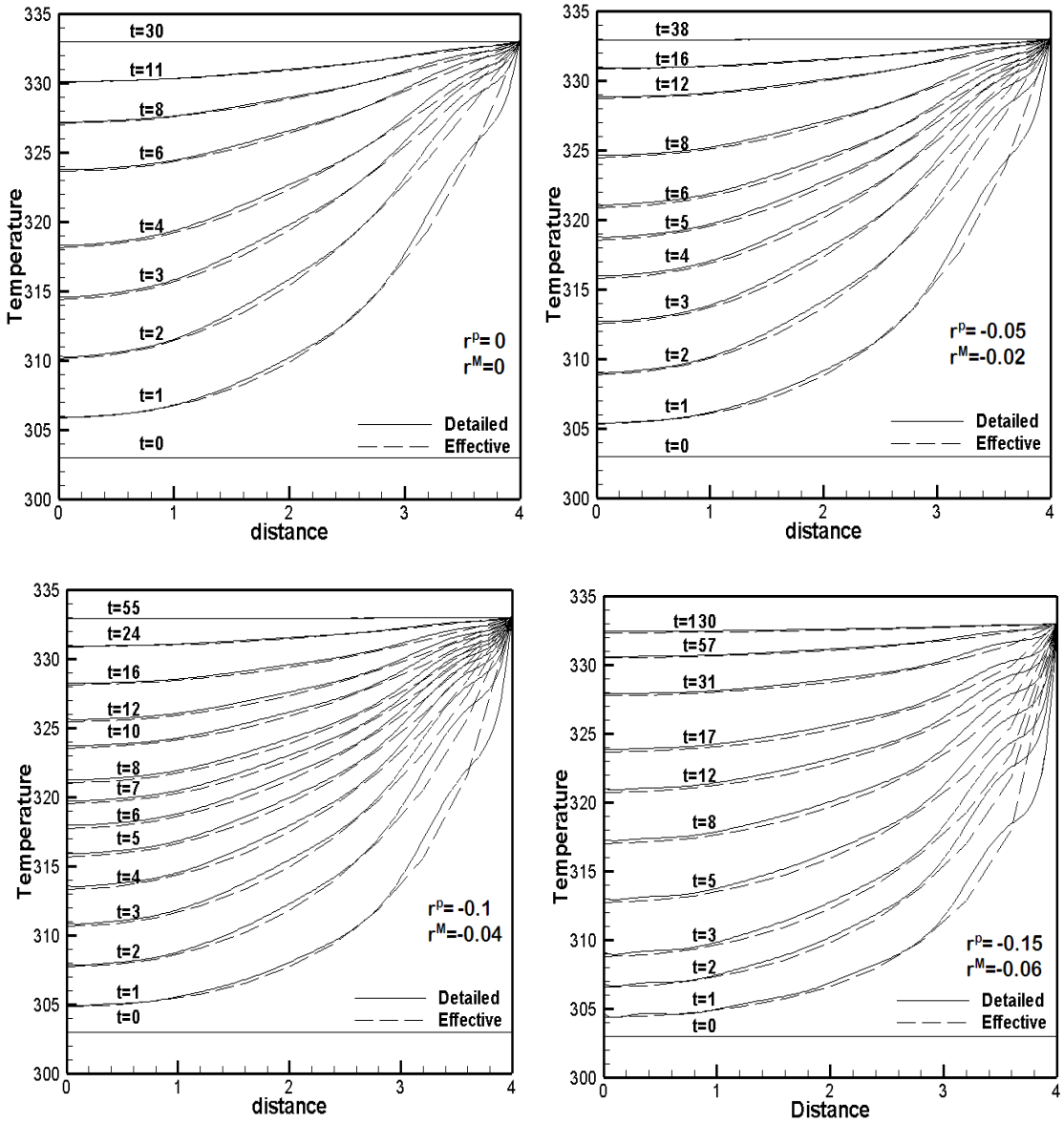

Fig.2.12. Temperature distribution along the slab for V_f =25% and K^o_P /K^o_M=6.84(K^o_P=13, K^o_M=1.9)

(c) V_f =50%

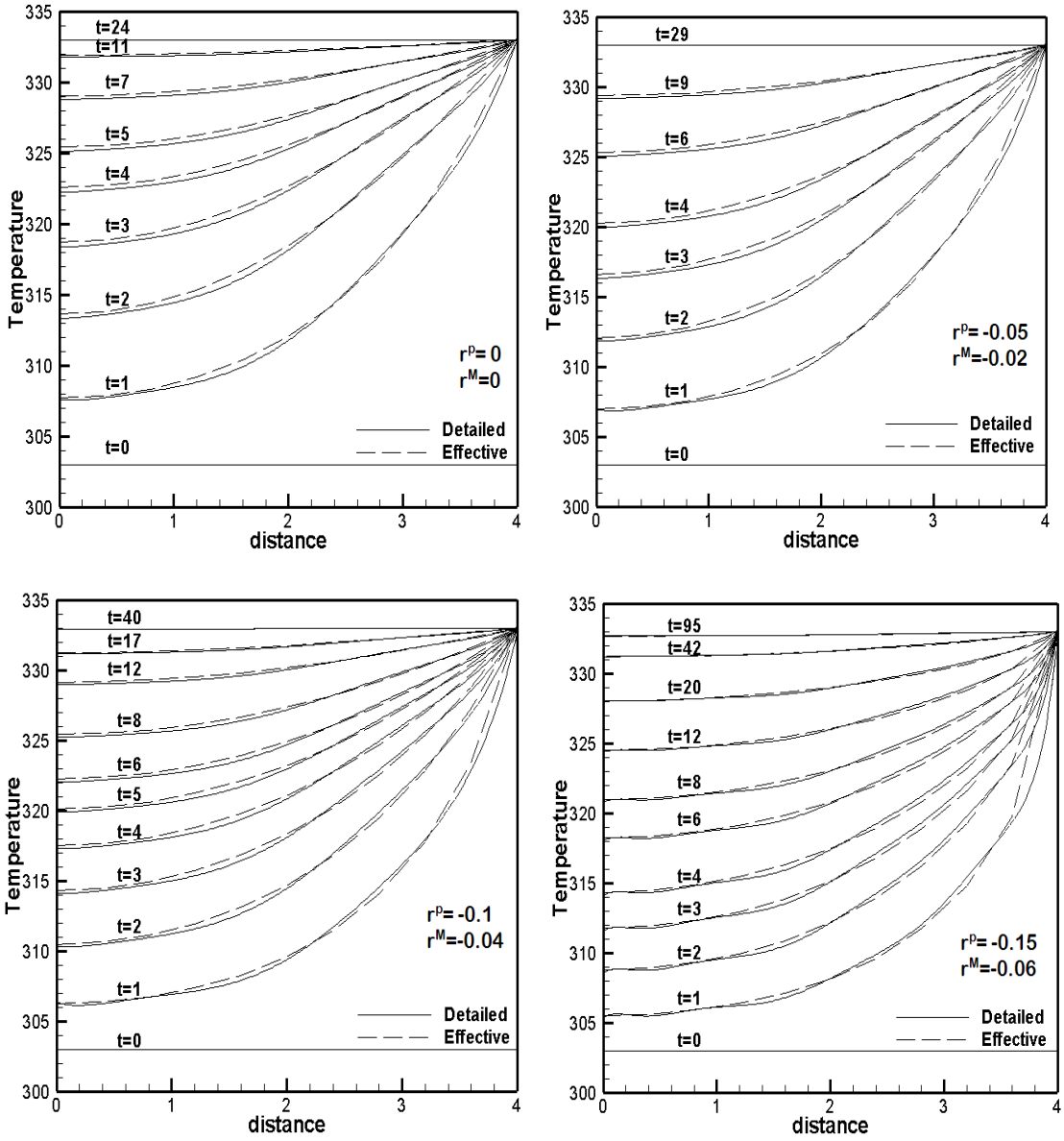

Fig.2.13. Temperature distribution along the slab for V_f =50% and K^o_P /K^o_M=6.84(K^o_P=13, K^o_M=1.9)

Case (2) $K^o_P / K^o_M = 50 (K^o_P = 95, K^o_M = 1.9)$

(a) V_f =12.5%

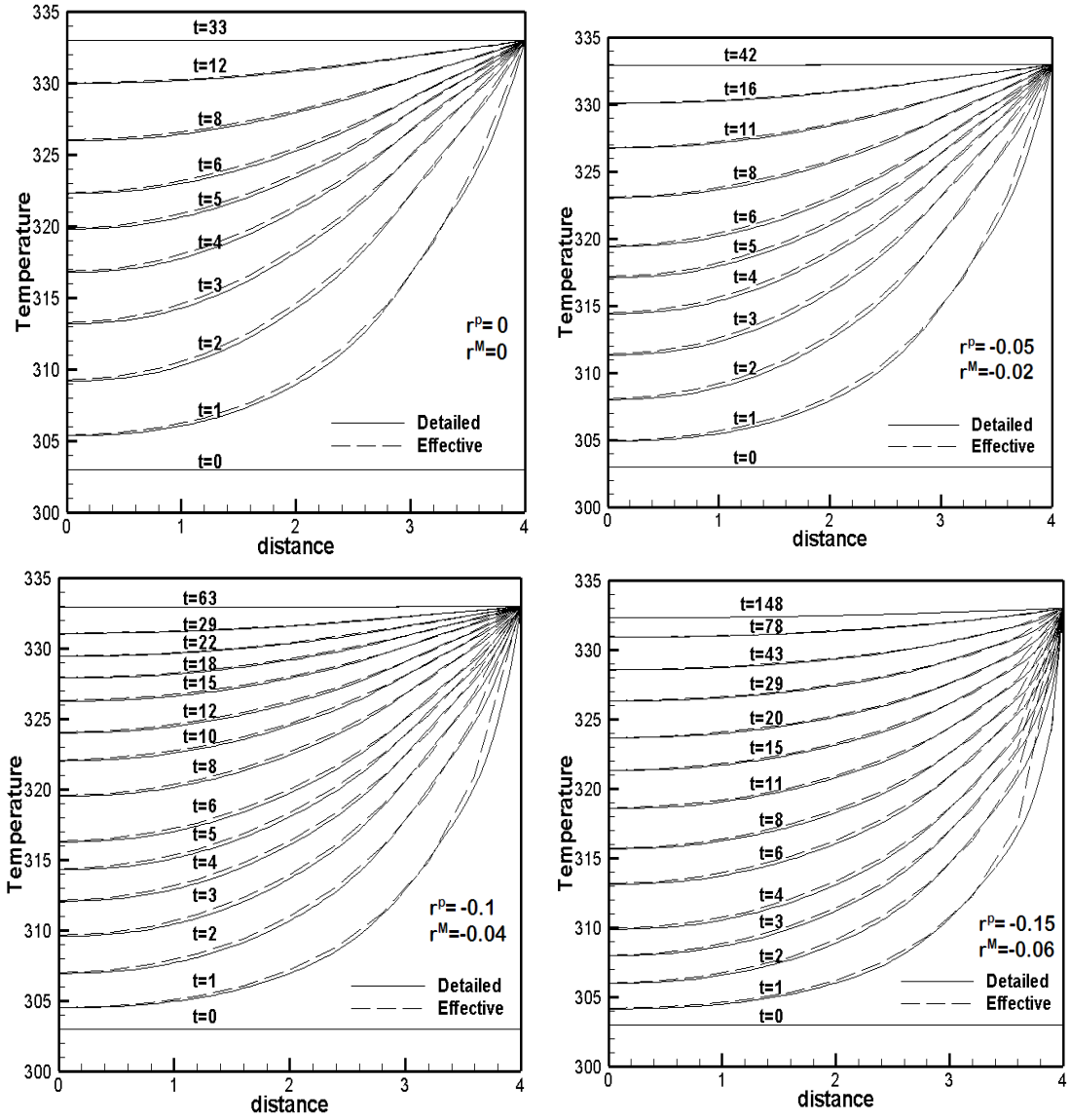

Fig. 2.14. Temperature distribution along the slab for V_f =12.5% and $K^o_P / K^o_M = 50 (K^o_P = 95, K^o_M = 1.9)$

(b) V_f =25%

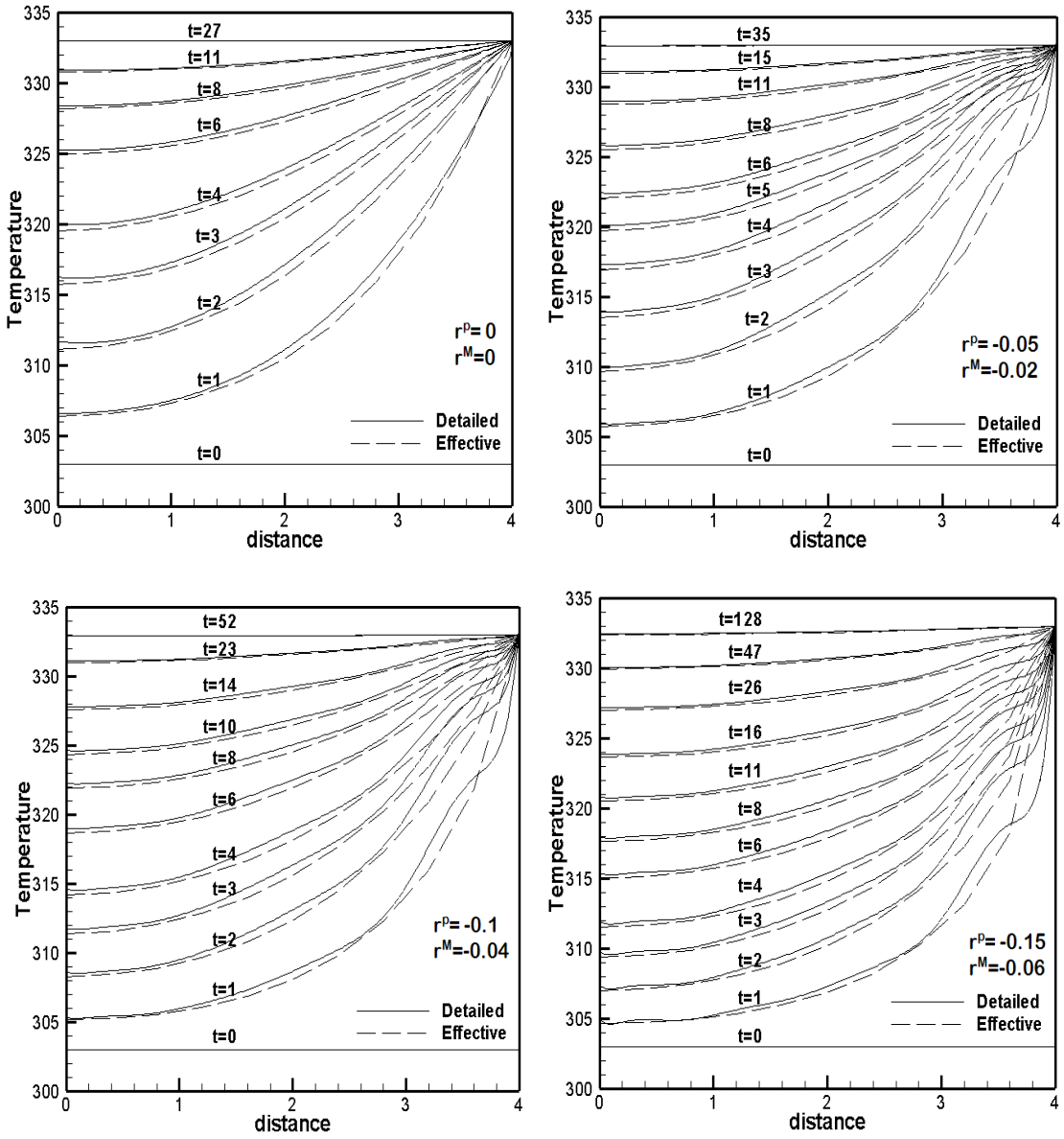

Fig. 2.15. Temperature distribution along the slab for V_f =25% and K^o_P /K^o_M=50(K^o_P=95, K^o_M=1.9)

(c) V_f =50%

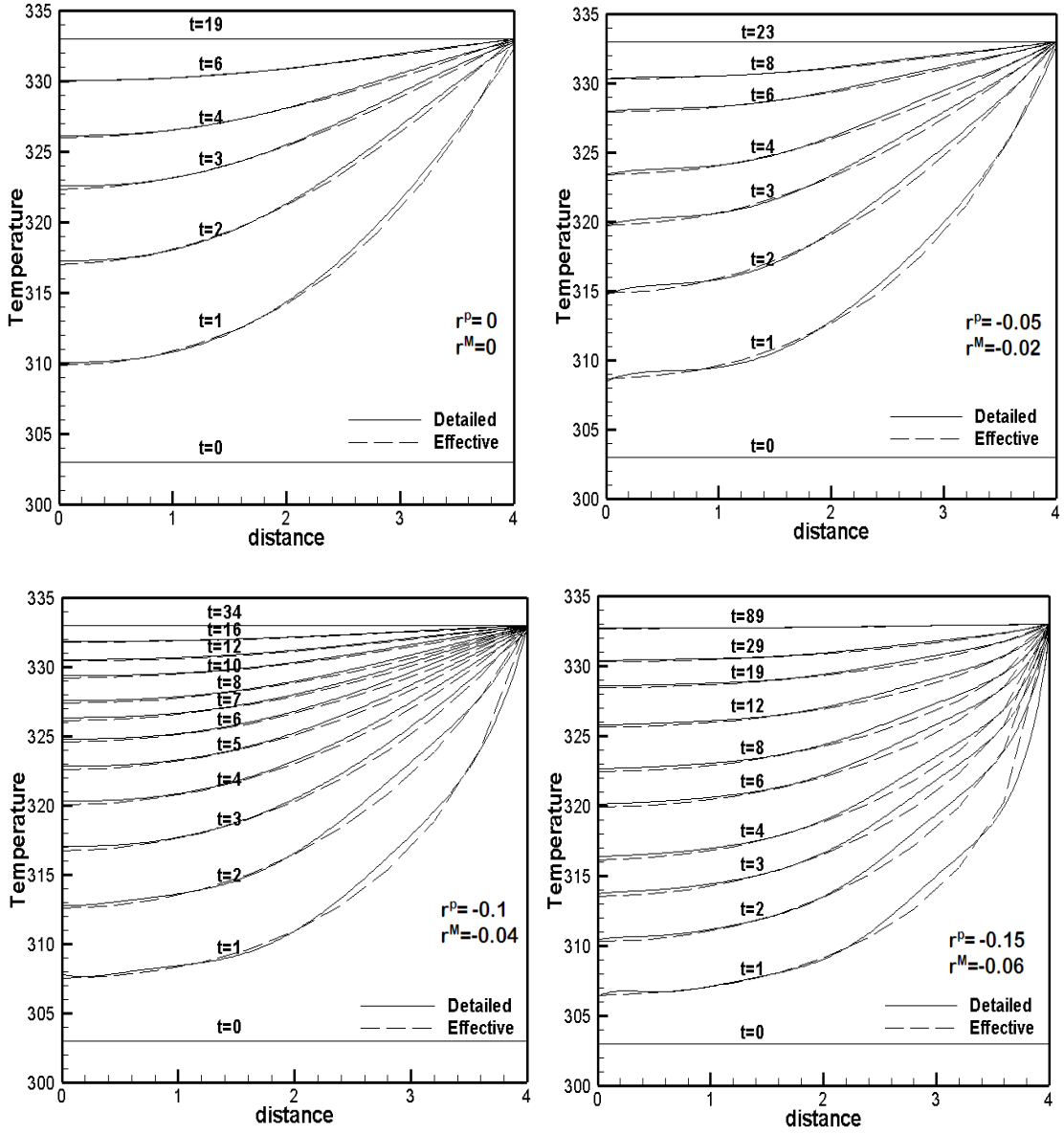

Fig. 2.16. Temperature distribution along the slab for V_f =50% and K^o_P /K^o_M=50(K^o_P=95, K^o_M=1.9)

Case (3) K^o_P / K^o_M=200(K^o_P=380, K^o_M=1.9)

(a) V_f =12.5%

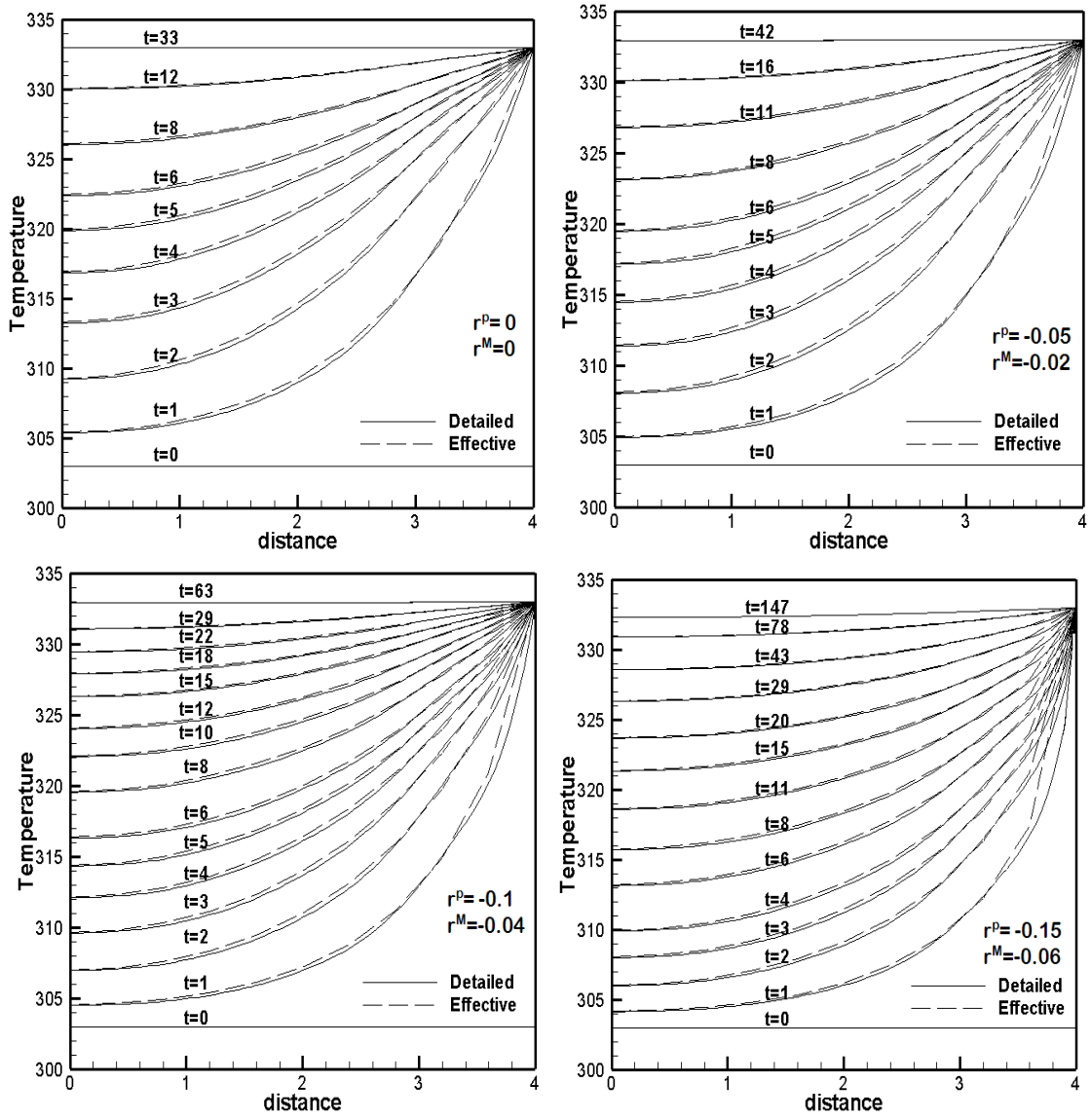

Fig. 2.17. Temperature distribution along the slab for V_f =12.5% and K^o_P /K^o_M=200(K^o_P=380, K^o_M=1.9)

(b) V_f =25%

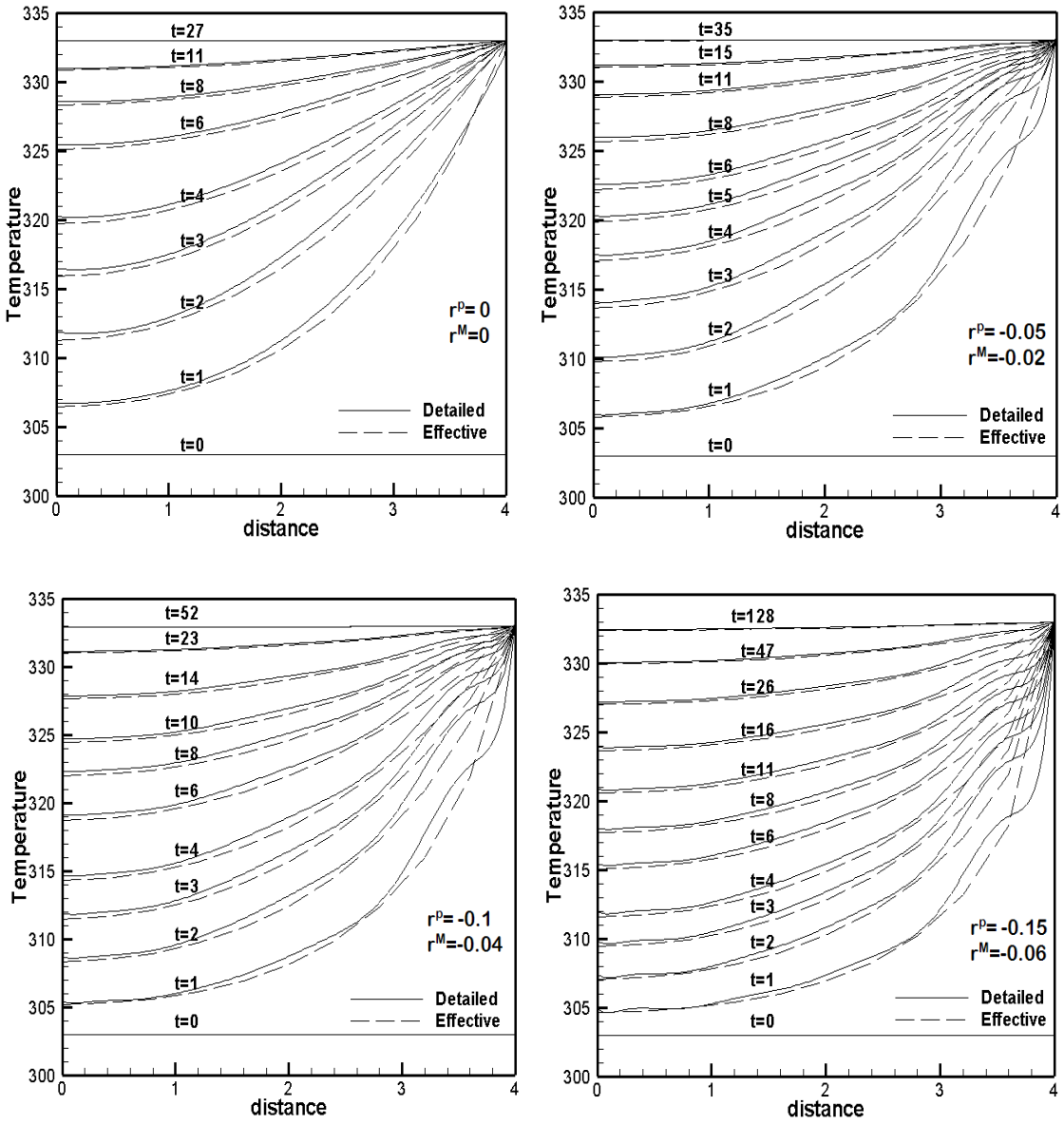

Fig. 2.18. Temperature distribution along the slab for V_f =25% and K^o_P /K^o_M=200(K^o_P=380, K^o_M=1.9)

(c) V_f =50%

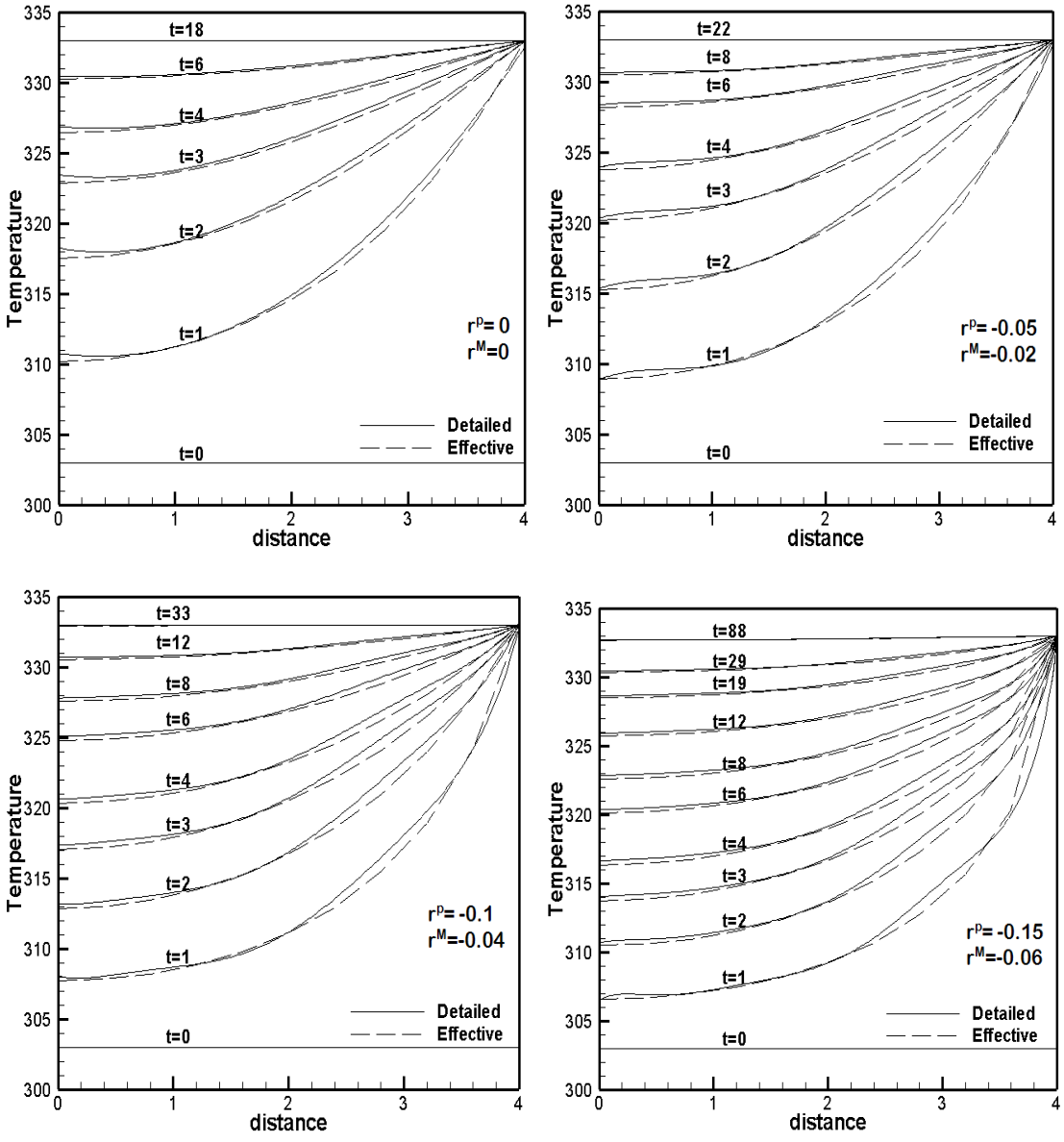

Fig. 2.19. Temperature distribution along the slab for V_f =50% and K^o_P /K^o_M=200(K^o_P=380, K^o_M=1.9)

Case (4) K^o_P / K^o_M=1000(K^o_P=1900, K^o_M=1.9)

(a) V_f =12.5%

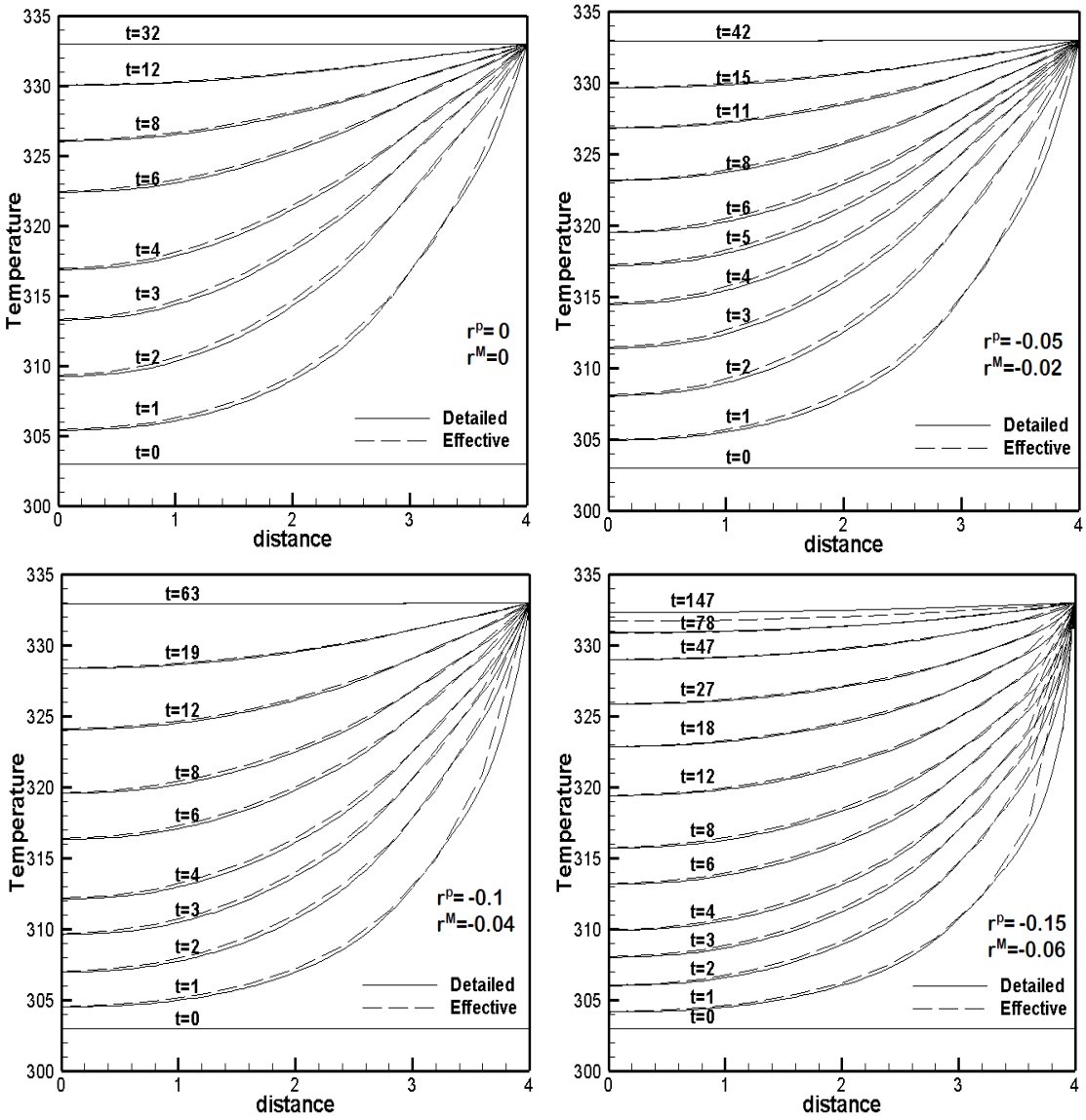

Fig. 2.20. Temperature distribution along the slab for V_f =12.5% and K^o_P / K^o_M=1000 (K^o_P=1900, K^o_M=1.9)

(b) V_f =25%

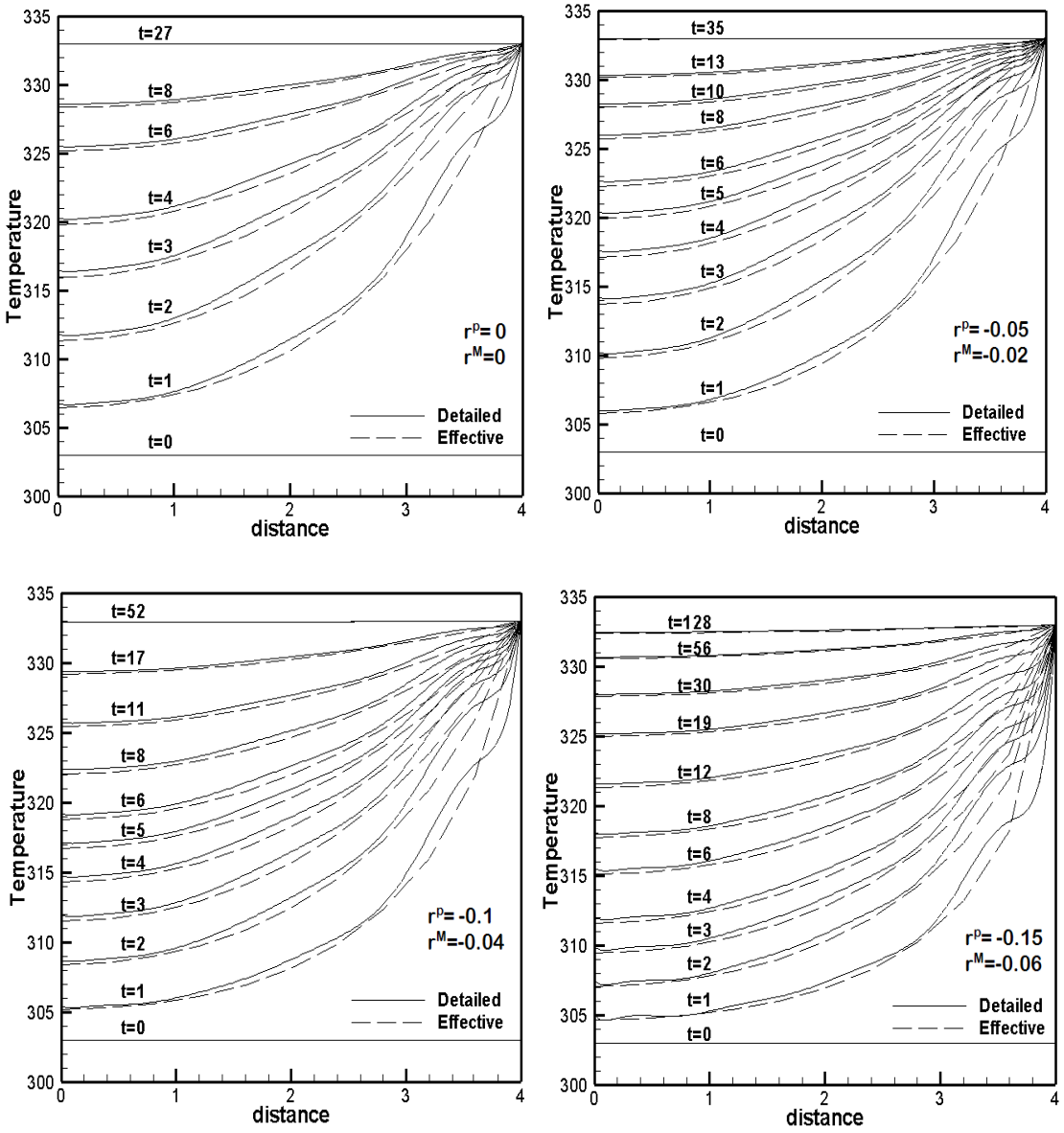

Fig. 2.21. Temperature distribution along the slab for V_f =25% and K^o_P /K^o_M=1000 (K^o_P=1900, K^o_M=1.9)

(c) V_f =50%

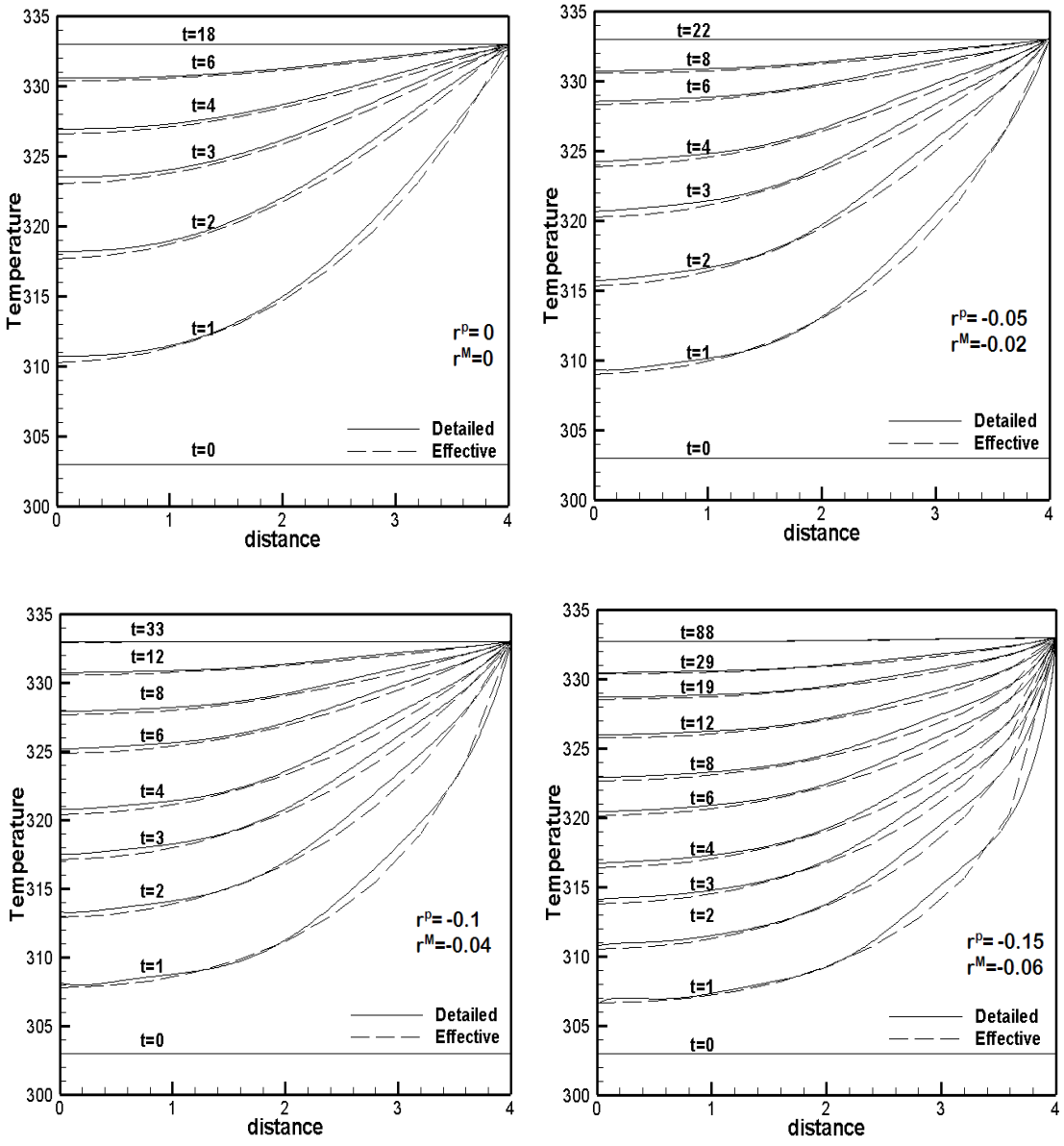

Fig. 2.22. Temperature distribution along the slab for V_f =50% and K^o_P /K^o_M=1000

(K^o_P=1900, K^o_M=1.9)

The effective thermal conductivity obtained using the present micromodel was compared with the apparent properties presented in Jiang et al. [25]. Apparent properties are defined as those under essential (displacement or temperature), natural (traction or heat flux), and mixed or periodic boundary conditions applied to finite size material domains (windows). The apparent conductivities obtained under Mixed boundary condition and Periodic boundary condition are equal and will always be bound by apparent conductivities obtained from Essential and Natural boundary conditions. For a periodic composite, apparent conductivity under Periodic boundary condition will be the Effective conductivity of the composite. For a particle volume fraction of 35% periodically distributed in a matrix having unit conductivity, Jiang et al. [25] determined the apparent conductivities under different boundary conditions for various conductivity ratios ranging from 0.001 to 1000.

The effective conductivity from the micromechanical model was compared with that presented in Jiang et al. [25] and a good match was found between the two. The corresponding results are presented in the Table 2.8. It is also seen from the table that the effective thermal conductivity values lie in between the lower and upper bounds of apparent conductivities i.e., the conductivities under natural and essential boundary conditions respectively.

Table 2.8. Comparison of effective conductivity values for different conductivity ratios

Conductivity ratio (K_P/K_M)	**Apparent conductivity obtained by using Natural B.C**	**Apparent conductivity obtained by using Periodic or Mixed B.C**	**Effective conductivity (determined form micromechanical model)**	**Apparent conductivity obtained by using Essential B.C**
0.001	0.0048	0.4821	0.504	0.5264
0.01	0.0458	0.489	0.5103	0.5327
0.1	0.3217	0.5546	0.57099	0.5927
10	1.689	1.803	1.8612	3.113
100	1.879	2.044	2.14614	21.86
1000	1.902	2.074	2.18135	208.8

This study also investigates the effect of K_P/K_M ratio on the effective thermal conductivity of composites. As the conductivity ratio increases or in other words as the conductivity of particles increase, Yin and Tu [22] observed that the effective conductivity of composite at first increases and then reaches an asymptotic value. This means that improvement in effective conductivity can be made by increasing the conductivity ratio only to a particular point. Similar observation is shown for effective conductivity obtained using the present micromechanical model. Fig. 2.23 shows the variation of effective conductivity with the conductivity ratio. It is evident from the graph that effective conductivity reached its maximum at $K_P / K_M = 200$ when K_P =380W/mk and K_M =1.9W/mk and after that the increase approach an asymptotic value.

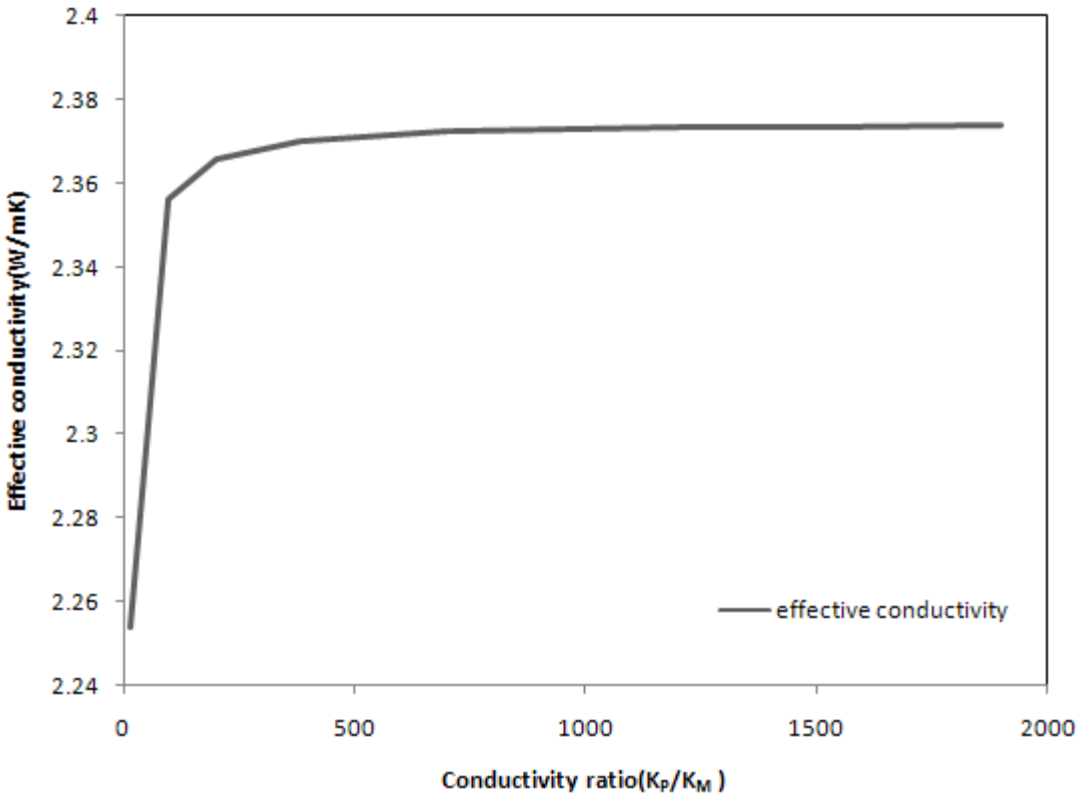

Fig. 2.23. Effective conductivity values for different conductivity ratios at V_f=12.5%

CHAPTER III

THERMO-ELASTIC DEFORMATION IN HETEROGENEOUS MEDIA

When composites are subjected to temperature changes, thermal stresses are developed in the microstructural constituents, i.e., reinforcement and matrix, due to difference in their thermal expansion properties, even when there are no external mechanical stimuli. For example, manufacturing processes of particle reinforced composites often involves high temperatures followed by rapid cooling to room temperature. Non negligible thermal stresses can influence both mechanical and thermal properties of the composites affecting overall behavior of the composite. Furthermore, different thermal and mechanical properties of the constituents cause discontinuities at the interphases between particles and matrix, which potentially induce debonding at the interphases.

To predict the overall mechanical performance of composites while at the same time monitoring nonlinear stress and temperature dependent constituent's responses, various homogenization methods have been proposed. Homogenization schemes rely on several assumptions to simplify the complex microstructural characteristics of composites. Thus, some fundamental characteristic or behavior at the microstructural levels may not be properly quantified when using homogenization methods. The advantage of using homogenization schemes is it allows predicting effective composite performance by incorporating microstructural information, such as volume contents, constituent properties and microstructural arrangement, which is essential for material

and structural design. However, the main drawback of such a homogenization scheme is that the discontinuity of effective stress and strain fields at the particle and matrix interface, which plays a vital role in the debonding of the composite, cannot be properly quantified

This chapter presents analysis of nonlinear thermo-elastic deformation in particle reinforced composites due to coupled heat conduction and mechanical loadings. The thermo-elastic material properties of the particle and matrix constituents are allowed to change with temperature and effective stress. Micromechanical model developed by Muliana and Kim [18] is used to incorporate this nonlinear thermo-elastic behavior and also to calculate the effective thermo-elastic properties of the entire composite. The responses from the micromechanical model that results in a homogenized medium are compared with the ones generated from detailed particle reinforced composite microstructures. For this purpose, two sets of FE meshes are generated for composites at different particle volume contents i.e., 12.5%, 25%, and 50%. The first FE represents a homogeneous composite panel, which is used along with the micromechanical model to determine the effective thermo-elastic properties of the composite. Whereas the second FE mesh, mimics the detailed composite microstructure with particles randomly distributed in matrix. In both the FE models an ABAQUS user material subroutine UMAT is used to input the variation of properties with temperature and stress. Sequentially coupled thermo-mechanical analyses are conducted for the two FE meshes generated for different volume fractions and their displacements in the two models are compared. Heat conduction in composites, discussed in CHAPTER II, is used as input to

prescribe the temperature fields during transient heat transfer analyses. A parametric study is conducted to investigate the effects of different CTE ratios, temperature changes, degree of nonlinearity, and volume fraction on the magnitude of discontinuity of effective stress and strain at the particle and matrix interphase.

3.1 Constitutive relations for thermo-elastic problem with isotropic constituents

Total strain is the sum of mechanical and thermal strains and for small deformation gradient problem is written as:

$$\varepsilon_{ij}^{\ t} = \varepsilon_{ij}^{\ T,t} + \varepsilon_{ij}^{\ M,t} \tag{3.1}$$

Thermal strain is given by:

$$\varepsilon_{ij}^{\ T,t} = \alpha(T^t - T_0)\delta_{ij} \tag{3.2}$$

And mechanical strain is given by:

$$\varepsilon_{ij}^{\ M,t} = e^t_{\ ij} + \frac{1}{3}\varepsilon_{kk}^{\ t}\delta_{ij} \tag{3.3}$$

Where the deviatoric and volumetric component of mechanical strain are:

$$e^t_{\ ij} = \frac{1}{2} g_0(\bar{\sigma}^t, T^t) J_0 S^t_{\ ij} \tag{3.4}$$

$$\varepsilon^t_{\ kk} = \frac{1}{3} g_0(\bar{\sigma}^t, T^t) B_0 \sigma^t_{\ kk} \tag{3.5}$$

Where J_0 and B_0 are the instantaneous elastic shear and bulk compliances respectively and are given by:

$$J_0 = \frac{2(1+\nu)}{E_0} \text{ and } B_0 = \frac{3(1-2\nu)}{E_0} \tag{3.6}$$

And E_0 is the instantaneous elastic modulus (under axial loading) and g_0 is the instantaneous nonlinear elastic compliance and is a measure of reduction or increase in compliance as a function of temperature and effective stress. As the problem is nonlinear, we need to solve the constitutive equation within an incremental formulation and perform iteration. The strain at current time can be obtained by:

$$\varepsilon_{ij}^{\ t} = \varepsilon_{ij}^{\ t-dt} + d\varepsilon_{ij}^{\ t} \tag{3.7}$$

$$d\varepsilon_{ij}^{\ t} = \frac{1}{2} g_0(\bar{\sigma}^t, T^t) J_0 . dS^t_{kk} + \frac{1}{3} g_0(\bar{\sigma}^t, T^t) B_0 . d\sigma^t_{kk} + \delta_{ij}\alpha(T).dT \tag{3.8}$$

Where the quantities at the previous converged time are indicated by a superscript t-dt and the increment quantities at the current time are indicated by a prefix 'd'. To determine strain at current time, we need to know increment of strain ($d\varepsilon_{ij}^{\ t}$). When a stress tensor is given as independent variables, Eq. (3.8) can be used to determine the corresponding strain tensor. When a strain tensor is given as independent variables, to calculate the corresponding stress tensor, iteration is performed as the g_0 parameter is also a function of effective stress. In the later case, to calculate initial value (trial) of g_0, it is assumed that $g_0^{\ trial} = g_0(\bar{\sigma}^{t-dt}, T^t)$. With the trial $g_0^{\ trial}$, one can calculate $d\sigma_{ij}^{\ t}$ using Eq. 3.8. The correct stress-strain tensor at current time is solved by minimizing residual tensor, which is defined as:

$$R^t_{\ ij} = d\varepsilon_{ij}^{\ t} + \frac{1}{3} d\varepsilon_{kk}^{\ t} \delta_{ij} - d\varepsilon_{ij}^{M,t} \tag{3.9}$$

Once convergent solution is achieved, consistent tangent stiffness matrix is obtained by taking the inverse of partial derivative of incremental strain with respect to incremental stress: $C^{t}_{ijkl} = \dfrac{\partial d\sigma^{t}_{ij}}{\partial d\varepsilon_{kl}^{M,t}}$ (3.10)

3.2 Micromechanical model for particle reinforced composites

This study uses a previously developed micromechanical model of Muliana et al. [18] the average stress and strain over a volume 'V' for a representative volume element can be written as

$$\overline{\sigma_{ij}} = \frac{1}{V}\int_{V}\sigma_{ij}dV \qquad \bar{\varepsilon}_{ij} = \frac{1}{V}\int_{V}\varepsilon_{ij}dV \tag{3.11}$$

The micromechanical relations derived by Muliana et al. [18] and Khan et al. [29] have been summarized here. Perfect bonding along sub cell's interface is assumed for determining these micromechanical relations. Effective stress and strain are related by the following constitutive equation:

$$\bar{\sigma}_{ij} = \bar{C}_{ijkl}\left[\bar{\varepsilon}_{kl} - \bar{\alpha}_{kl}(\bar{T} - \bar{T}_{o})\right] \text{ or } \bar{\varepsilon}_{ij} = \bar{S}_{ijkl}\bar{\sigma}_{kl} + \bar{\alpha}_{ij}(\bar{T} - \bar{T}_{o}) \tag{3.12}$$

The average stresses in a unit cell model:

$$\overline{\sigma}_{ij} = \frac{1}{V}\sum_{\alpha=1}^{N}\int_{V^{(\alpha)}}\sigma_{ij}^{(\alpha)}(x_{k}^{(\alpha)})dV^{(\alpha)} \approx \frac{1}{V}\sum_{\alpha=1}^{N}V^{(\alpha)}\sigma_{ij}^{(\alpha)} \tag{3.13}$$

The average strains in a unit cell model:

$$\bar{\varepsilon}_{ij} = \frac{1}{V}\sum_{\alpha=1}^{N}\int_{V^{(\alpha)}}\varepsilon_{ij}^{(\alpha)}(x_{k}^{(\alpha)})dV^{(\alpha)} \approx \frac{1}{V}\sum_{\alpha=1}^{N}V^{(\alpha)}\varepsilon_{ij}^{(\alpha)} \tag{3.14}$$

In each sub-cell, stress and strain are related by:

$$\sigma^{\alpha}{}_{ij} = C^{\alpha}{}_{ijkl}\left[\varepsilon^{\alpha}{}_{kl} - \alpha^{\alpha}{}_{kl}(T^{\alpha} - T^{\alpha}{}_{o})\right] \text{ or } \varepsilon^{\alpha}{}_{ij} = S^{\alpha}{}_{ijkl}\sigma^{\alpha}{}_{kl} + \alpha^{\alpha}{}_{ij}(T^{\alpha} - T^{\alpha}{}_{o}) \qquad (3.15)$$

where T^{α} in each sub-cell has to be determined by solving the transient heat conduction equation. The total stress and strain at current time t are given by

$$\bar{\sigma}^{t}_{ij} = \bar{\sigma}^{t-\Delta t}_{ij} + d\bar{\sigma}^{t}_{ij} \quad \text{and} \quad \bar{\varepsilon}^{t}_{ij} = \bar{\varepsilon}^{t-\Delta t}_{ij} + d\bar{\varepsilon}^{t}_{ij} \qquad (3.16a)$$

$$\sigma^{(\alpha),t}_{ij} = \sigma^{(\alpha),t-\Delta t}_{ij} + d\sigma^{(\alpha),t}_{ij} \text{ and } \varepsilon^{(\alpha),t}_{ij} = \varepsilon^{(\alpha),t-\Delta t}_{ij} + d\varepsilon^{(\alpha),t}_{ij} \qquad (3.16b)$$

Homogenized incremental stresses and strains are related by:

$$d\bar{\sigma}_{ij} = \bar{C}_{ijkl}\ d\bar{\varepsilon}_{kl} - \bar{\alpha}_{kl} d\Delta T \qquad (3.17)$$

The displacement compatibility results in:

$$d\bar{\varepsilon}_{ij} = \frac{1}{V^{(1)} + V^{(2)}}\left[V^{(1)} d\varepsilon^{(1)}{}_{ij} + V^{(2)} d\varepsilon^{(2)}{}_{ij}\right] = d\varepsilon^{(3)}{}_{ij} = d\varepsilon^{(4)}{}_{ij} \qquad (3.18a)$$

$$d\bar{\gamma}_{ij} = V^{(1)} d\gamma^{(1)}{}_{ij} + V^{(2)} d\gamma^{(2)}{}_{ij} + V^{(3)} d\gamma^{(3)}{}_{ij} + V^{(4)} d\gamma^{(4)}{}_{ij} \qquad (3.18b)$$

The stress continuity condition gives:

$$d\bar{\sigma}^{t}_{ij} = V^{(A)} d\sigma^{(A),t}_{ij} + V^{(3)} d\sigma^{(3),t}_{ij} + V^{(4)} d\sigma^{(4),t}_{ij} \quad \text{for } i = j \qquad (3.19)$$
$$d\sigma^{(A),t}_{ij} = d\sigma^{(1),t}_{ij} = d\sigma^{(2),t}_{ij}$$

$$d\bar{\sigma}^{t}_{ij} = d\sigma^{(1),t}_{ij} = d\sigma^{(2),t}_{ij} = d\sigma^{(3),t}_{ij} = d\sigma^{(4),t}_{ij} \quad \text{for } i \neq j \qquad (3.20)$$

Using the micromechanical relations in Eqs. (3.19)-(3.20) and constitutive relation in Eq. (3.16), effective stress and strain relations in Eq. (3.17) can be written as:

$$d\bar{\sigma}_{ij} = \bar{C}_{ijkl} d\bar{\varepsilon}_{kl} - \frac{\Delta T}{V}\left[V^{(A)} C^{A}{}_{ijkl} \alpha^{A}{}_{kl} + V^{(3)} C^{3}{}_{ijkl} \alpha^{3}{}_{kl} + V^{(4)} C^{4}{}_{ijkl} \alpha^{4}{}_{kl} \right]$$
$$= \bar{C}_{ijkl}\ d\bar{\varepsilon}_{kl} - d\Delta T \bar{\alpha}_{kl}$$

where $\bar{C}_{ijkl}$ is the effective tangent stiffness and $\bar{\alpha}_{kl}$ is the effective coefficient of thermal expansion given by

$$\bar{\alpha}_{kl} = \bar{\alpha}\delta_{ij} = \frac{\bar{C}^{-1}_{ijkl}}{V}\left[V^{(A)} C^{A}{}_{ijkl} \alpha^{A}{}_{kl} + V^{(3)} C^{3}{}_{ijkl} \alpha^{3}{}_{kl} + V^{(4)} C^{4}{}_{ijkl} \alpha^{4}{}_{kl} \right] \tag{3.21}$$

$$\text{where } \alpha^{(A)}{}_{ij} = \alpha^{(A)}\delta_{ij} = \frac{1}{V^{(A)}}\left[V^{(1)} \alpha^{(1)}{}_{ij} + V^{(2)} \alpha^{(2)}{}_{ij} \right] \tag{3.22}$$

$$\text{and } C^{A}{}_{ijkl} = \left[\frac{1}{V^{(A)}} (V^{(1)} (C^{1}{}_{ijkl})^{-1} + V^{(2)} (C^{2}{}_{ijkl})^{-1} \right]^{-1} \tag{3.23}$$

3.3 Verification of effective properties

The effective properties obtained by micromechanical model are first compared with the upper and lower bounds of Voigt and Reuss models and also the compared with the ones from Mori-Tanaka model. For isotropic material, the stiffness matrix is given by

$$C = \frac{E}{(1+\nu)(1-2\nu)}\begin{bmatrix} 1-\nu & \nu & \nu & 0 & 0 & 0 \\ \nu & 1-\nu & \nu & 0 & 0 & 0 \\ \nu & \nu & 1-\nu & 0 & 0 & 0 \\ 0 & 0 & 0 & 1-2\nu & 0 & 0 \\ 0 & 0 & 0 & 0 & 1-2\nu & 0 \\ 0 & 0 & 0 & 0 & 0 & 1-2\nu \end{bmatrix} \quad (3.24)$$

Consider $E_M = 2710.03$; $E_P = 72000$; $\nu_M = 0.35$; $\nu_P = 0.25$

Hence stiffness of matrix can be obtained from Eq. (3.24) as

$$C_M = \begin{bmatrix} 4349.43 & 2342 & 2342 & 0 & 0 & 0 \\ 2342 & 4349.43 & 2342 & 0 & 0 & 0 \\ 23422 & 2342 & 4349.43 & 0 & 0 & 0 \\ 0 & 0 & 0 & 2007.42 & 0 & 0 \\ 0 & 0 & 0 & 0 & 2007.42 & 0 \\ 0 & 0 & 0 & 0 & 0 & 2007.42 \end{bmatrix} \quad (3.25)$$

And stiffness of particle is obtained as

$$C_P = \begin{bmatrix} 86400 & 28800 & 28800 & 0 & 0 & 0 \\ 28800 & 86400 & 28800 & 0 & 0 & 0 \\ 28800 & 28800 & 86400 & 0 & 0 & 0 \\ 0 & 0 & 0 & 57600 & 0 & 0 \\ 0 & 0 & 0 & 0 & 57600 & 0 \\ 0 & 0 & 0 & 0 & 0 & 57600 \end{bmatrix} \quad (3.26)$$

Comparison of Effective Model Results with Voigt and Reuss's Bounds

$$\text{According to Voigt's model, Effective stiffness, } C_{eq} = V_f C_p + (1-V_f)C_m \quad (3.27)$$

$$\text{According to Reuss model, Effective stiffness, } \frac{1}{C_{eq}} = \frac{V_f}{C_p} + \frac{(1-V_f)}{C_m} \quad (3.28)$$

For V_f = 12.5%

From Voigt's model:

$$C^{V}_{eq} = \begin{bmatrix} 14605.75 & 5649.25 & 5649.25 & 0 & 0 & 0 \\ 5649.25 & 14605.75 & 5649.25 & 0 & 0 & 0 \\ 5649.25 & 5649.25 & 14605.75 & 0 & 0 & 0 \\ 0 & 0 & 0 & 8956.5 & 0 & 0 \\ 0 & 0 & 0 & 0 & 8956.5 & 0 \\ 0 & 0 & 0 & 0 & 0 & 8956.5 \end{bmatrix}$$

From our effective model, we obtained stiffness as:

$$C_{eff} = \begin{bmatrix} 5337.8 & 2850.7 & 2850.7 & 0 & 0 & 0 \\ 2850.7 & 5324.8 & 2843.2 & 0 & 0 & 0 \\ 2850.7 & 2843.2 & 5324.8 & 0 & 0 & 0 \\ 0 & 0 & 0 & 2276.3 & 0 & 0 \\ 0 & 0 & 0 & 0 & 2276.3 & 0 \\ 0 & 0 & 0 & 0 & 0 & 2276.3 \end{bmatrix}$$

From Reuss model,

$$C^{R}_{eq} = \begin{bmatrix} 4932.615 & 2649.776 & 2649.776 & 0 & 0 & 0 \\ 2649.776 & 4932.615 & 2649.776 & 0 & 0 & 0 \\ 2649.776 & 2649.776 & 4932.615 & 0 & 0 & 0 \\ 0 & 0 & 0 & 2282.83 & 0 & 0 \\ 0 & 0 & 0 & 0 & 2282.83 & 0 \\ 0 & 0 & 0 & 0 & 0 & 2282.83 \end{bmatrix}$$

It is clear from above that $C^{R}_{eq} \leq C_{eff} \leq C^{V}_{eq}$

For V_f = 25%

From Voigt's model:

$$C^{V}_{eq} = \begin{bmatrix} 24862.07 & 8956.5 & 8956.5 & 0 & 0 & 0 \\ 8956.5 & 24862.07 & 8956.5 & 0 & 0 & 0 \\ 8956.5 & 8956.5 & 24862.07 & 0 & 0 & 0 \\ 0 & 0 & 0 & 15905.57 & 0 & 0 \\ 0 & 0 & 0 & 0 & 15905.57 & 0 \\ 0 & 0 & 0 & 0 & 0 & 15905.57 \end{bmatrix}$$

And from our effective model:

$$C_{eff} = \begin{bmatrix} 6896 & 3635 & 3635 & 0 & 0 & 0 \\ 3635 & 6875 & 3622.1 & 0 & 0 & 0 \\ 3635 & 3622.1 & 6875.5 & 0 & 0 & 0 \\ 0 & 0 & 0 & 2621.4 & 0 & 0 \\ 0 & 0 & 0 & 0 & 2621.4 & 0 \\ 0 & 0 & 0 & 0 & 0 & 2621.4 \end{bmatrix}$$

From Reuss Model:

$$C^{R}_{eq} = \begin{bmatrix} 5696.5 & 3050.67 & 3050.67 & 0 & 0 & 0 \\ 3050.67 & 5696.5 & 3050.67 & 0 & 0 & 0 \\ 3050.67 & 2649.776 & 5696.5 & 0 & 0 & 0 \\ 0 & 0 & 0 & 2645.83 & 0 & 0 \\ 0 & 0 & 0 & 0 & 2645.83 & 0 \\ 0 & 0 & 0 & 0 & 0 & 2645.83 \end{bmatrix}$$

Clearly $C^{R}_{eq} \leq C_{eff} \leq C^{V}_{eq}$

For V_f = 50%

From Voigt's model:

$$C^{V}_{eq} = \begin{bmatrix} 45374.72 & 15571 & 15571 & 0 & 0 & 0 \\ 15571 & 45374.72 & 15571 & 0 & 0 & 0 \\ 15571 & 15571 & 45374.72 & 0 & 0 & 0 \\ 0 & 0 & 0 & 29803.71 & 0 & 0 \\ 0 & 0 & 0 & 0 & 29803.71 & 0 \\ 0 & 0 & 0 & 0 & 0 & 29803.71 \end{bmatrix}$$

From effective model:

$$C_{eff} = \begin{bmatrix} 12519.2 & 6328 & 6328 & 0 & 0 & 0 \\ 6328 & 12478.4 & 6301.1 & 0 & 0 & 0 \\ 6328 & 6301.1 & 12478.4 & 0 & 0 & 0 \\ 0 & 0 & 0 & 3763.4 & 0 & 0 \\ 0 & 0 & 0 & 0 & 3763.4 & 0 \\ 0 & 0 & 0 & 0 & 0 & 3763.4 \end{bmatrix}$$

From Reuss Model:

$$C^{R}_{eq} = \begin{bmatrix} 8253.24 & 4373.59 & 4373.59 & 0 & 0 & 0 \\ 4373.59 & 8253.24 & 4373.59 & 0 & 0 & 0 \\ 4373.59 & 4373.59 & 8253.24 & 0 & 0 & 0 \\ 0 & 0 & 0 & 3879.65 & 0 & 0 \\ 0 & 0 & 0 & 0 & 3879.65 & 0 \\ 0 & 0 & 0 & 0 & 0 & 3879.65 \end{bmatrix}$$

Therefore, $C^{R}_{eq} \leq C_{eff} \leq C^{V}_{eq}$

Hence for all the volume fractions considered (V_f=12.5,25 &50%), the effective stiffness values always lie between the Voigt and Reuss estimates of stiffness which form upper and lower bound respectively. It is observed that the shear components of the stiffness matrix are slightly under the lower bounds.

Comparison of Effective Properties with Mori-Tanaka Method

Effective properties determined form the micromechanical model are compared with those obtained from Mori-Tanaka's method. Figs.3.1 to 3.4 shows the comparison for effective elastic modulus, Poisson's ratio, bulk and shear modulus respectively. At lower volume fractions, the effective properties obtained from the micromechanical model are in good agreement with those obtained from Mori-Tanaka method. As the volume fraction increases, the difference between effective properties from both the methods increases, with micromechanical model resulting in higher estimates of properties than Mori-Tanaka's method. The difference at higher volume contents are due to the effect of particle-particle interaction, which is not considered in the present micromodel.

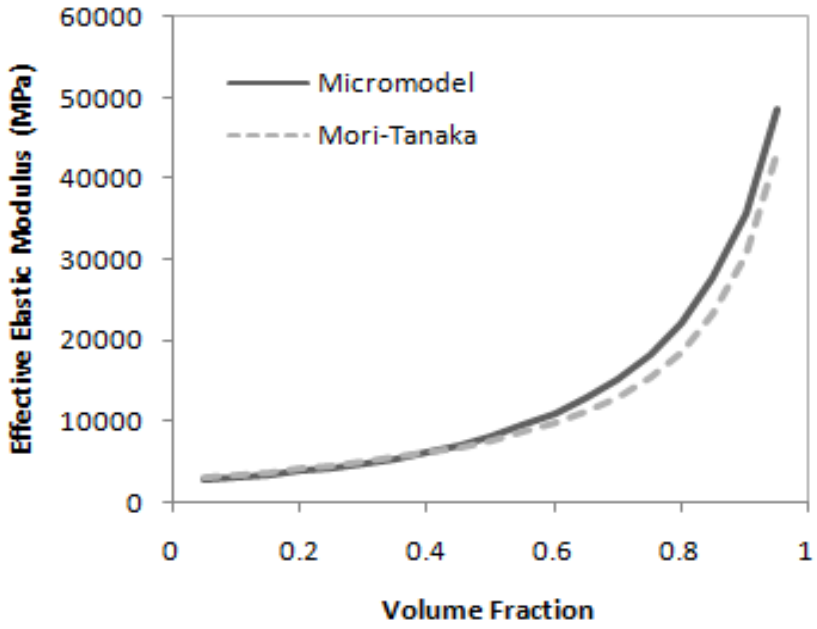

Fig. 3.1. Comparison of effective elastic modulus of micromodel with Mori-Tanaka

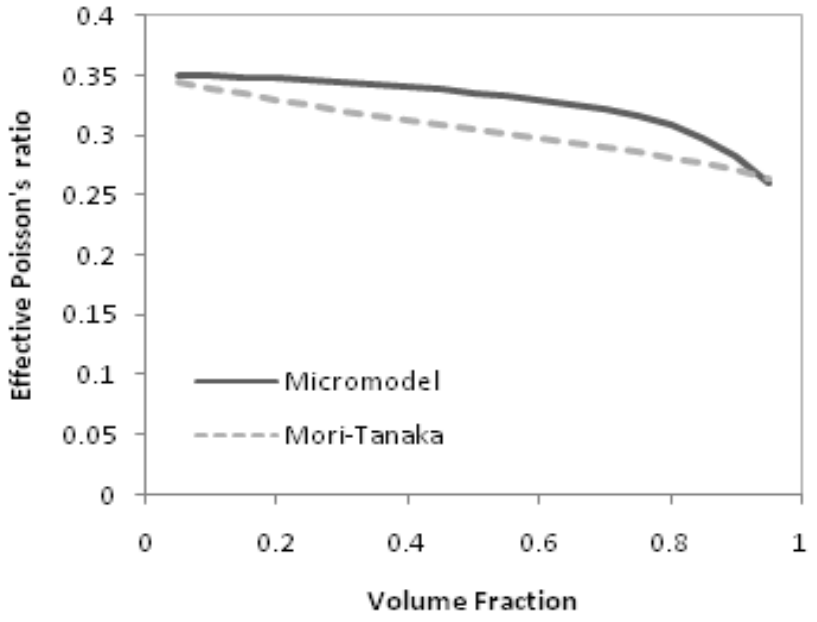

Fig. 3.2. Comparison of effective Poisson's ratio of micromodel with Mori-Tanaka

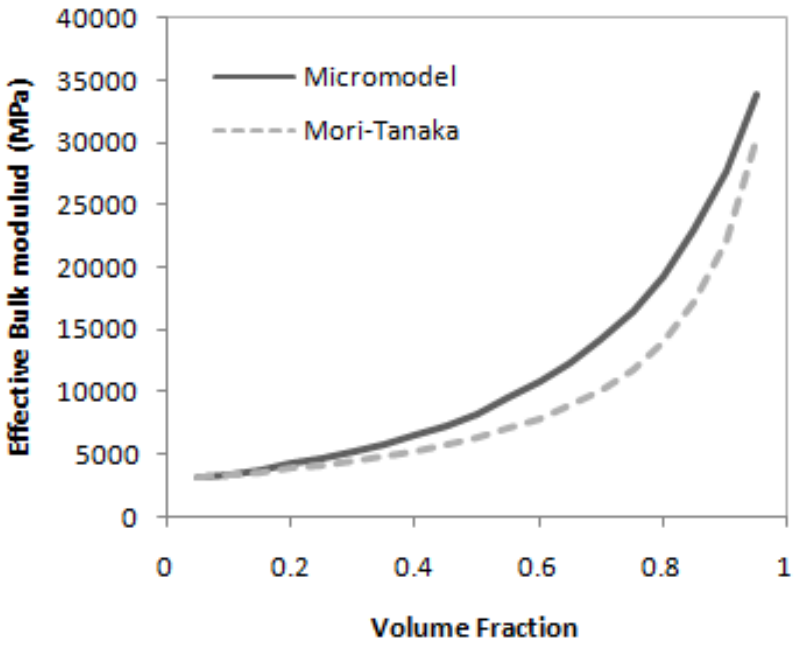

Fig. 3.3. Comparison of effective bulk modulus of micromodel with Mori-Tanaka

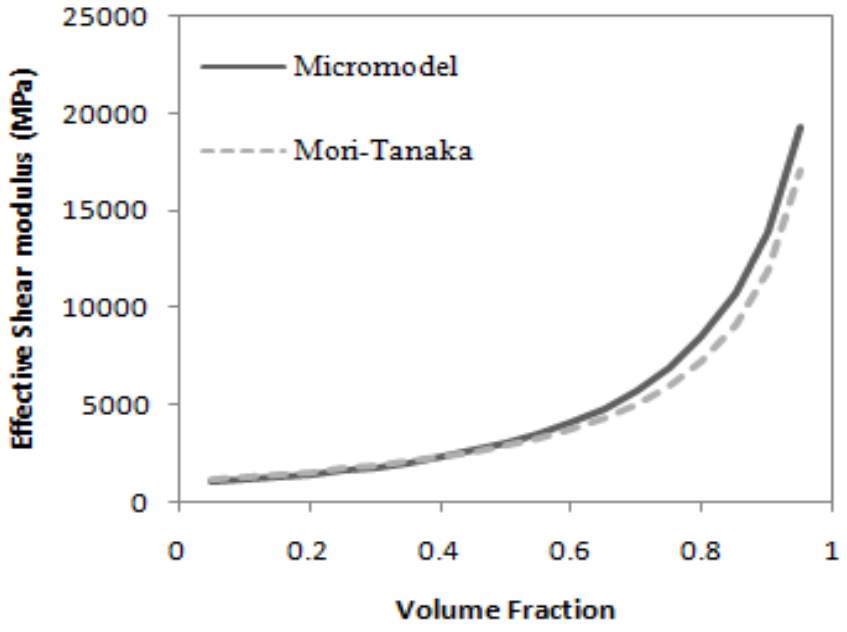

Fig. 3.4. Comparison of effective shear modulus of micromodel with Mori-Tanaka

The responses of the homogenization model are now compared with the ones of detailed microstructure of the composite. Two sets of FE meshes are generated for composites at different particle volume contents, i.e. 12.5%, 25%and 50%. The first FE mesh represents a homogeneous composite panel, which uses the micromechanical model to obtain the effective thermo-elastic properties. The second FE mimics detailed composite microstructure with particles randomly distributed in matrix.

Consider a square composite panel of 4μmx4μm as shown in Fig 3.5. The following boundary and initial conditions are prescribed:

$$T(X,Y,0) = T_0 = T_{ref} \quad \forall\, 0 \le X \le 4 \text{ and } 0 \le Y \le 4$$

$$T(4,Y,t) = T_1 \quad \forall\, 0 \le Y \le 4 \tag{3.29}$$

$$t_x(4,Y,t) = \sigma_0 = 40\,\text{MPa} \quad \text{and} \quad t_y(X,4,t) = 0$$

$$u_x(0,Y,t) = 0 \quad \text{and} \quad u_y(X,0,t) = 0$$

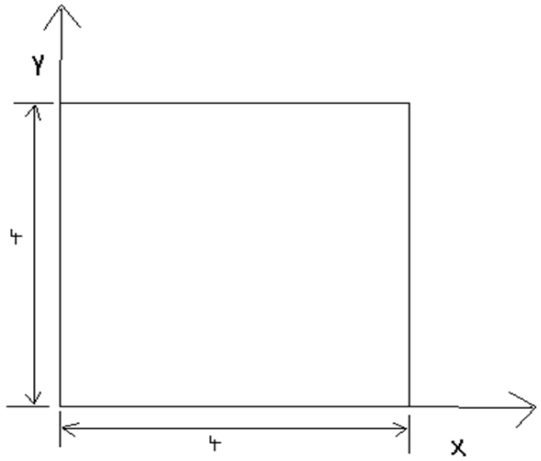

Fig. 3.5. Square composite panel

A sequentially coupled thermo-mechanical analysis is conducted. The basic assumption of such a type of analysis is that only the temperature field can influence the mechanical field but not vice versa. Hence temperature field can be determined independent of stress distribution. A heat transfer analysis is conducted with temperature dependent thermal conductivity for both the particle and matrix, as discussed in section 2.4. The temperature distribution thus obtained is brought into the stress analysis. Particles are assumed to be isotropic and linearly elastic; whereas matrix is assumed as isotropic and nonlinear elastic material. It is assumed that the elastic modulus of the matrix is dependent on stress and temperature as shown in Eqs. (3.30 a)-(3.30 b)

$$E_m\ \sigma_m, T\ = f_S f_T E^o{}_m \tag{3.30a}$$

$$f_S = e^{\left(-\frac{\sigma_m}{B_0}\right)} \quad ; \quad f_T = 1 - A_0\ \ T - T_{ref} \tag{3.30b}$$

A detailed model of 4µmx4µm, with randomly distributed solid spherical particles of fixed diameter 0.4µm for volume fractions 12.5, 25 and 50% are developed. The mesh shown in Fig. 3.6 is for 12.5% volume fraction of particles. For the stress analysis the boundary conditions described in Eq. (3.29) are used. The mesh is made up of CPS3 and CPS4 elements. The material properties used for particle and matrix constituents are given in Table 3.1.

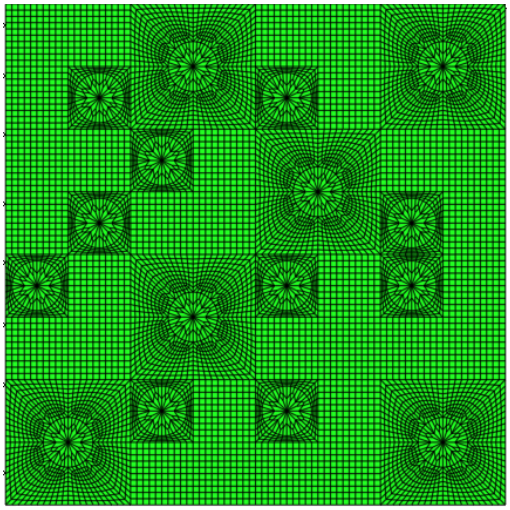

Fig. 3.6. Detailed mesh representing volume fraction 12.5%

Table 3.1. Properties of particle and matrix of the composite

Material	Properties	Values
Particle	Young's Modulus, E (MPa)	72000
	Poisson's ratio, ν	0.22
	CTE α ($^0K^{-1}$)	$5x10^{-6}$
	Heat capacity ρC (J/m^3K)	2.0898
	Conductivity K^0_p (W/mK)	13
Matrix	Young's Modulus, E (MPa)	2710.03
	Poisson's ratio, ν	0.35
	CTE α ($^0K^{-1}$)	$6x10^{-6}$
	Heat capacity ρC (J/m^3K)	1.47
	Conductivity K^0_M (W/mK)	1.9

A FE model of homogenized composite as shown in Fig. 3.7 is generated. The length of each element in the mesh is 0.4µm. Sequentially coupled analysis is performed on the model. Thermal conductivity and elastic modulus for particle and matrix are assumed the same way as done for detailed model. Thermal analysis is performed as discussed in section 2.4. For structural analysis the elements are made up of C3D8 elements. The homogenized model developed was used to calculate effective properties for thermal conductivity, Poisson's ratio, CTE and elastic modulus for different volume fractions. For all the other properties like density and specific heat, rule of mixtures have been used to find out the effective properties for each volume fraction.

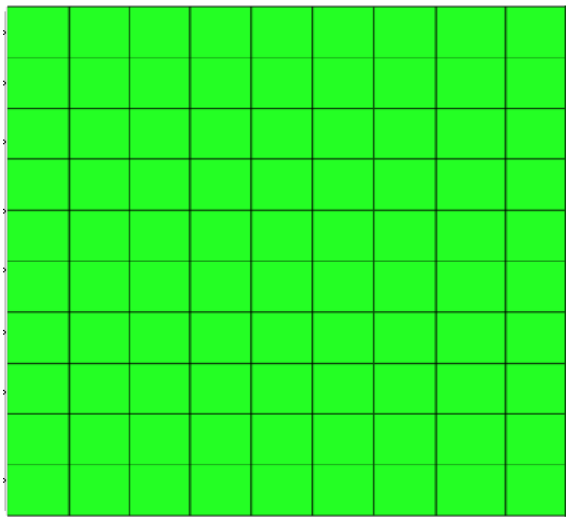

Fig. 3.7. Effective model mesh representing volume fraction 12.5%

Heat capacity per unit volume of composite is assumed as:

$$\rho C = V_f \rho_p C_p + 1 - V_f \quad \rho_m C_m \tag{3.31}$$

Density of the composite is given as:

$$\rho = V_f \rho_p + 1 - V_f \quad \rho_m \tag{3.32}$$

Comparison of Detailed Model with Effective Model

The displacements obtained with effective model are compared with that of the detailed FE microstructural model as shown in the Figs. 3.8 (a) to 3.10 (b). The following nonlinear parameters are used for the two FE models:

$$r^P = -0.02; \quad r^M = -0.05; \; A_0 = 1e-5; \quad B_0 = 5000$$

Fig. 3.8 (a) to Fig. 3.10 (a) shows the plots for axial displacement in x direction (U_1) for both detailed and effective models for different volume fractions; and Fig. 3.8 (b)-3.10 (b) show the plots for transverse displacement in y direction (U_2). As expected, the axial displacement (U_1) values for all the plots increases as the time progresses due to the mechanical load initially acting, and continues to increase further due to the thermal strains developed along with the deformation due to load. The transverse displacement (U_2), at first decreases because of the load acting in the axial direction (due to the effect of Poisson's ratio) and then increases because of the temperature effect.

The axial and transverse displacements for the detailed microstructural and effective models are in good agreement with each other for lower volume fractions. At higher volume fractions because of particle-particle interactions, mismatches are observed in the transverse displacement for composite with 50% volume content as shown in Fig 3.10 (b). This is due to the fact that the effective responses micromechanical model does not incorporate particle interactions.

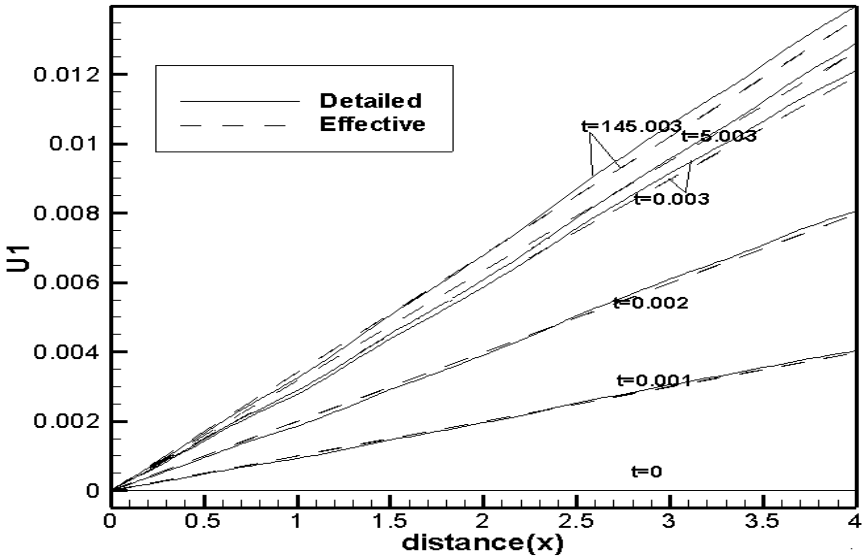

(a)

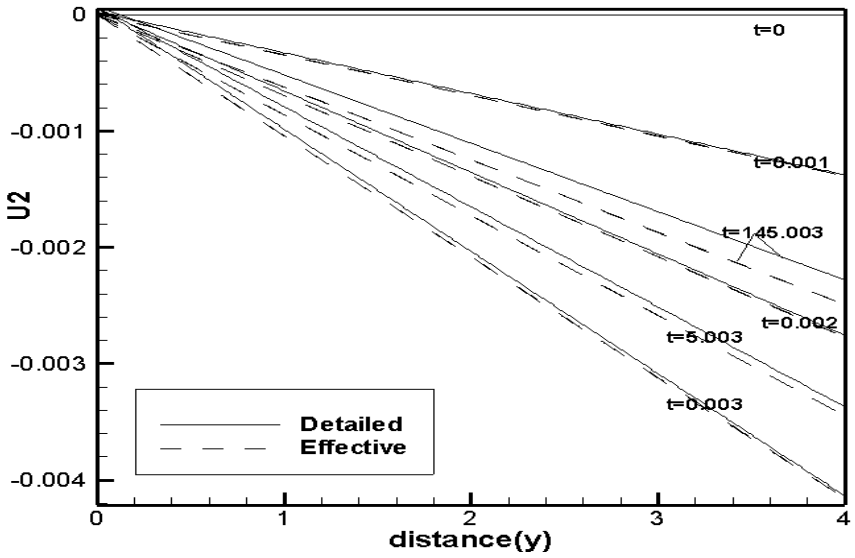

(b)

Fig. 3.8. Axial and transverse displacement plots for effective and detailed model for volume fraction 12.5%

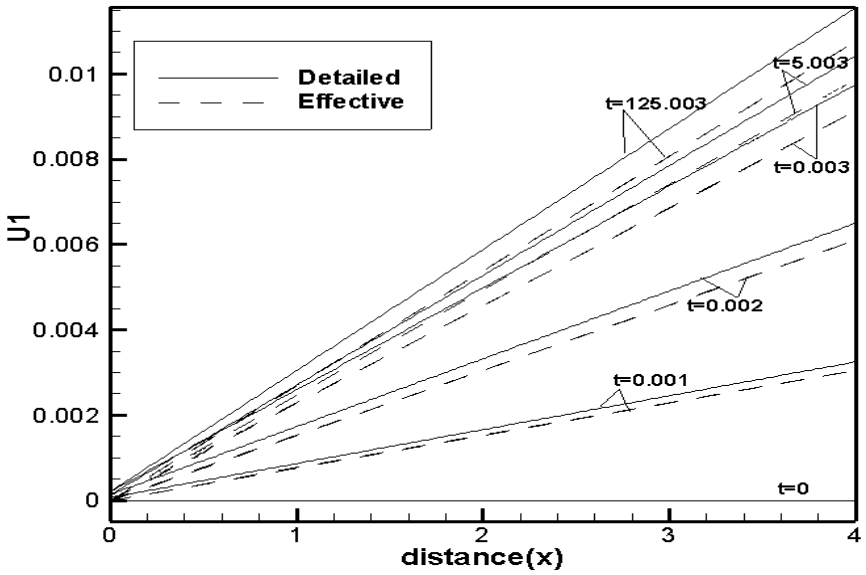

(a)

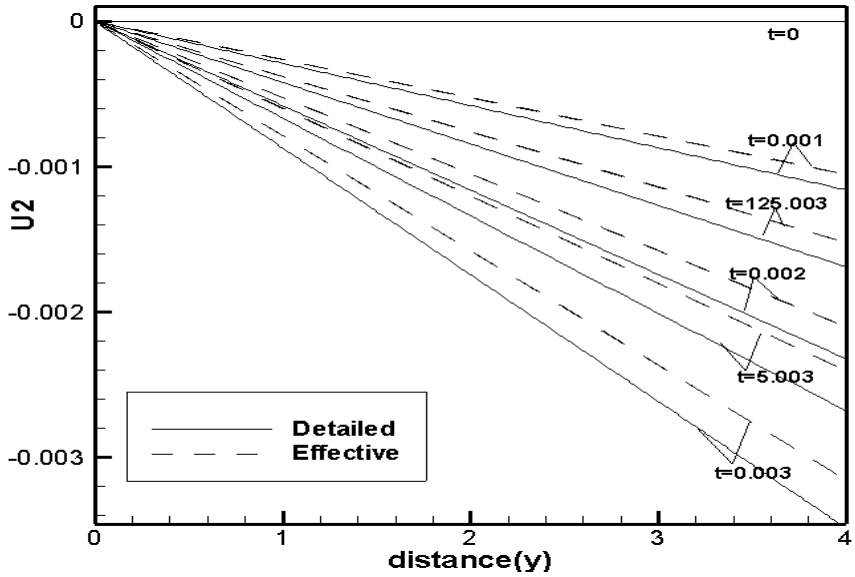

(b)

Fig. 3.9. Axial and transverse displacement plots for effective and detailed model for volume fraction 25%

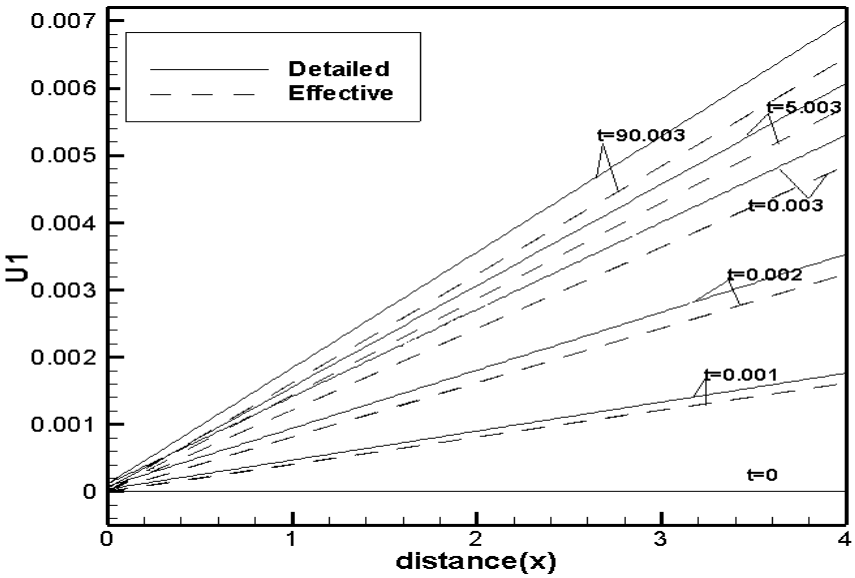

(a)

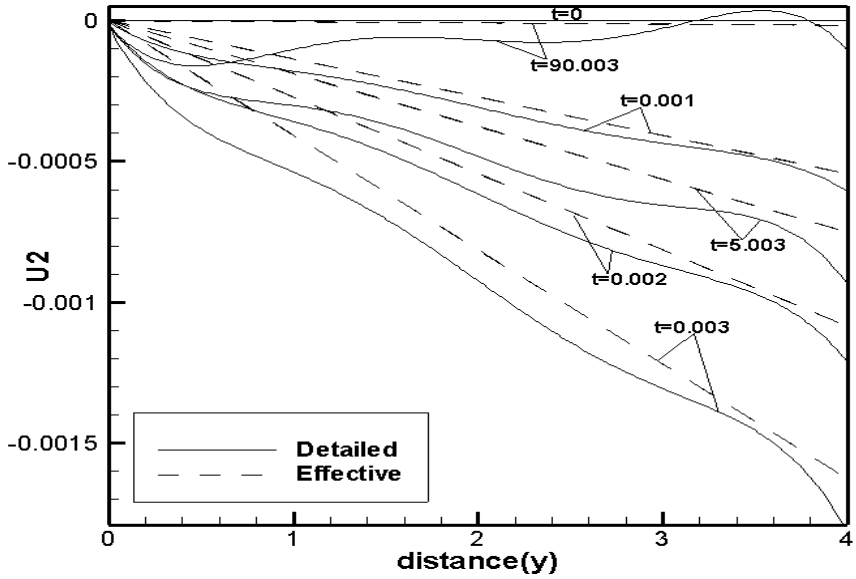

(b)

Fig. 3.10. Axial and transverse displacement plots for effective and detailed model for volume fraction 50%

3.4 Parametric studies on Discontinuity of stress and strain

In particle reinforced composites, as there is a sudden transition of properties from particle to matrix, it is expected that the interphase between particle and matrix experiences a jump in the magnitude of effective stress and strain. This jump in magnitude or discontinuity of effective stress and strain has an important role in the debonding between particles and matrix. In the present section, a study has been conducted on understanding the discontinuity of stress and strain at the interphase and the influence of various parameters, such as CTE ratio of particle and matrix, volume fraction of particles, temperature difference and degree of non-linearity on the discontinuities. The detailed model mesh as shown in Fig. 3.6 is used to study the stress discontinuity at the particle-matrix interphase. In order to study the influence of various parameters on the discontinuity of stress and strain at the particle-matrix interphase, the following procedure is followed.

The entire composite panel is assumed to be at a temperature of 303K initially. In the next step, the entire composite panel is brought to a temperature of ‘T’ by uniformly heating it. In the final step, a traction boundary condition of 40MPa is applied. Because of the difference in CTE for matrix and particle, the particles and matrix exhibit different thermal deformations. As displacement continuity at the bonded interphase has to be maintained, the mismatches in thermal deformation results in thermal stresses in the constituents and jump discontinuities in the stress values at the interphase. A parametric study is conducted to observe the influence of volume fraction of particles, CTE ratio, degree of nonlinearity and temperature change on the discontinuity of stress and strain.

Influence of Temperature changes and CTE ratio on Discontinuity

A parametric study is conducted by varying temperature changes ($\Delta T = 50$, 80, 100, and 300^0K) and the CTE ratio between particle and matrix $\alpha_P / \alpha_M = 0.01, 0.1, 1$ for composites with volume fraction of particles 12.5%. The von Mises stresses are monitored at three different locations, shown in Fig. 3.11.

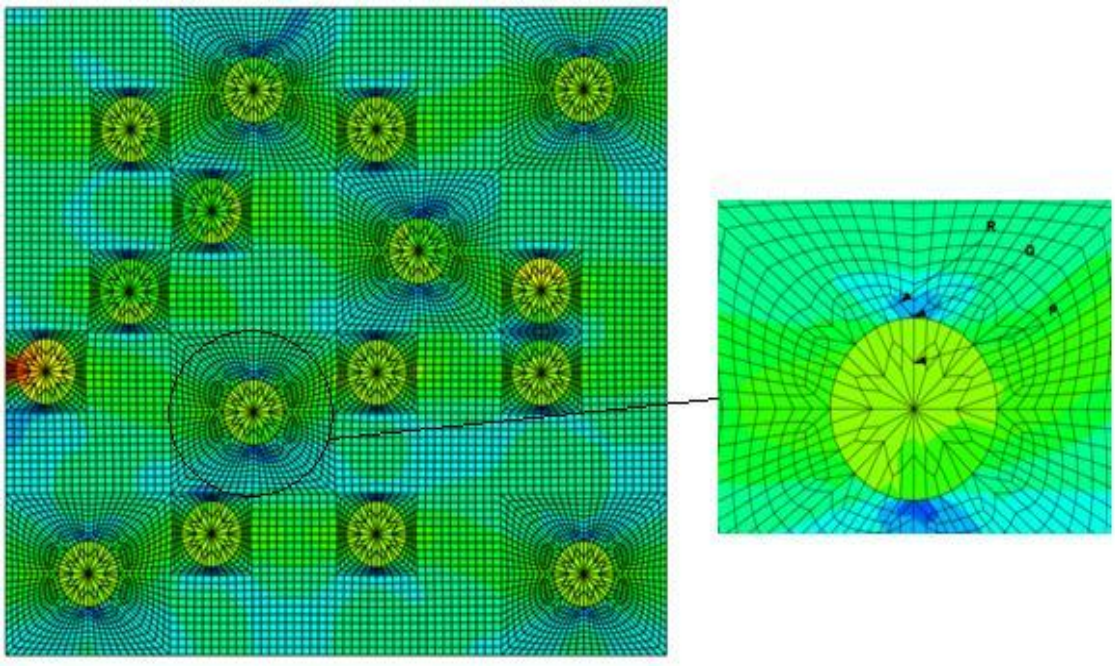

Fig. 3.11. Contour plot for von Mises for volume fraction 12.5% at location 1

The nodes P, Q and R are chosen in such a way that

P is inside the particle,

R is inside the matrix and

Q is on the matrix-particle interface.

We expect two distinct values of stress at the point Q. The difference between these values is represented by symbol $\Delta\sigma$, which is the magnitude of discontinuity in stress at a particular node. Tables 3.2 to 3.5 present the thermal stresses and combined thermal and mechanical stresses at locations P,Q and R for composites with various α_P / α_M ratios and temperature changes. As expected, thermal stress occurs when the CTE of particles and matrix are different. These values increase with increasing temperature changes and CTE ratio. Significant thermal stresses are observed in case d, where $\Delta T = 300$ and $\alpha_P / \alpha_M = 0.01$. The addition of thermal stress will eventually affect the overall or total stresses in the microstructural constituents. The difference in α_P and α_M increases jump discontinuity in stresses at the interphase. For example at $\Delta T = 300$, when $\alpha_P / \alpha_M = 1$, jump discontinuity is shown to be 12.29MPa, with $\alpha_P / \alpha_M = 0.01$, the jump discontinuity increases to 14.56MPa.

Case (1) DTEMP=50

Table 3.2. Influence of CTE ratio for a temperature change of 50^0K

CTE ratio	**node**	**Thermal Stress (MPa)**	**Combined Stress (Thermal+ Mechanical) (MPa)**
$(\alpha)_p/(\alpha)_M$ =1;	P	0.779452E-12	15.5786
$(\alpha)_p$ = 6e-06;	Q	0.74887E-12 } $\Delta\sigma = 0$	16.4167 } $\Delta\sigma = 12.293$
$(\alpha)_M$ = 6e-06	Q	1.76124E-12	4.12316
	R	1.56525E-12	5.59984
$(\alpha)_p/(\alpha)_M$=0.1;	P	5.84267E-01	15.8937
$(\alpha)_p$= 0.6e-06;	Q	5.79269E-01 } $\Delta\sigma$ = 0.257	16.7439 } $\Delta\sigma = 13.027$
$(\alpha)_M$ = 6e-06	Q	8.36927E-01	3.71674
	R	7.83483E-01	5.22183
$(\alpha)_p/(\alpha)_M$=0.01;	P	6.42686E-01	15.9261
$(\alpha)_p$= 0.06e-06;	Q	6.3719E-01 } $\Delta\sigma$ = 0.283	16.7773 } $\Delta\sigma = 13.095$
$(\alpha)_M$ = 6e-06	Q	9.20606E-01	3.68214
	R	8.61818E-01	5.18852

Case (2) DTEMP=80

Table 3.3. Influence of CTE ratio for a temperature change of 80^0K

CTE ratio	**node**	**Thermal Stress (MPa)**	**Combined Stress (Thermal+ Mechanical) (MPa)**
$(\alpha)_p/(\alpha)_M$ =1;	P	1.15406E-12	15.5787
$(\alpha)_p$ = 6e-06;	Q	1.18104E-12 } $\Delta\sigma = 0$	16.4168 } $\Delta\sigma = 12.293$
$(\alpha)_M$ = 6e-06	Q	2.81829E-12	4.12312
	R	2.50426E-12	5.5998
$(\alpha)_p/(\alpha)_{M=}$ 0.1;	P	9.3464	16.09
$(\alpha)_p$=0.6e-6;	Q	9.2667 } $\Delta\sigma =$ 0.412	16.9467 } $\Delta\sigma = 13.42$
$(\alpha)_M$ = 6e-06	Q	1.3388	3.52669
	R	1.25331	5.03575
$(\alpha)_p/(\alpha)_M$=0.01;	P	1.02809	16.1432
$(\alpha)_p$= 0.06e-06;	Q	1.01933 } $\Delta\sigma =$ 0.453	17.0016 } $\Delta\sigma = 13.51$
$(\alpha)_M$ = 6e-06	Q	1.47264	3.48322
	R	1.3786	4.99202

Case (3) DTEMP=100

Table 3.4. Influence of CTE ratio for a temperature change of 100^0K

CTE ratio	node	Thermal Stress (MPa)	Combined Stress (Thermal+ Mechanical) (MPa)
$(\alpha)_p/(\alpha)_M$ =1;	P	1.48964E-12	15.5788
$(\alpha)_p$ = 6e-06;	Q	1.58798E-12 } $\Delta\sigma = 0$	16.4169 } $\Delta\sigma = 12.29$
$(\alpha)_M$ = 6e-06	Q	3.52712E-12 }	4.12309 }
	R	3.1378E-12	5.59977
$(\alpha)_p/(\alpha)_M$=0.1;	P	1.16816	16.2237
$(\alpha)_p$= 0.6e-06;	Q	1.15822 } $\Delta\sigma$ = 0.515	17.0846 } $\Delta\sigma = 13.66$
$(\alpha)_M$ = 6e-06	Q	1.67327 }	3.42391 }
	R	1.56642	4.93154
$(\alpha)_p/(\alpha)_M$=0.01;	P	1.28494	16.2913
$(\alpha)_p$= 0.06e-06;	Q	1.27402 } $\Delta\sigma$ = 0.566	17.1542 } $\Delta\sigma = 13.77$
$(\alpha)_M$ = 6e-06	Q	1.84054 }	3.37993 }
	R	1.72301	4.88603

Case (4) DTEMP=300

Table 3.5. Influence of CTE ratio for a temperature change of 300^0K

CTE ratio	node	Thermal Stress (MPa)	Combined Stress (Thermal+ Mechanical) (MPa)
$(\alpha)_p/(\alpha)_M$ =1;	P	2.16426E-12	15.5795
$(\alpha)_p$ = 6e-06;	Q	2.00791E-12 } $\Delta\sigma = 0$	16.4178 } $\Delta\sigma = 12.29$
$(\alpha)_M$ = 6e-06	Q	3.83184E-12 }	4.12284 }
	R	3.40558E-12	5.5995
$(\alpha)_p/(\alpha)_M$ =0.1;	P	3.49999	17.6725
$(\alpha)_p$ = 0.6e-06;	Q	3.47084 } $\Delta\sigma$ = 1.54	18.5649 } $\Delta\sigma = 14.67$
$(\alpha)_M$ = 6e-06	Q	5.01283 }	3.88575 }
	R	4.69274	5.07459
$(\alpha)_p/(\alpha)_M$=0.01;			
	P	3.8497	17.9057
$(\alpha)_p$ = 0.06e-06	Q	3.81774 } $\Delta\sigma$ = 1.695	18.8014 } $\Delta\sigma = 14.56$
	Q	5.51361 }	4.23311 }
$(\alpha)_M$ = 6e-06	R	5.16155	5.26256

Influence of Degree of nonlinearity and Volume fraction on Discontinuity

The effect of linearity and nonlinearity in elastic modulus and thermal conductivity of the constituents on the magnitude of discontinuity in stress and strain is examined. The composites with volume fraction of particles 12.5%, 25% and 50% are subjected to temperature changes 300K. To include the thermal stress effects in the overall nonlinear responses, composites with $\alpha_p / \alpha_m = 0.01 \text{and} 1$ are also studied.

(a) V_f = 12.5%

The stress and strains are monitored at the particle, interphase and matrix regions indicated by A, B, C respectively as shown in Fig 3.12.

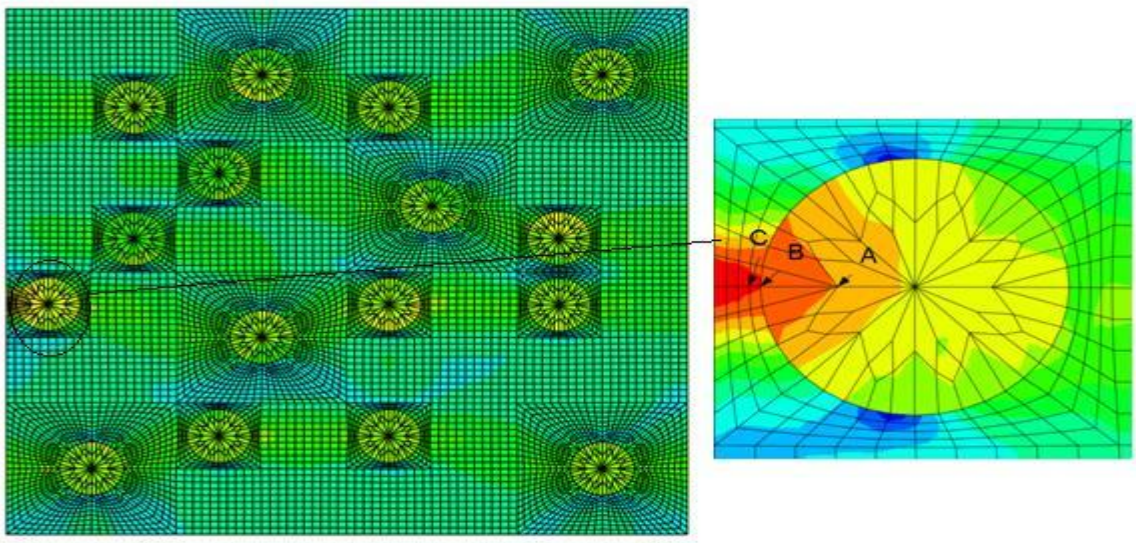

Fig. 3.12. Contour plot of von Mises at volume fraction 12.5% at location 2

Tables 3.6 and 3.7 present the measured strains and stresses at these three locations. It is seen when $(\alpha)_p/(\alpha)_M$ =1, the thermal stress is absent but significant jump in

the radial stain is observed. As discussed above, the interphase maintain displacement continuity condition without imposing strain continuity.

Table 3.6. Effect of CTE ratio on stress and strain discontinuity at volume fraction 12.5% for a temperature change of 300^0K and for a linear case (E^P=72000; E^M=2710.03; K^P=13; K^M=1.9)

CTE ratio	**Node**	**Radial Strain E11**	**Hoop Strain E22**	**Thermal Stress (MPa)**	**Combined Stress (Thermal+ Mechanical) (MPa)**
$(\alpha)_p/(\alpha)_M$ =1;	A	2.07E-03	1.76E-03	0	19.01
	B	2.08E-03	1.77E-03	0	19.78
$(\alpha)_p$ = 6e-06;	B	9.57E-03	1.74E-03	0	21.09
$(\alpha)_M$ = 6e-06	C	9.79E-03	0.83E-03	0	21.36
$(\alpha)_p/(\alpha)_M$ =0.01;	A	0.36E-03	-0.016E-03	5.17	24.07
	B	0.38E-03	-0.007E-03	5.64	25.38
$(\alpha)_p$ = 0.06e-06;	B	12.58E-03	-0.039E-03	8.74	28.84
$(\alpha)_M$ = 6e-06	C	12.83E-03	-1.176E-03	9.08	29.61

$\Delta\sigma$ = 1.31

$\Delta\sigma$ = 3.45

Table 3.7. Effect of CTE ratio on stress and strain discontinuity at volume fraction 12.5% for a temperature change of 300^0K and for a nonlinear case (temperature and stress dependent properties)

CTE ratio	**Node**	**Radial Strain E11**	**Hoop Strain E22**	**Thermal Stress (MPa)**	**Combined Stress (Thermal+ Mechanical) (MPa)**	
$(\alpha)_p/(\alpha)_M$ =1;	A	2.09E-03	1.76E-03	0	20.22	
$(\alpha)_p$ = 6e-06;	B	2.11E-03	1.76E-03	0	21.17	$\Delta\sigma$ = 1.14
$(\alpha)_M$ = 6e-06	B	10.06E-03	1.745E-03	0	22.31	
	C	10.29E-03	0.94E-03	0	22.66	
$(\alpha)_p/(\alpha)_M$ =0.01;	A	0.39E-03	-0.024E-03	6.24	26.33	
$(\alpha)_p$ = 0.06e-06;	B	0.42E-03	-0.027E-03	6.80	27.92	$\Delta\sigma$ = 3.04
$(\alpha)_M$ = 6e-06	B	13.42E-03	-0.59E-03	9.59	30.95	
	C	13.73E-03	-1.214E-03	10.12	31.85	

(b) V_f = 25%

Fig. 3.13 shows the contour of von Mises stress for 25% volume fraction of particles. The thermo-elastic analyses are performed both for linear and nonlinear constituent properties.

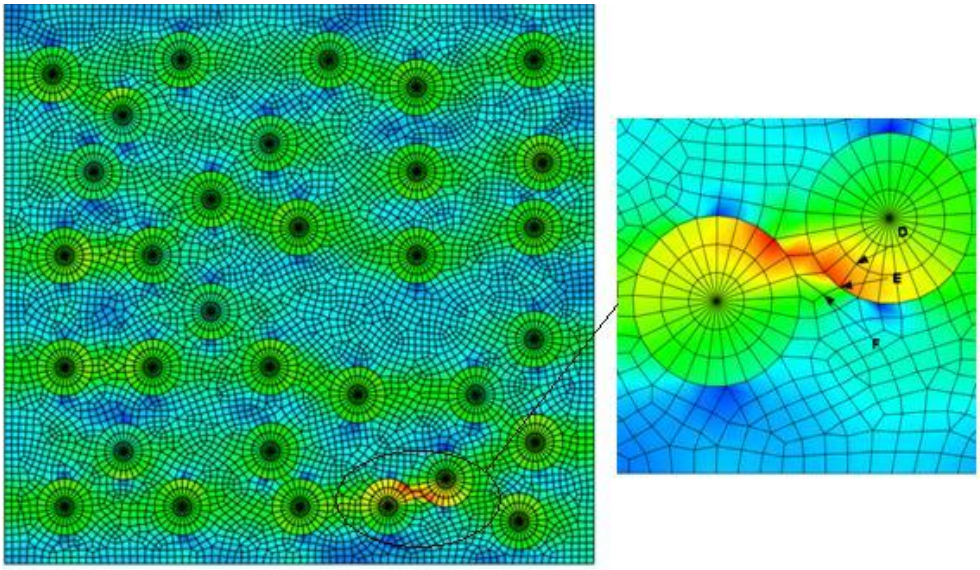

Fig. 3.13. Contour plot of von Mises at volume fraction 25%

The nodes D, E and F are chosen in such a way that

D is inside the particle,

F is inside the matrix and

E is on the matrix-particle interface.

Tables 3.8 and 3.9 present strains and stresses for the linear and nonlinear cases. It is observed that the stress discontinuities are more significant for composites with

volume fraction 25% as compared to the one with 12.5%. This is due to the particle interactions that may exist in the measured locations, as can be seen in Fig 3.13.

Table 3.8. Effect of CTE ratio on stress and strain discontinuity at volume fraction 25% for a temperature change of 300^0K and for a linear case

CTE ratio	**Node**	**Radial Strain E11**	**Hoop Strain E22**	**Thermal Stress (MPa)**	**Combined Stress (Thermal+ Mechanical) (MPa)**
$(\alpha)_p/(\alpha)_M$ =1;	D	2.10E-03	1.75E-03	0	21.04
$(\alpha)_p$ = 6e-06;	E	2.14E-03	1.75E-03	0	24.54 } $\Delta\sigma$ = 10.38
$(\alpha)_M$ = 6e-06	E	6.17E-03	-0.39E-03	0	14.16 }
	F	7.14E-03	0.62E-03	0	14.37
$(\alpha)_p/(\alpha)_M$ =0.01;	D	0.40E-03	-0.052E-03	6.39	27.33
$(\alpha)_p$ = 0.06e-06;	E	0.47E-03	-0.061E-03	7.93	32.33 } $\Delta\sigma$ = 13.34
$(\alpha)_M$ = 6e-06	E	6.49E-03	-1.437E-03	6.39	18.99 }
	F	8.23E-03	-0.475E-03	5.44	18.24

Table 3.9. Effect of CTE ratio on stress and strain discontinuity at volume fraction 25% for a temperature change of 300^0K and for a nonlinear case

CTE ratio	**Node**	**Radial Strain E11**	**Hoop Strain E22**	**Thermal Stress (MPa)**	**Combined Stress (Thermal+ Mechanical) (MPa)**
$(\alpha)_p/(\alpha)_M$ =1;	D	2.11E-03	1.75E-03	0	22.30
$(\alpha)_p$ = 6e-06;	E	2.17E-03	1.75E-03	0	26.08 } $\Delta\sigma$ = 8.62
$(\alpha)_M$ = 6e-06	E	6.09E-03	-0.66 E-03	0	17.45 }
	F	7.30E-03	0.56E-03	0	14.92
$(\alpha)_p/(\alpha)_M$ =0.01;	D	0.43E-03	-0.045E-03	6.99	29.17
$(\alpha)_p$ = 0.06e-06;	E	0.5E-03	-0.061E-03	8.38	34.22 } $\Delta\sigma$ = 8.35
$(\alpha)_M$ = 6e-06	E	6.20E-03	-2.004E-03	10.03	25.87 }
	F	8.401E-03	-0.684 E-03	6.41	19.29

(c) $V_f = 50\%$

The von Mises contour plot for volume fraction 50% is as shown below in Fig. 3.14.

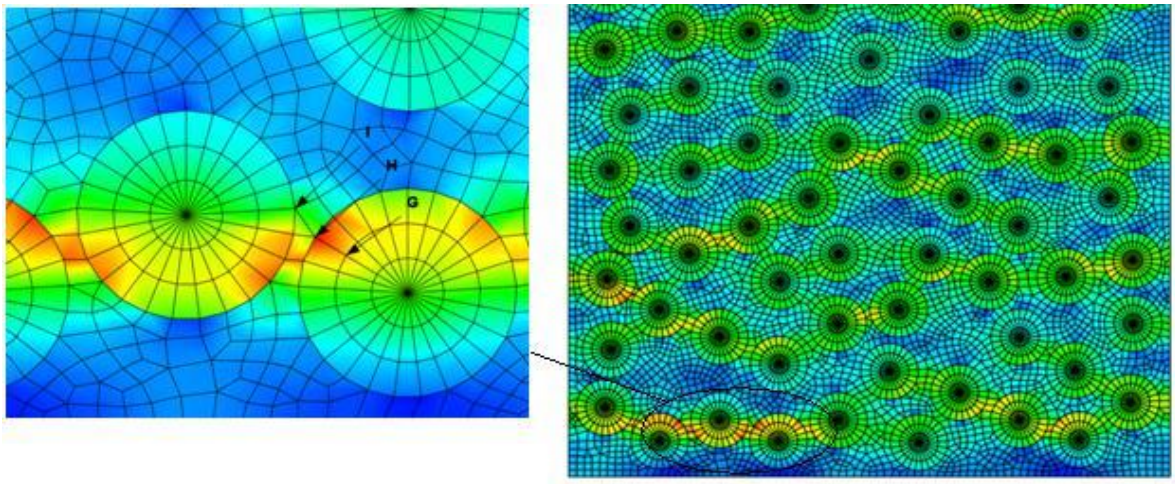

Fig. 3.14. Contour plot of von Mises at volume fraction 50%

The nodes G, H and I are chosen in such a way that

G is inside the particle,

H is on the matrix-particle interface and

I is inside the matrix (also an interphase node for an adjacent particle)

Stress and strain discontinuity is studied at the particle matrix interphase. For 50% volume fraction of particles, the particles are very close to each other. Hence the thermal stresses resulting from the mismatch of CTE contribute a good amount to the total stress. Tables 3.10 and 3.11 present the influence of CTE ratio on stress and strain discontinuity for linear and nonlinear cases when the volume fraction of particles is 50%. When CTE ratio is 1, the thermal stresses are of the order of 10^{-15} where as when

the CTE ratio is 0.01, the thermal stresses are absent. The magnitude of discontinuity of stress is less for a nonlinear case than the linear elastic case. For example (from table above), the $\Delta\sigma$ value for CTE ratio of 0.01 at node H was 14.62MPa where as for a nonlinear case it reduced to 13.05MPa.

Table 3.10. Effect of CTE ratio on stress and strain discontinuity at volume fraction 50% for a temperature change of 300^0K and for a linear case

CTE ratio	**Node**	**Radial Strain E11**	**Hoop Strain E22**	**Thermal Stress (MPa)**	**Combined Stress (Thermal+ Mechanical) (MPa)**
$(\alpha)_p/(\alpha)_M$ =1;	G	2.13E-03	1.71E-03	0	24.23
	H	2.22E-03	1.77E-03	0	30.05 $\Delta\sigma$ = 10.68
$(\alpha)_p$ = 6e-06;	H	8.92E-03	0.87E-03	0	19.36
$(\alpha)_M$ = 6e-06	I	7.33E-03	1.28E-03	0	15.23 $\Delta\sigma$ = 0.2748
	I	1.96E-03	1.76E-03	0	14.96
$(\alpha)_p/(\alpha)_M$ =0.01;	G	0.44E-03	-84.19E-06	7.077	31.10
	H	0.58E-03	-24.88E-06	10.35	40.31 $\Delta\sigma$ = 14.62
$(\alpha)_p$ = 0.06e-06;	H	11.01E-03	-534.62E-06	8.022	25.69
	I	8.83E-03	-287.56E-06	6.466	19.63 $\Delta\sigma$ = 0.25
$(\alpha)_M$ = 6e-06	I	0.19E-03	7.85E-06	6.262	19.38

Table 3.11. Effect of CTE ratio on stress and strain discontinuity at volume fraction 50% for a temperature change of 300^0K and for a nonlinear case

CTE ratio	**Node**	**Radial Strain E11**	**Hoop Strain E22**	**Thermal Stress (MPa)**	**Combined Stress (Thermal+ Mechanical) (MPa)**
$(\alpha)_p/(\alpha)_M$ =1;	G	2.12E-03	1.71E-03	0	23.93
	H	2.21E-03	1.76E-03	0	29.57 } $\Delta\sigma$ = 10.4
$(\alpha)_p$ = 6e-06;	H	8.64E-03	0.88E-03	0	19.16 }
$(\alpha)_M$ = 6e-06	I	7.29E-03	1.27E-03	0	15.76 } $\Delta\sigma$ = 0.75
	I	1.95E-03	1.74E-03	0	15.01 }
	G	0.43E-03	-91.96E-06	6.88	30.40 } $\Delta\sigma$ = 13.05
$(\alpha)_p/(\alpha)_M$ =0.01;	H	0.56E-03	-43.661E-06	9.68	38.94 }
	H	0.01E-03	-707.33E-06	9.32	25.89 }
$(\alpha)_p$ = 0.06e-06;	I	8.75E-03	-376.71E-06	6.79	20.27 } $\Delta\sigma$ = 1.20
$(\alpha)_M$ = 6e-06	I	0.19E-03	10.95E-06	6.95	19.06

The following observations are summarized from the above parametric studies:

1) **CTE ratio**: For all the volume fractions and for both linear and nonlinear cases, as expected the thermal stresses increase the overall stress in the composite. The thermal stress increases with increasing temperature changes and the CTE ratios between particle and matrix.
2) **Volume Fraction**: For all the CTE ratios studied, as the volume fraction increases, the stresses developed also increases, which may be due to the particle interactions. The magnitude of $\Delta\sigma$ also increases with volume fraction.
3) **Degree of Nonlinearity**: For all the CTE ratios and for all volume fractions studied, the stress developed was more with nonlinearity in elastic moduli then the linear elastic case. However, the magnitude of discontinuity was more for a linear case than the nonlinear case.

For all the cases considered, the magnitudes of discontinuity for radial strains are more pronounced than the one of hoop strains. Hoop strains show mild discontinuities.

CHAPTER IV

COUPLED HEAT CONDUCTION AND THERMO-ELASTIC ANALYSIS OF THERMAL BARRIER COATING

The thermal efficiency of a gas turbine engine increases with increase in operating temperatures. Hence they are usually made up of different Ni based super alloy compositions, as discussed by Pusch [35] and Kulkarni [36]. For aerospace and other applications, the gas turbine engines need to be operated at an operating temperature of 1700^0C or above, where as the melting point of most of the super alloys is less than 1300^0C. To prevent them from melting and to protect them from the damaging effects of heat, an advanced material system called "Thermal Barrier Coating (TBC)" is used now-a-days.

TBC's are made of materials with low thermal conductivity that coats a substrate of less thermal resistance in order to protect it from damaging effects of heat. They are designed in such a way that they not only reduce the temperature of the substrate via reducing the heat transfer through the coating layers, but also protect it from hot corrosion and oxidation as the material is prone to these damaging effects when subjected to thermal and mechanical loads simultaneously at high temperatures. Fig. 4.1 illustrates typical TBC systems.

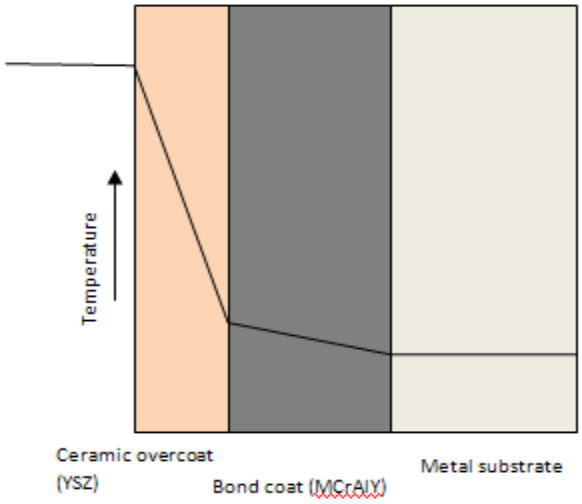

Fig. 4.1. Thermal barrier coating

The materials for TBCs should have

- Low thermal conductivity (to reduce the amount of heat transferred to the substrate or to maximize the temperature drop).
- High melting point
- High resistance to thermal shock and mechanical erosion, as discussed by Hass [37].
- Thermal expansion same or approximately equal to that of the substrate (otherwise there is a chance of debonding between the TBC and the substrate resulting in exposing the surface of the metal substrate to extremely high temperatures).

Ceramic overcoats form good TBCs, as they have very low thermal conductivity. But the thermal expansion coefficient of ceramics is significantly less when compared to

that of metal substrate. In order to reduce the debonding effect between the TBC and substrate, an additional layer called bond coat is commonly used. As discussed by Kulkarni [36] and Hass [37], bond coat is usually an Aluminum-rich layer of the form (MCrAlY) where M represents metal and is usually Nickel or Cobalt. As it is an Al-rich layer, it protects the metal substrate from oxidation by forming Aluminium oxide. Different thermal expansion coefficients between layers in TBCs often lead to stress concentrations at the interface layers leading to debonding. To reduce stress discontinuities, functionally graded concept is used between the ceramic and metallic zones in the TBCs.

Functionally graded materials (FGMs) are composites in which the distribution of the constituents is spatially varied in a controlled manner to obtain the desired spatial variation of macroscopic properties. The use of FGMs in TBCs can effectively separate a region of high temperature with a region of low temperature. A typical functionally graded material used for Thermal barrier applications is as shown in the Fig 4.2. It usually consists of 3 zones viz. Ceramic zone, Ceramic-metallic zone and metallic zone.

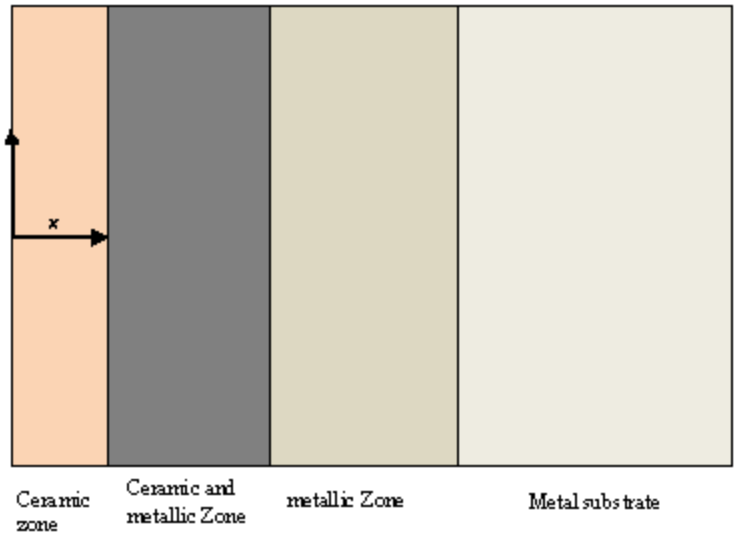

Fig. 4.2. Functionally graded thermal barrier coating

Ceramic zone is usually made up of Yttrium Stabilized Zirconia (YSZ). It has very low conductivity and acts as a good insulating material. Hence, the maximum drop in temperature is observed in this zone. Ceramic-metallic zone consists of ceramic particles embedded in a metallic matrix. The region nearer to the ceramic phase consists of more ceramic particles and the concentration of ceramic particles gradually decreases towards the metallic zone. The primary purpose of this layer is to ensure that the transition of thermo-mechanical properties is gradual from ceramic zone to metallic zone and thus prevents any spallation or delamination between these zones.

This chapter demonstrates the capability of the integrated micromechanical model and FE analyses in simulating coupled heat conduction and thermo-elastic deformation of TBCs. An example of TBC is considered and the micromechanical model is used to determine the effective thermal and mechanical properties of particle

reinforced composites used in TBCs under thermal stimuli. The TBC system considered consists of rectangular plates piled one over the other in such a way that the layers with higher ceramic concentration are bonded to the metal substrate via the lower ceramic concentration layers. Sequentially coupled heat conduction and stress analysis are performed. The purpose is to quantify thermal stresses developed during temperature changes in a composite system having different layers of materials like in TBCs.

Fig. 4.3 illustrates a TBC layup which can be used for insulating purposes at extremely high temperatures. It consists of six layers which are piled up as shown in the figure. The first bottom layer is made up of metal substrate (like Inco HX) where as the 2nd layer is made up of NiCrAlY matrix reinforced with YSZ (Yttrium Stabilized Zirconia) particles with volume fraction 4%. From 2^{nd} layer to 6^{th} layer, the concentration of YSZ particles increases gradually with 3^{rd}, 4^{th}, 5^{th} & 6^{th} layers containing 25%, 50%, 75% & 88% of YSZ particles, respectively.

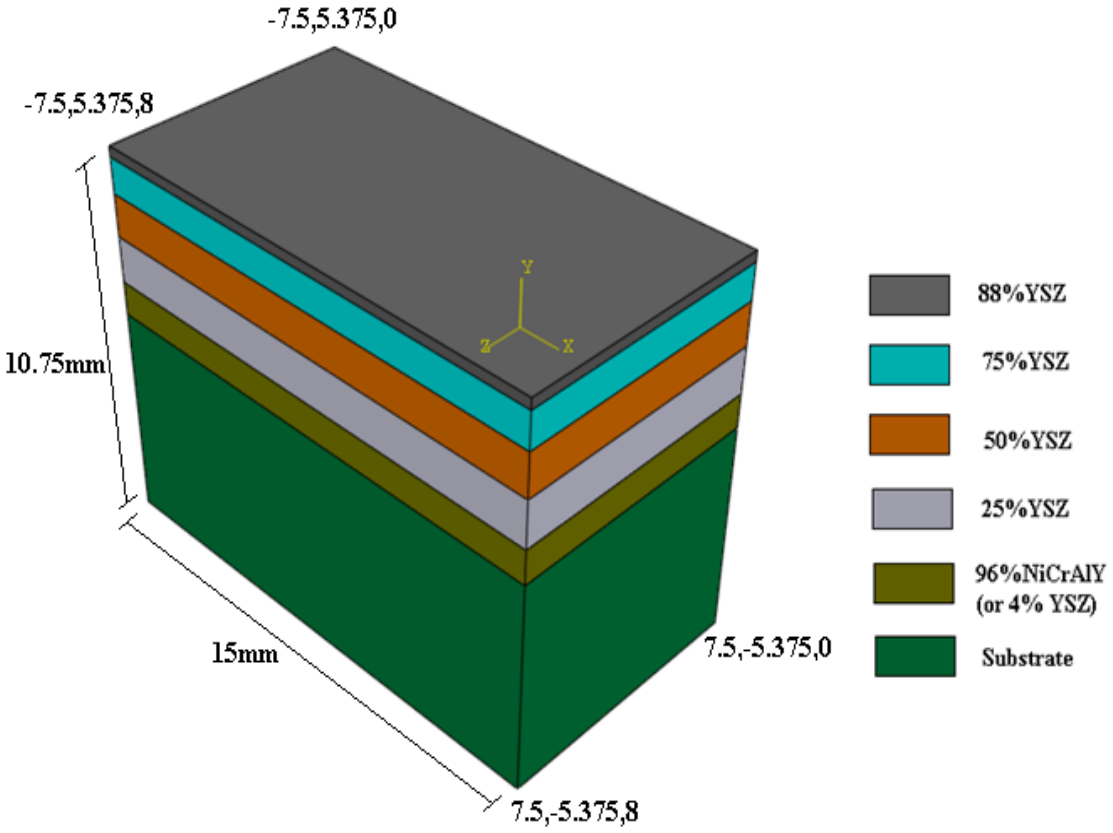

Fig. 4.3. Geometry of TBC plate

TBCs are manufactured by either Electronic beam vapor deposition process (EB-PVD) or Air Plasma (APS) methods. The fabrication temperature of TBC in these manufacturing methods is around 427^0C, as discussed in Zhu et al. [38]. From this temperature, they are rapidly cooled to room temperature before they can be put into use for thermal insulation applications. Because of this rapid cooling, residual stresses would develop which could result in premature failure of the composite. Sequentially coupled heat conduction and thermo elastic analysis are performed on the TBC layup to simulate

the cooling down process before applying other external stimuli. FE analyses with integrated micromechanical model are used. The FE mesh is shown in Fig 4.4 and it is made up of DC3D8 and C3D8 elements for the thermal and structural analysis, respectively. The following steps are followed to conduct the thermal and mechanical analysis:

- Initially all the nodes are assumed to be at a temperature of 427^0C.

$$T(x, y, z, 0) = 427 \;\; \forall -7.5 \le x \le 7.5; -5.375 \le y \le 5.375 \& 0 \le z \le 8$$

- Constant temperature boundary condition is applied on all the faces of the composite layup , which can be written as:

$$T(\pm 7.5, y, z, t) = T(x, \pm 5.375, z, t) = T(x, y, 0, t) = T(x, y, 8, t) = 30^0\,\text{C}$$
$$\forall -7.5 \le x \le 7.5; -5.375 \le y \le 5.375 \& 0 \le z \le 8$$

Where t (=10 sec) is the time period for which the cooling is performed on the composite system.

- For heating the composite, a constant temperature boundary condition is used on the top surface of 6^{th} layer for a time period of 13 seconds, after the cooling period ends.

$$T(x, 5.375, z, t) = 1300 \;\; \forall \;\; t \ge 11$$

The heat conduction process is monitored until this period of time. Thermal stresses are also monitored during the heating and cooling process.

- During the cooling and heating periods, the following mechanical constraints are also applied

$$u_x(-7.5, y, z, t) = u_y(x, -5.375, z, t) = u_z(x, y, 0) = 0$$
$$\forall -7.5 \le x \le 7.5; -5.375 \le y \le 5.375 \& 0 \le z \le 8$$

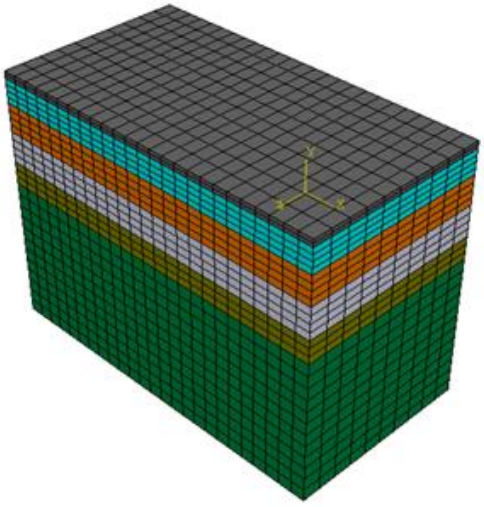

Layer	Material	Thickness(mm)
1	Metal Substrate	6
2	96% NiCrAlY or 4% YSZ	0.95
3	25% YSZ	1.3
4	50%YSZ	1.2
5	75%YSZ	1.0
6	88%YSZ	0.3

Fig. 4.4. Finite element mesh of a TBC plate and thickness of layers

The material properties used in the TBC plate are taken from Seo et al. [39] and are as listed in the following tables. Table 4.1, Table 4.2 and Table 4.3 give the material properties of metal substrate, 100%NiCrAlY and 100%YSZ at various temperatures.

Table 4.1. Material properties of metal substrate

Temperature (^{0}C)	Conductivity (W/mmK)	Elastic modulus (MPa)	Expansion (/^{0}C)	Specific Heat (J/Kg^{o}C)	Density (kg/mm^3)	Poissons ratio
20	90.5e-3	207e03	1.27e-05	460	8880e-9	0.312
400	65.3e-3	182e03	1.64e-05	460	8880e-9	0.312
800	73.9e-3	150e3	1.8e-05	460	8880e-9	0.312

Table 4.2. Material properties of 100% NiCrAlY

Temperature (^{0}C)	Expansion (/^{0}C)	SpecificHeat (J/Kg^{o}C)	Density (kg/mm^3)	Poissons ratio
20	1.4e-05	600	7320e-9	0.3
400	2.4e-05	600	7320e-9	0.3
800	4.7e-05	600	7320e-9	0.3
1200	7.1e-05	600	7320e-9	0.3

Table 4.3. Material properties of 100%YSZ

Temperature (^{0}C)	Expansion (/^{0}C)	Specific Heat (J/Kg^{o}C)	Density (kg/mm^3)	Poisson's ratio
20	7.2e-06	600	6037e-9	0.25
400	9.4e-06	600	6037e-9	0.25
800	1.6e-06	600	6037e-9	0.25
1200	2.2e-06	600	6037e-9	0.25

Matrix (NiCrAlY) is assumed to be nonlinear elastic, (i.e., dependent on temperature) and the particle (YSZ) is assumed to be linear elastic:

$$E_M = 0.0258T^2 - 80T + 200000 \text{ and } E_P = 52e03 \text{ Mpa} \quad (4.1)$$

Conductivity of both particle and matrix are assumed to degrade linearly with temperature:

$$K_M = 10^{-9}T^3 + 4*10^{-6}T^2 + 0.003T + 4.222 \text{ and} \quad (4.2)$$

$$K_P = -10^{-9}T^3 + 2*10^{-6}T^2 - 0.001T + 1.531 \quad (4.3)$$

These nonlinearities are accommodated through a user subroutine, and the material properties for each layer (for varying YSZ concentration) can be obtained with the help of the same subroutine. Micromechanical model is used to determine the effective properties of each layer and thereby the overall response of the composite, as discussed in CHAPTERS II and III. The responses from the coupled heat conduction and thermo-elastic deformation in the studied TBC are discussed as follows.

4.1 Temperature profiles

During the cooling period, a constant temperature boundary condition is applied on all the outer surfaces of the composite, in order to cool it to room temperature from fabricating temperature (427^0C). The purpose of doing this is to investigate the thermal stresses developed within layers in the TBC during the cooling down process. This process is done for a time period of 10 seconds. After the cooling down process is completed, a constant temperature boundary condition is applied on outer surface of 88% YSZ layer during the heating process for a time period of 13 seconds, after the

cooling period ends. Fig. 4.5 shows the contour plot through the thickness of all layers during heating process at t=23 seconds, and Fig.4.6 shows temperature distribution through the thickness during the cooling and heating process. From Fig. 4.6, at t=10 sec the entire composite is approximately at 30^0C. At the end of heating process i.e., when t=23 sec, the outer surface of 88% YSZ layer has reached 1300^0C where as the metal substrate is at a temperature of 180^0C. Maximum temperature drop is observed in 88% YSZ layer, as expected.

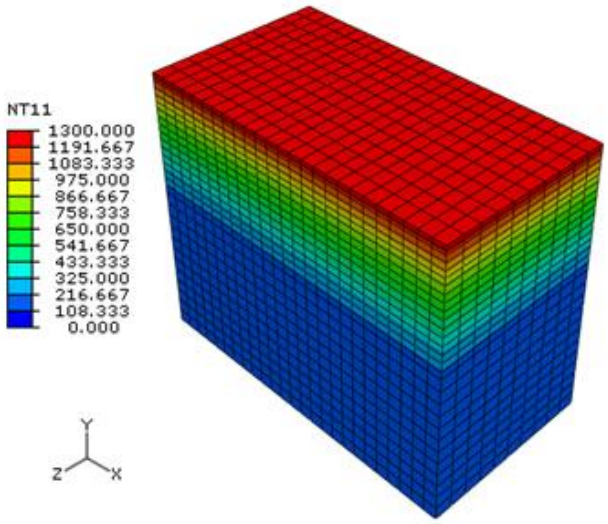

Fig. 4.5. Contour plot of temperature during heating process at t=23 sec

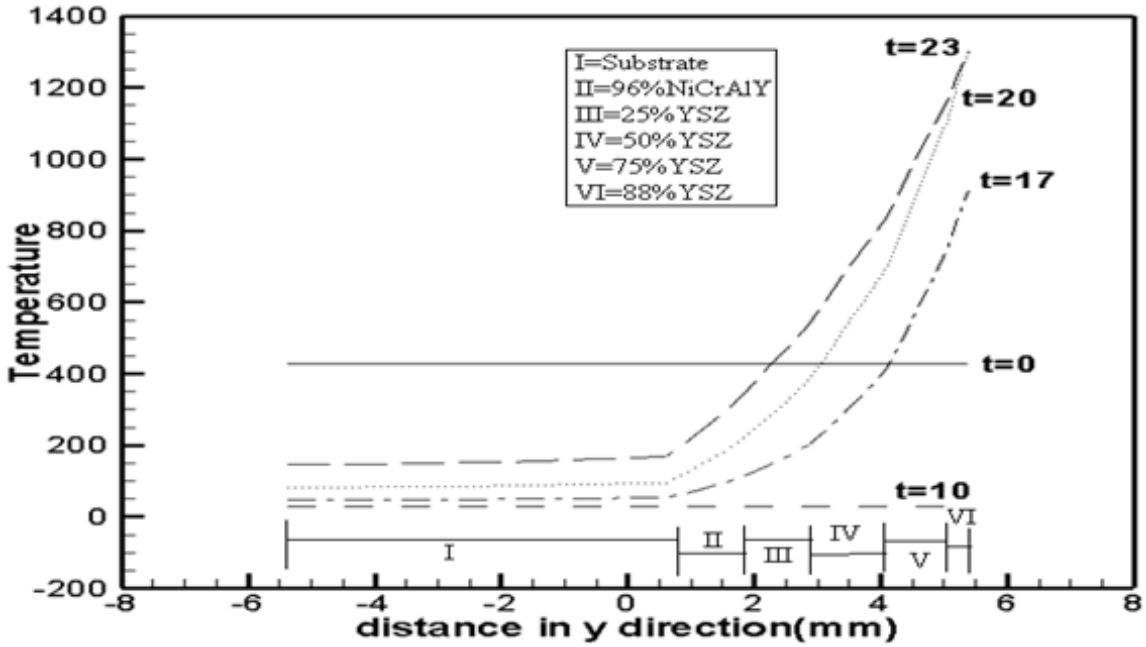

Fig. 4.6. Temperature distribution through the thickness of TBC layers during cooling and heating steps

4.2 Stress distribution

The contour stress plots shown in Fig.4.7 (a) and Fig.4.8 (a) are at the initial time increments in the cooling period and the contour stress plots shown in Fig.4.7 (b) and Fig.4.8 (b) are at t=23 sec during heating step. Stress distribution plots through the thickness of various layers at different times for both cooling and heating periods are as shown in Fig.4.9 to Fig.4.12.

The longitudinal stress (S_{11}), transverse stress (S_{33}) and shear stress (S_{12}) values during both cooling and heating steps are observed to be higher in metal substrate than

the ceramic layers. When the TBC is cooled, as the thermal expansion coefficient is higher for the metal substrate than that of ceramic, it tries to contract more than the ceramic layer but the ceramic layer prevents it from contracting. Thus tensile stresses develop in the metal substrate and compressive stresses develop in the ceramic. This fact can be seen in both the contour profiles shown in Fig. 4.7 and Fig. 4.8.

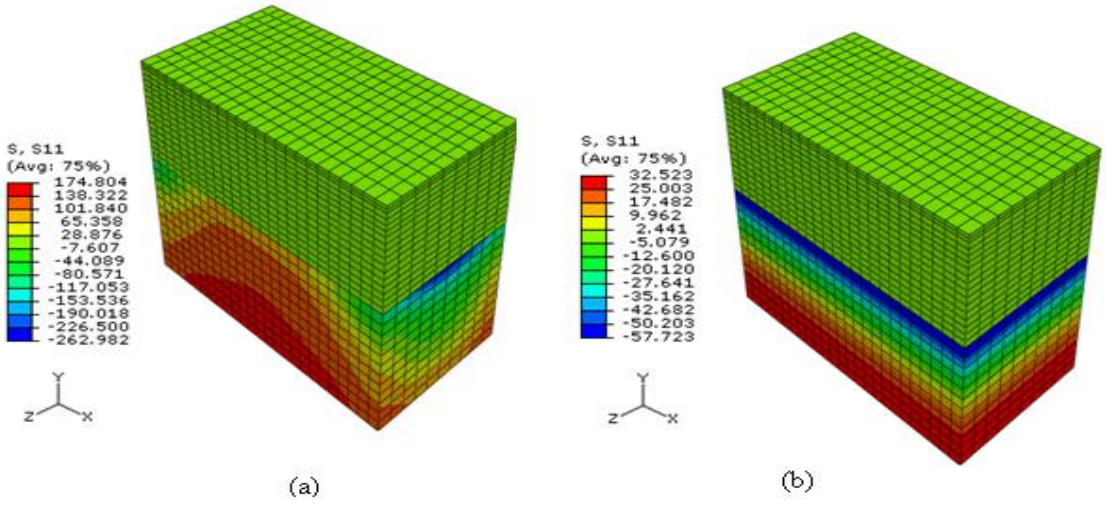

Fig. 4.7. Longitudinal stress contour plot for (a) cooling process and (b) heating process

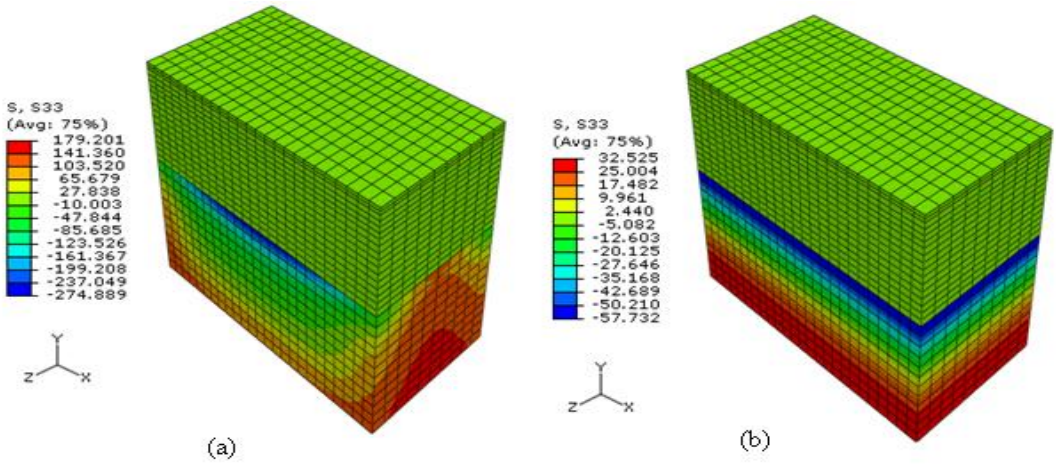

Fig. 4.8. Transverse stress contour plot for (a) cooling process and (b) heating process

Fig. 4.8(a) shows that the residual stresses developed in the metal substrate during the initial cooling period are very high when compared to the other layers. This cause can be attributed to the fact that thermal expansion coefficient is higher for metal substrate. During the heating period, when composite is heated the stresses developed in metal substrate are more than that in ceramic. As the TBC is heated, the metal substrate tries to expand more than the ceramic as it has higher CTE. Because of this compressive stress develops in metal and tensile in ceramic. This is the reason for the stresses to decrease from the cooling step to heating step in the metal substrate. However, as the young's modulus of the metal substrate is higher than ceramic, it offers more resistance to deformation and develops more stresses. This increase in stress combined with the

residual stresses developed in the cooling step ensures that the stresses in metal substrate are tensile and higher than ceramic. Even though the thermal effect (because of heating) tries to reduce these stresses, the reduction is not significant enough to make the tensile stresses in metal substrate to become compressive, for the time period monitored.

Fig 4.9(a) shows the longitudinal stress distribution plot through the thickness of different layers, for the cooling period. During the initial times, the residual stress developed in the metal substrate is very high and it gradually reduces as time progresses in the cooling period (as the composite reaches steady state temperature). Fig 4.9(b) shows the longitudinal stress distribution plot through the thickness of various layers in the heating step. It can be seen that the stress developed is increasing, as the time progresses in the heating period.

Discontinuity in stresses ($S_{11,}$ S_{22} & S_{12}) is observed at all the interphases between layers. But the maximum discontinuity is observed at the metal substrate and 96%NiCrAlY layer. This fact can be seen in Fig. 4.9 to 4.12. As time progresses in the heating period, the discontinuity at this interphase is also increasing. The discontinuity at this interphase is very high and hence the possibility of debonding at this interphase is high.

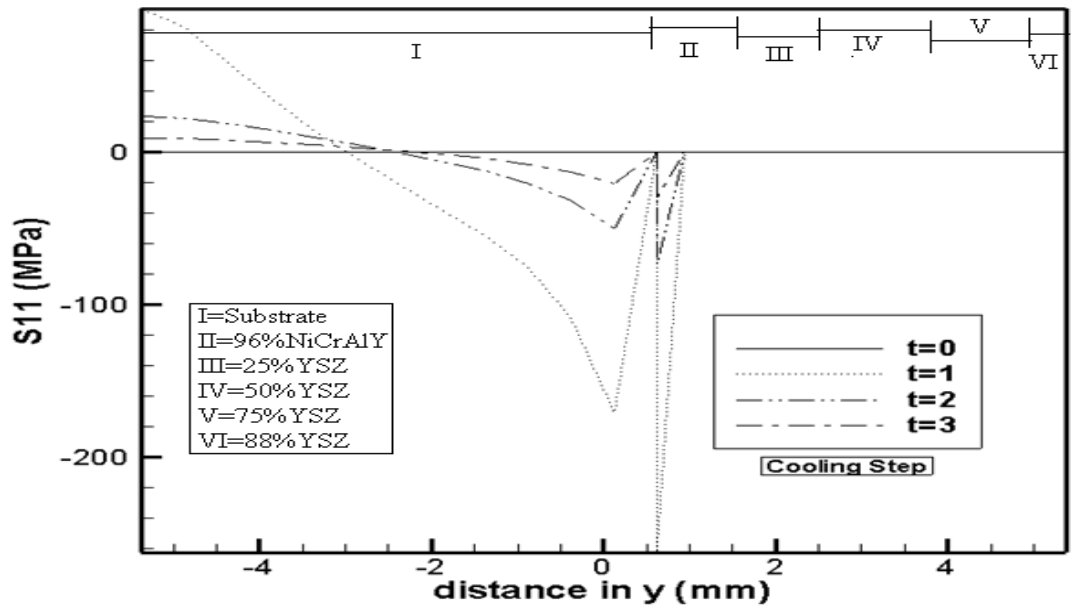

(a)

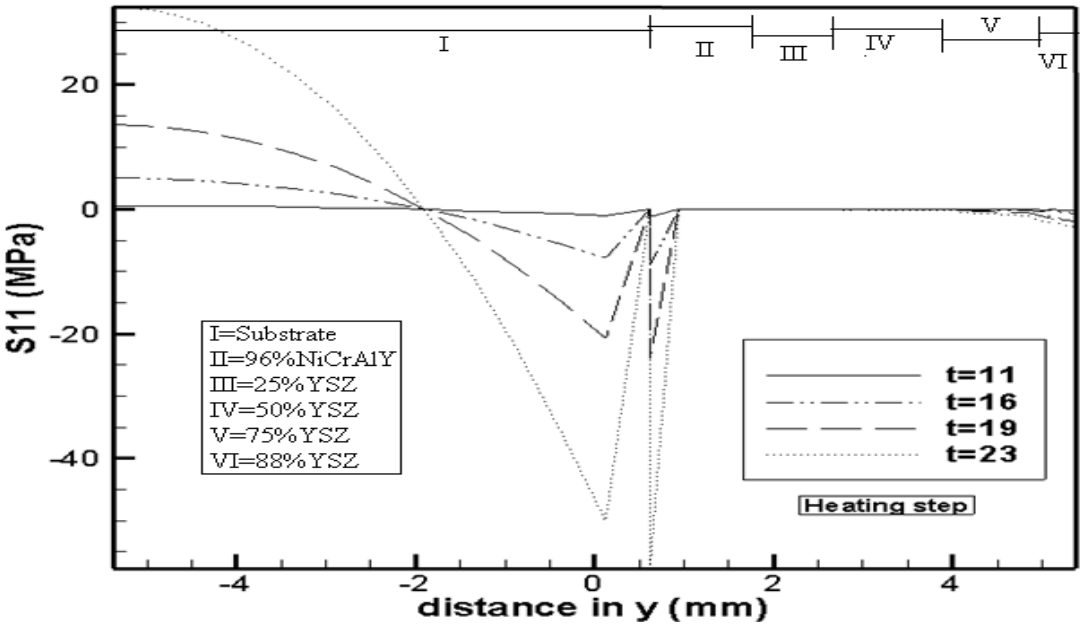

(b)

Fig. 4.9. Longitudinal stress (S_{11}) distribution through the thickness of TBC layers for (a) cooling and (b) heating period

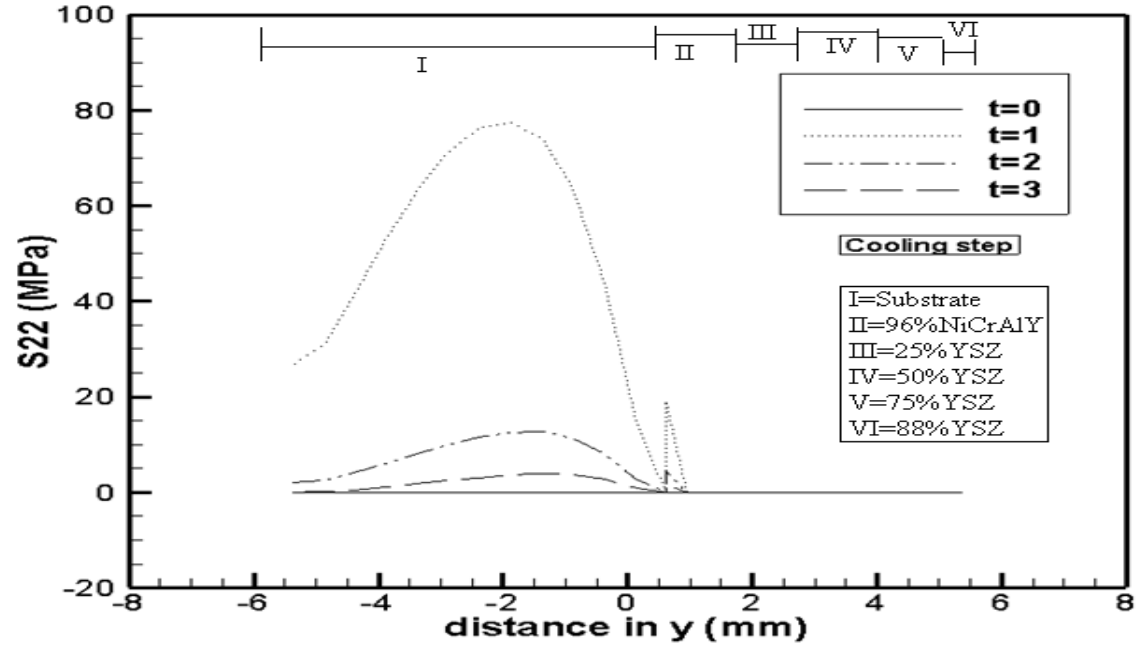

(a)

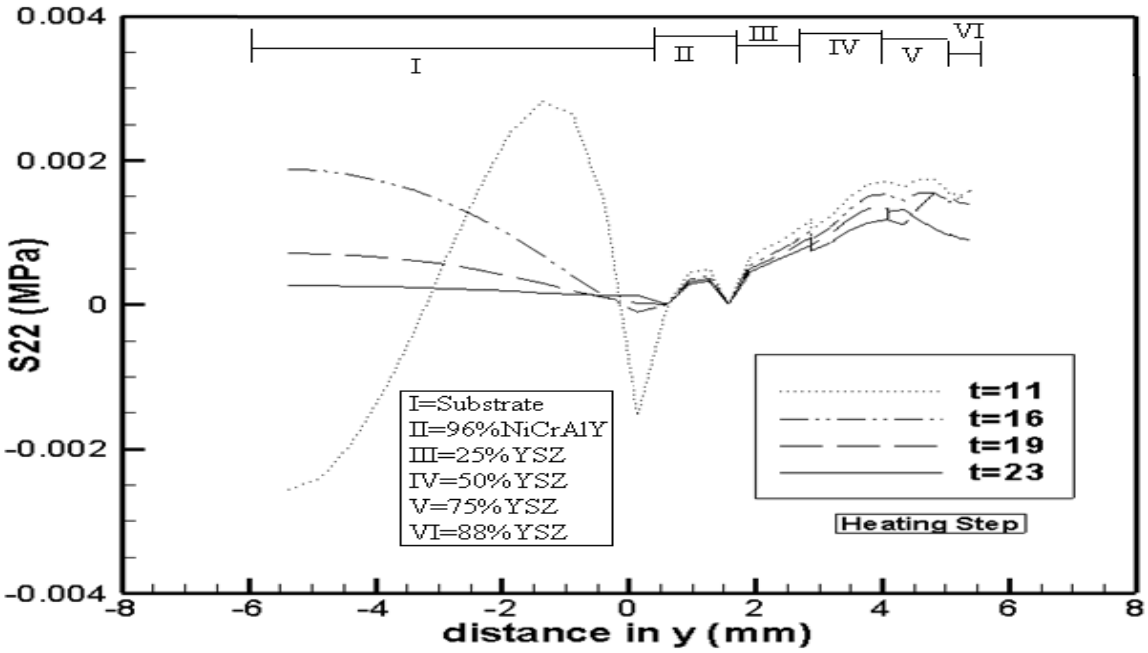

(b)

Fig. 4.10. Transverse stress (S_{22}) distribution through the thickness of TBC layers for (a) cooling and (b) heating period

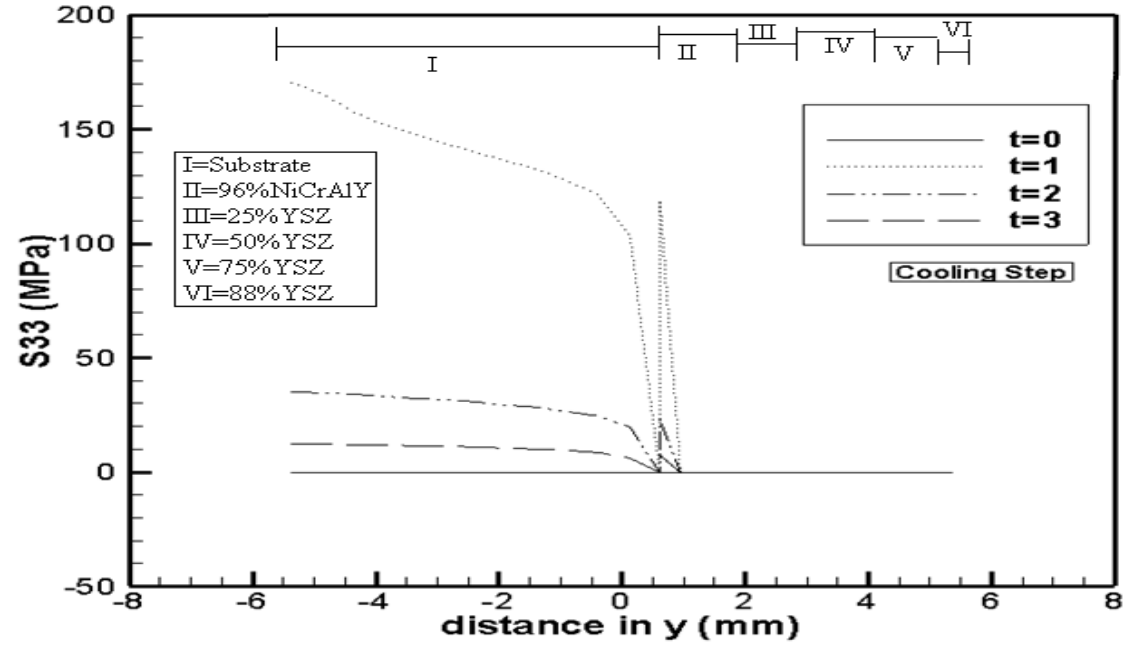

(a)

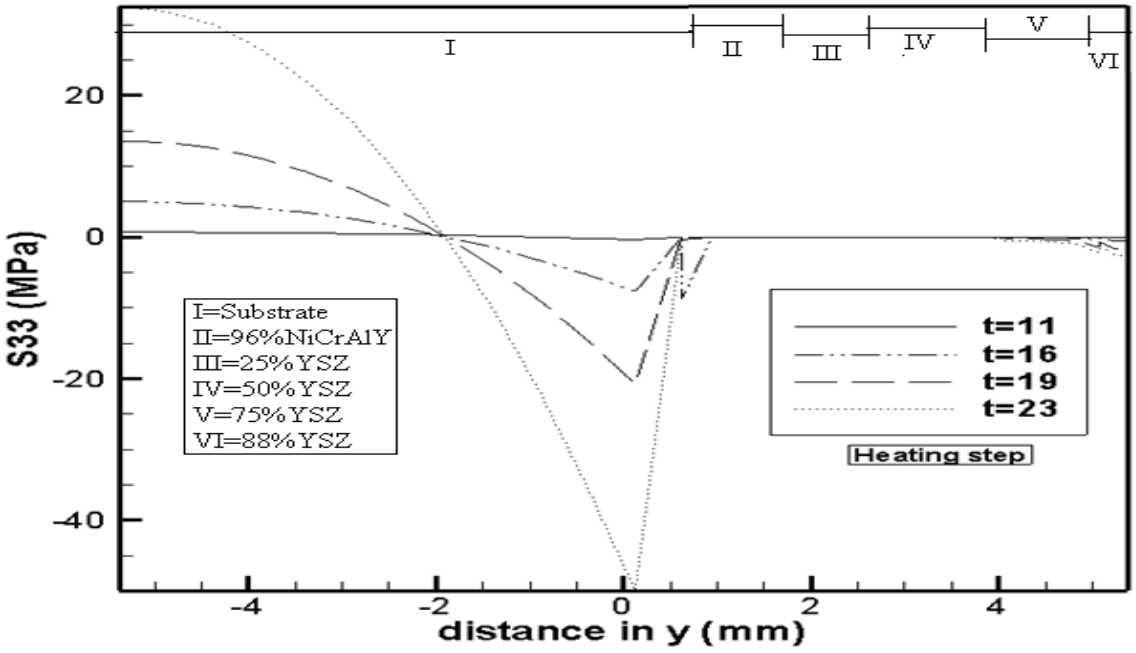

(b)

Fig. 4.11. Transverse stress (S_{33}) distribution through the thickness of TBC layers for (a) cooling and (b) heating period

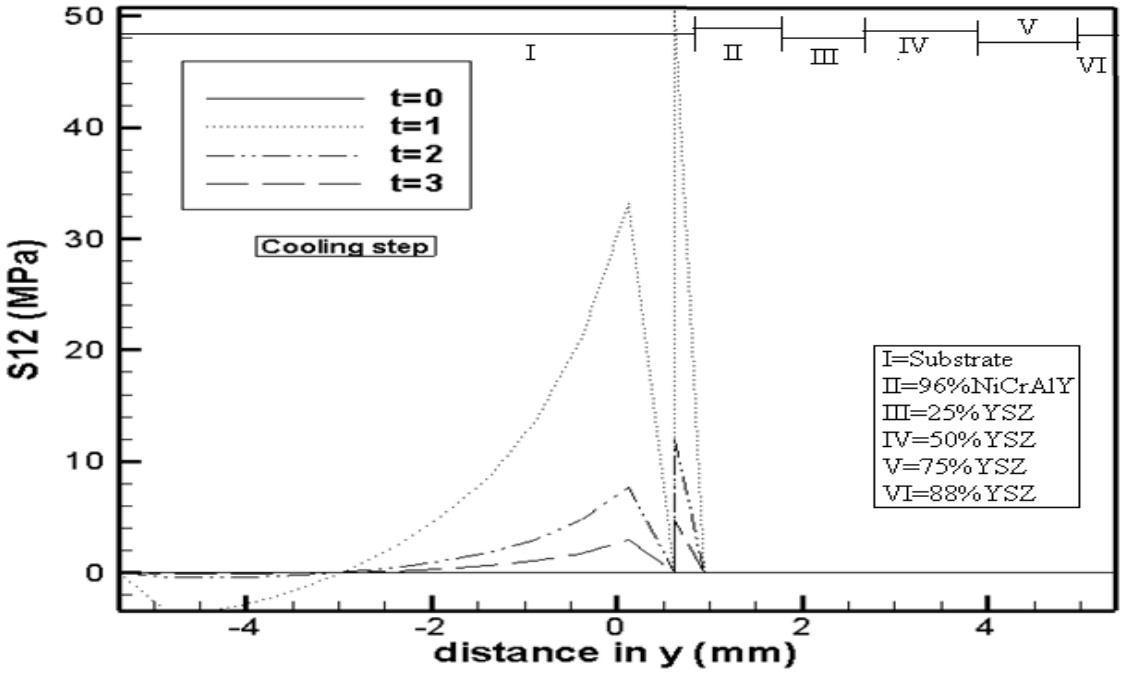

(a)

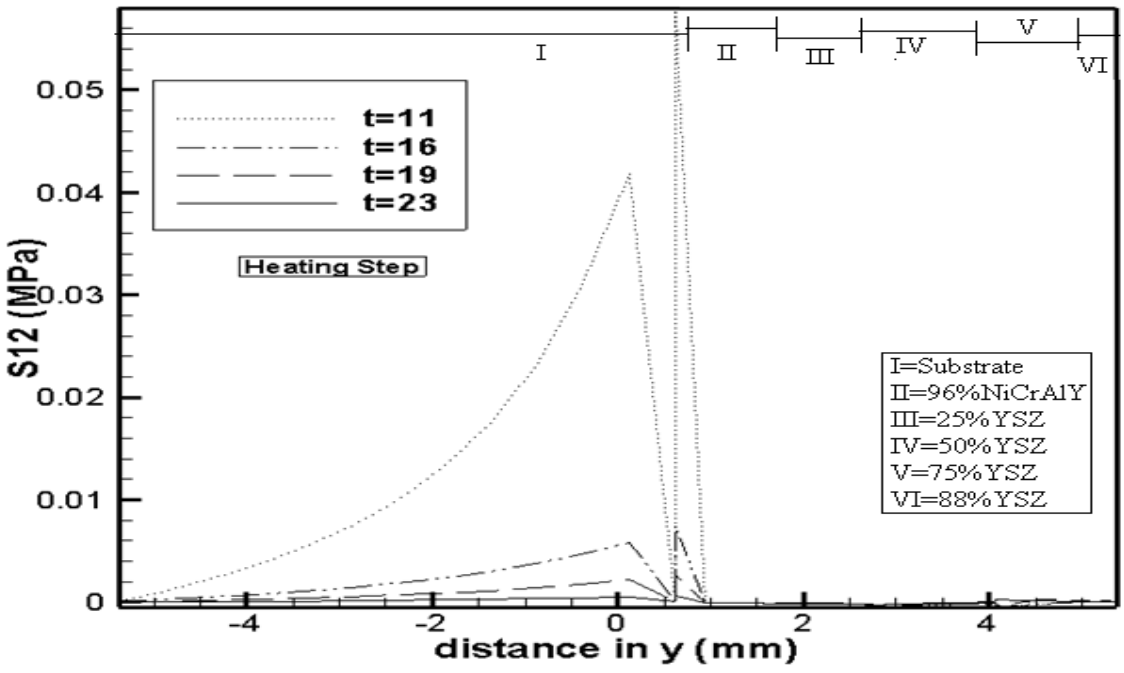

(b)

Fig. 4.12. Shear stress (S_{12}) distribution through the thickness of TBC layers for (a) cooling and (b) heating period

CHAPTER V

CONCLUSIONS AND FUTURE RESEARCH

5.1 Conclusions

A micromechanical model is used to determine effective (macroscopic) thermal and mechanical properties of particle reinforced composites. The micromechanical model is implemented in FE framework for analyzing coupled heat conduction and thermo-elastic deformation of a homogenized composite medium. The responses from the micromechanical model are compared with the ones generated from particles dispersed in homogeneous matrix, which represents more realistic composite microstructures. For that reason, a FE model that represents detailed particles randomly dispersed in a homogeneous matrix is generated. Sequentially coupled thermo-mechanical analyses are conducted for the two FE meshes for different volume fractions and the temperature, stress, and displacement fields in both models are compared. For both the cases ABAQUS user material subroutines UMATHT and UMAT are used to input the variation of thermal conductivity with temperature and elastic modulus with stress and temperature, respectively. Parametric studies on effects of conductivity ratio between particle and matrix, degree of nonlinearity, and volume fraction on the temperature distribution and steady state times have been studied.

From the above studies, it has been observed that at constant volume fraction, as the nonlinearity in thermal conductivity of the particle and matrix constituents increases, the steady state time significantly deviates from the ones with constant constituent properties. When the volume fraction of particles in the composite increases, the steady

state is reached in less time, since the thermal conductivity of particles are taken larger than that of the matrix. As the conductivity ratio increases while keeping constant volume fraction of particles, there has not been any significant difference in the effective thermal conductivities. The temperature profiles are compared for the homogenized and heterogeneous composite models at different times until the composite reaches steady state. For lower volume fractions (12.5 and 25%), the temperature profiles of both models are in good agreement with each other. But for higher volume fractions (50%), deviation has been observed between the models. The detailed model showed a wavy profile for temperature but the effective model showed no signs of it. The cause for this could be attributed to the fact that particle-particle interactions at higher volume fractions cannot be neglected and as effective model does not take into account these interactions, it deviates from the heterogeneous model behavior.

The effective thermo-elastic properties from the micromechanical model are compared with those of FE microstructural heterogeneous model. As expected, the axial displacement values for all the cases increases along with distance from the fixed end as the time progresses during the transient heat transfer analysis and continues to increase due to the stress and temperature dependency of the elastic modulus of matrix and the thermal strains developed in structural analysis. Transverse displacement initially decreases due to Poisson's ratio and then increases because of the temperature effect. The effective and heterogeneous model profiles for the axial and transverse displacements are in good agreement with each other for lower volume fractions. At

higher volume fractions because of particle-particle interactions, mismatches are observed in the transverse displacement for composite with 50% volume content.

In particle reinforced composites, as there is a sudden transition of properties from particle to matrix, it is expected that the interphase between particle and matrix experiences a jump in the magnitudes of stress and strain. This jump discontinuity of stress and strain has an important role in the debonding between particles and matrix. A study has been conducted on understanding the discontinuity of stress and strain at the interphase and the influence of various parameters like CTE ratio of particle and matrix, volume fraction of particles, temperature difference and degree of non-linearity on the discontinuities. The detailed FE microstructural model has been used to study the effective stress discontinuity at the particle-matrix interface. The entire composite panel is uniformly heated to a temperature from its initially uniform temperature and then a static uniaxial load is applied. Because of the difference in CTE for matrix and particle, the particles and matrix exhibit different thermal deformations. As displacement continuity at the bonded interphase has to be maintained, the mismatches in thermal strains results in thermal stresses in the constituents and jump discontinuities in the stress values at the interphase.

A parametric study is conducted by varying temperature changes ($\Delta T = 50$, 80, 100, and 300^0K) and the CTE ratio between particle and matrix $\alpha_P / \alpha_M = 0.01, 0.1, 1$ for composites with different volume fraction of particles. The von Mises stresses are monitored at the interphase of particle and matrix and two distinct values of stress are expected at the interphase nodes. The difference between these values represents the

magnitude of discontinuity in stress at that particular node. For all the volume fractions and for both linear and nonlinear thermo-elastic cases, as expected the stresses developed were more when the difference in thermal expansions were higher and the magnitude of discontinuity also follows the same trend. As the volume fraction increases keeping all other parameters constant, the stresses developed also increases. The magnitude of discontinuity also increases with volume fraction. For all the CTE ratios and for all volume fractions studied, the stress developed was higher with nonlinearity in the elastic modulus and thermal conductivity of the constituents involved than when linear constituent properties are assumed. However, the magnitude of discontinuity observed was higher for a linear case than the nonlinear case.

To demonstrate the applicability of the micromechanical model in simulating overall thermo-mechanical responses of larger scale of composite systems, sequentially coupled analysis has been performed on an example of functionally graded thermal barrier coatings (TBCs). A rectangular layup consisting of a metal substrate bonded to functionally graded plates is considered with gradually increasing ceramic particles in the metallic matrix for each layer.

5.2 Future research

The current study focuses on the determination of effective properties and the influence of various parameters at the microscale on the macroscopic behavior of the particle reinforced composites, but has been limited to only linear and nonlinear elastic cases. Further study can be conducted by extending the mechanical responses to include viscoelastic constitutive models.

In the present study only one way thermo-mechanically coupled analyses has been performed where in only the thermal field is assumed to influence the mechanical field. Further study can be conducted to include two way thermo-mechanically coupled analyses, i.e. both thermal and mechanical fields contributing to each other, can be analyzed.

It is also possible to extend the proposed micromechanical analysis approach to study other multi-field effects, such as coupled thermo-electro-mechanical responses in piezoelectric composites.

REFERENCES

[1]. Hashin Z, Shtrikman S. A variational approach to the theory of the elastic behaviour of multiphase materials. J Mech Phys Solids 1963;11(2):127-140.

[2]. Kari S, Berger H, Ramos RR, Gabbert U. Computational evaluation of effective material properties of composites reinforced by randomly distributed spherical particles. Compos Struct 2007;77(2):223-231.

[3]. Chen J, Xu L, Li H. Investigation on a direct modeling strategy for the effective elastic moduli prediction of composite material. Mater Sci Eng 2008;491(1-2):385-389.

[4]. Cho J, Joshia MS, Sun CT. Effect of inclusion size on mechanical properties of polymeric composites with micro and nano particles. Compos Sci Technol 2006;66(13):1941-1952.

[5]. Kanit T, Forest S, Galliet I, Mounoury V, Jeulin D. Determination of the size of the representative volume element for random composites: stastical and numerical approach. Int J Solids Struct 2003;40(13-14):3647-3679.

[6]. Kari S, Berger H, Gabbert U, Guinovart-Diaz R, Bravo-Castillero J, Rodriguez-Ramos R. Evaluation of influence of interphase material parameters on effective material properties of three phase composites. Compos Sci Technol 2008;68(3-4):684-691.

[7]. Hollister SJ, Kikuchi N. A comparison of homogenization and standard mechanics analyses for periodic porous composites. Computational Mechanics 1992;10(2):73-95.

[8]. Kaminski M. Boundary element method homogenization of the periodic linear elastic fiber composites. Eng Anal Bound Elem 1999;23(10):815-823.

[9]. Tszeng TC. The effects of particle clustering on the mechanical behavior of particle reinforced composites. Compos B Eng 1998;29(3):299-308.

[10]. Segurado J, Gonzalez C, Llorca J. A numerical investigation of the effect of particle clustering on the mechanical properties of composites. Acta Mater 2003;51(8):2355-2369.

[11]. Drugan WJ, Willis JR. A micromechanics-based nonlocal constitutive equation and estimates of representative volume element size for elastic composites. J Mech Phys Solids 1996;44(4):497-524.

[12]. Drugan WJ. Micromechanics-based variational estimates for a higher-order nonlocal constitutive equation and optimal choice of effective moduli for elastic composites. J Mech Phys Solids 2000;48(6-7):1359-1387.

[13]. Levesque M, Derrien K, Mishnaevski L, Baptiste D, Gilchrist MD. A micromechanical model for nonlinear viscoelastic particle reinforced polymeric composite materials-undamaged State. Compos Appl Sci Manuf 2004;35(7-8):905-913.

[14]. Hine PJ, Lusti HR, Gusev AA. Numerical simulation of the effects of volume fraction, aspect ratio and fibre length distribution on the elastic and thermoelastic properties of short fibre composites. Compos Sci Technol 2002;62(10-11):1445-1453.

[15]. Aboudi J. Thermomechanically coupled micromechanical analysis of multiphase composites. J Eng Math 2008;61(2-4):111-132.

[16]. Aboudi J. Mechanics of composite materials: A unified micromechanical approach. New York: Elsevier; 1991.

[17]. Li G, Castaneda PP. The effect of particle shape and stiffness on the constitutive behavior of metal-matrix composites. Int J Solids Struct 1993;30(23):3189-3209.

[18]. Muliana AH, Kim JS. A concurrent micromechanical model for predicting nonlinear viscoelastic responses of composites reinforced with solid spherical particles. Int J Solids Struct 2007;44(21):6891-6913.

[19]. Muliana AH. Multi-scale framework for the thermo-viscoelastic analyses of polymer composites. Mech Res Comm 2008;35(1-2):89-95.

[20]. Kolodziej JA, Konczak Z. Determination of effective thermal conductivity for a laminated composite slab in non-linear case. Int Comm Heat Mass Trans 1994;21(3):403-410.

[21]. Fan Z. A microstructural approach to the effective transport properties of multiphase composites. Phil Mag 1996;73(6):1663-1684.

[22]. Yin Y, Tu ST. Thermal conductivities of PTFE composites with random distributed graphite particles. J Reinforc Plast Compos 2002;21(18):1619-1627.

[23]. Jiang M, Starzewski MO, Jasiuk I. Scale-dependent bounds on effective elastoplastic response of random composites. J Mech Phys Solids 2001;49(3):655-673.

[24]. Jiang M, Jasiuk I, Starzewski MO. Apparent elastic and elastoplastic behavior of periodic composites. Int J Solids Struct 2002;39(1):199-212.

[25]. Jiang M, Jasiuk I, Starzewski MO. Apparent thermal conductivity of periodic two-dimensional composites. Comput Mater Sci 2002;25(3):329-338.

[26]. Kim JY, Yoon BJ. The effective conductivities of composites with cubic arrays of spheroids and cubes. J Compos Mater 1999;33(14):1344-1362.

[27]. Hasselman DPH. Effect of cracks on thermal conductivity. J Compos Mater 1978;12(4):403-407.

[28]. Rajput RK. Heat and mass transfer in SI units. New Delhi: S.Chand & Company LTD; 2003.

[29]. Khan KA, Muliana AH. Effective thermal properties of viscoelastic composites having field dependent constituent properties, 2008. Currently under review.

[30]. Reddy JN. An introduction to the finite element method. New York: Tata McGraw-Hill Edition; 2005.

[31]. White JR. Math methods-section X: analytical solution of PDEs, http://www.tmt.ugal.ro/crios/Support/ANPT/Curs/math/s10/s10intro/s10intro.html, 2004.

[32]. Geiger AL, Hasselman DPH, Donaldson KY. Effect of reinforced particle size on the thermal conductivity of a particulate silicon carbide-reinforced aluminium-matrix composite. J Mater Sci 1993;12(6):420-423.

[33]. Chawla N, Shen YL. Mechanical behavior of particle reinforced metal matrix composites. Adv Eng Mater 2001;3(6):357-370.

[34]. Santos DWN. Experimental investigation of the effect of moisture on thermal conductivity and specific heat of porous ceramic materials. J Mater Sci 2000;35(16):3977-3982.

[35]. Pusch M. Historical development and processing of TBCs, http://www.mspusch.de/Ing-Diplomarbeit/2_GeneralBackground.htm, 2002.

[36]. Kulkarni AA, Goland A, Herman H, Allen AJ, Ilavsky J, Long GG, Johnson CA, Ruud JA. Microstructure-property correlations in industrial thermal barrier coatings. J Am Ceram Soc 2004;87(7):1294-1300.

[37]. Hass DD. Directed vapor deposition of thermal barrier coatings, Chapter 2: Thermal Barrier Coatings, PhD Dissertation. Charlottesville: University of Virginia, 2000.

[38]. Zhu D, Miller RA. Thermophysical and thermomechanical properties of thermal barrier coating systems. J Am Ceram Soc 2000;91(8):2630-2635.

[39]. Seo DW, Na EG. Finite element analysis of residual stress in NiCrAlY/Yttria-stabilized zirconia coatings by nanoscale multi-layered deposition. Key Eng Mater 2004;270-273(1):58-63.

[40]. Sadd MH. Elasticity: theory, applications and numerics. Oxford: Academic Press; 2005.

[41]. ABAQUS, user's manual, version, 6.7. Providence, RI: Hibbitt, Karlsson and Sorensen Inc.; 2007.

[42]. ASM International., Superalloys: A technical guide, http://asmcommunity.asm international.org/content/ASM/StoreFiles/ACFAAD4.pdf, 2002.

VITA

Name: Pradeep Gudlur

Address: Department of Mechanical Engineering, 3123 TAMU,
College Station, TX 77843, USA

Email Address: deepu_mechanics@tamu.edu

Education: B. Tech., Mechanical Engineering,
Vidya Jyothi Institute of Technology, India, 2006

M.S., Mechanical Engineering, Texas A&M University,
College Station, Texas, 2008